

สาเหตุของการให้สีแดงในพลอยแพลจีโอเคลสเฟลด์สปาร์



นางสาวนาร์วี สุเสวี

จุฬาลงกรณ์มหาวิทยาลัย

CHULALONGKORN UNIVERSITY

วิทยานิพนธ์นี้เป็นส่วนหนึ่งของการศึกษาตามหลักสูตรปริญญาวิทยาศาสตรมหาบัณฑิต

สาขาวิชาธรณีวิทยา ภาควิชาธรณีวิทยา

คณะวิทยาศาสตร์ จุฬาลงกรณ์มหาวิทยาลัย

บทคัดย่อและแฟ้มข้อมูลฉบับเต็มของวิทยานิพนธ์ตั้งแต่ปีการศึกษา 2554 ที่ให้บริการในคลังปัญญาจุฬาฯ (CUIR)

ปีการศึกษา 2556

เป็นแฟ้มข้อมูลของนิสิตเจ้าของวิทยานิพนธ์ ที่ส่งผ่านทางบัณฑิตวิทยาลัย

ลิขสิทธิ์ของจุฬาลงกรณ์มหาวิทยาลัย

The abstract and full text of theses from the academic year 2011 in Chulalongkorn University Intellectual Repository (CUIR)

are the thesis authors' files submitted through the University Graduate School.

CAUSE OF RED COLORING IN GEM PLAGIOCLASE FELDSPAR

Miss Namrawee Susawee

The logo of Chulalongkorn University, featuring a central emblem with a sunburst and a tiered structure, set against a light background.

จุฬาลงกรณ์มหาวิทยาลัย  
CHULALONGKORN UNIVERSITY

A Thesis Submitted in Partial Fulfillment of the Requirements  
for the Degree of Master of Science Program in Geology

Department of Geology

Faculty of Science

Chulalongkorn University

Academic Year 2013

Copyright of Chulalongkorn University

Thesis Title	CAUSE OF RED COLORING IN GEM PLAGIOCLASE FELDSPAR
By	Miss Namrawee Susawee
Field of Study	Geology
Thesis Advisor	Associate Professor Chakkaphan Sutthirat, Ph.D.

---

Accepted by the Faculty of Science, Chulalongkorn University in Partial  
Fulfillment of the Requirements for the Master's Degree

.....Dean of the Faculty of Science  
(Professor Supot Hannongbua, Dr. rer. nat.)

THESIS COMMITTEE

.....Chairman  
(Associate Professor Montri Choowong, Ph.D.)

.....Thesis Advisor  
(Associate Professor Chakkaphan Sutthirat, Ph.D.)

.....Examiner  
(Associate Professor Visut Pisutha-Arnon, Ph.D.)

.....Examiner  
(Assistant Professor Pitsanupong Kanjanapayont, Dr. rer. nat.)

.....External Examiner  
(Bhuwadol Wathanachaisaeng, Dr. rer. nat.)

นำรวี สุเสวี : สาเหตุของการให้สีแดงในพลอยแพลงจิโอเคลสเฟลด์สปาร์. (CAUSE OF RED COLORING IN GEM PLAGIOCLASE FELDSPAR) อ.ที่ปรึกษาวิทยานิพนธ์หลัก: รศ. ดร.จักรพันธ์ สุทธิรัตน์ , 88 หน้า.

แอนติซินและแลบราดอไลต์เป็นแร่ในกลุ่มแพลงจิโอเคลสเฟลด์สปาร์ชนิดที่มีสมบัติทางอัญมณี ในตลาดอัญมณีและผู้บริโภคมีการยอมรับซื้อขายกัน แต่เนื่องจากกลุ่มพลอยชนิดที่มีสีแดงนั้น มีทั้งที่เกิดขึ้นเองตามทำธรรมชาติและที่ผ่านการปรับปรุงคุณภาพขึ้น ทำให้เกิดความสับสนในกลุ่มผู้ขายและผู้บริโภค จึงทำให้เป็นที่มาของการศึกษาถึงกลไกสาเหตุการเกิดสีแดงของพลอยชนิดนี้ โดยตัวอย่างที่นำมาใช้ในการศึกษาได้มาจากแหล่งที่น่าเชื่อถือ ในการศึกษาได้อาศัยเครื่องมือขั้นพื้นฐานและขั้นสูงต่างๆ โดยลักษณะมลทินที่เด่นชัดที่พบภายใต้กล้องจุลทรรศน์ ได้แก่ มลทินท่อสีแดงทั้งที่มีลักษณะการเรียงตัวเป็นแนวดีและที่มีลักษณะผิดปกติ บริเวณที่ขอบรอบผิวพลอยจะแสดงลักษณะไม่มีสี พบมลทินลักษณะคล้ายกลุ่มหมอกบริเวณโซนสีแดง โดยในตัวอย่างพลอยที่ไม่ผ่านการปรับปรุงคุณภาพจะพบลักษณะสีที่ไม่สม่ำเสมอ มีสีเขียวกระจายปนอยู่ และพบลักษณะประกายเหลือบแสงเฉพาะในพลอยกลุ่มนี้ ขณะที่ลักษณะเด่นที่พบเฉพาะในกลุ่มตัวอย่างพลอยปรับปรุงคุณภาพที่เผาให้เกิดสีจากการแพร่ของทองแดงนั้น ได้แก่ ลักษณะชั้นสีที่เห็นเป็นวงสีแดงเข้มสลับอ่อนจากขอบนอกเข้ามาตรงกลางด้านในพลอย เมื่อนำตัวอย่างไปวิเคราะห์ด้วยเครื่อง EPMA ผลการวิเคราะห์เคมีที่ได้ทำให้สามารถสรุปชนิดของพลอยตัวอย่างทั้งหมดได้ว่าเป็นชนิดพลอยแอนติซิน-แลบราดอไรต์ โดยมีลักษณะการดูดกลืนแสงช่วง UV-VIS ของพลอยตัวอย่างสีแดงทั้งหมดทั้งที่ผ่านการปรับปรุงคุณภาพและไม่ผ่านการปรับปรุงคุณภาพนั้น ต่างแสดงลักษณะการดูดกลืนแสงที่ตำแหน่งประมาณ 568 - 599 nm อย่างชัดเจน ซึ่งน่าจะเป็นผลการดูดของ  $\text{Cu}^0$  colloid ที่เป็นมลทินอนุภาคนาโนขนาดเล็ก เพื่อยืนยันผลและกลไกการเกิดสีในพลอย จึงได้ทำการวิเคราะห์ด้วยเครื่อง LA-ICP-MS พบว่าปริมาณของธาตุทองแดงที่น่าจะเป็นสาเหตุการเกิดสีแดง แสดงความสัมพันธ์ระหว่างปริมาณธาตุทองแดงที่พบกับแนวระนาบแฝดหรือมลทินท่อหรือมลทินกลุ่มหมอกสีแดงในพลอย จากหลักฐานที่กล่าวมาทั้งหมดข้างต้นนั้น ได้นำมาใช้สรุปผลการศึกษากการเกิดสีแดงและกลไกการให้สีในพลอยแพลงจิโอเคลสเฟลด์สปาร์สีแดงได้ว่า สีแดงที่พบน่าจะเกิดจากกลไกการแพร่ของทองแดงที่เป็นมลทินขนาดเล็กมากแทรกตัวหรือเกิดการแพร่ของสีไปตามโครงสร้างที่เป็นท่อหรือช่องว่างภายในพลอย รวมถึงการแพร่จากผิวภายนอกเข้ามาในเนื้อพลอยกรณีที่พลอยผ่านการปรับปรุงคุณภาพ

ภาควิชา ธรณีวิทยา

ลายมือชื่อนิสิต .....

สาขาวิชา ธรณีวิทยา

ลายมือชื่อ อ.ที่ปรึกษาวิทยานิพนธ์หลัก .....

ปีการศึกษา 2556

# # 5372273523 : MAJOR GEOLOGY

KEYWORDS: RED FELDSPAR / COPPER-DIFFUSED ANDESINE / RED PLAGIOCLASE

NAMRAWEE SUSAWEE: CAUSE OF RED COLORING IN GEM PLAGIOCLASE  
FELDSPAR. ADVISOR: ASSOC. PROF. CHAKKAPHAN SUTTHIRAT, Ph.D., 88 pp.

Andesine and labradorite, members of plagioclase feldspar, may have gemological properties. In the gem market, red gem plagioclases have been sold but they may contain natural and treated stones. Consequently, confusion has been made to both trader and customer. Mechanism and cause of red coloring in gem plagioclase feldspar were then investigated in this study. Two sample groups, natural red plagioclase and red copper-diffused plagioclase were collected for this study. Microscopic examination revealed some typical internal features such as oriented and irregular red tubes, colorless rim, mottled colors of red and green, milky cloud along red zone and glistering cloud were found in natural group while red concentric color layer is typically observed in copper-diffused samples. EPMA analyses revealed that all samples have their end-member composition in the range of andesine–labradorite. UV-Vis spectra of all red samples show distinct absorption band at 568-599 nm probably due to  $\text{Cu}^0$  colloid. LA-ICP-MS analyses supported that copper content is related to red cloud zone, red tubes or twinning plane. In conclusion, the red coloring in gem plagioclase feldspar is probably due to copper nanoparticle that could be diffused into the stones by natural process as well as artificial process. The copper diffusion mechanism could have been taken place along twinning plane, or dislocation tubes as pipe diffusion in both natural and treated samples. Moreover, the surface diffusion maybe caused clearly by diffusion treatment leading to red color intense from outer rim inward core.

CHULALONGKORN UNIVERSITY

Department: Geology

Student's Signature .....

Field of Study: Geology

Advisor's Signature .....

Academic Year: 2013

## ACKNOWLEDGEMENTS

I would like to express my special gratitude to my thesis advisor, Associate Professor Dr. Chakkaphan Sutthirat for his guidance throughout the thesis project. I am also thoughtful to Mrs. Wilawan Atichat (Former Director of The Gem and Jewelry Institute of Thailand (Public Organization) and Mr.Thanong Leelawattanasuk, Cheif of GIT-GTL for sample collections and their very useful suggestions. Thanks are also extended to thesis committee; Associate Professor Dr. Montri Choowong, Associate Professor Dr. Visut Pisutha-Armond, Dr. Bhuwadol Wathanachaisaeng and Assistant Professor Pitsanupong Kanjanapayont for their valuable comments. I would like to express my sincere gratitude to all instructors who have been given knowledge since undergraduate to graduate programs.

Research facilities and analytical techniques were provided by the Department of Geology, Faculty of Science, Chulalongkorn University and the Gem and Jewelry Institute of Thailand (Organization) for use of.

My study could not have been accomplished without the kind support of my classmates, especially Mr. Alongkot Fanka, Miss Sutipa Arsirapoj, Mr. Supattarachai Saksakulkrai, Mr. Tasnara Sripoonjan and many peoples. Last but not least, I must thank my parents, sisters and doctor who want to see my good health after my graduation

## CONTENTS

	Page
THAI ABSTRACT .....	iv
ENGLISH ABSTRACT .....	v
ACKNOWLEDGEMENTS .....	vi
CONTENTS .....	vii
LIST OF TABLES .....	ix
LIST OF FIGURES.....	x
CHAPTER 1 INTRODUCTION .....	1
1.1 General Statement .....	1
1.2 Objective.....	1
1.3 Scope of Work.....	2
1.4 Methodology.....	2
1.5 Advanced Analytical Techniques.....	5
1.5.1 UV-VIS-NIR spectrophotometer.....	5
1.5.2 Laser Raman spectroscopy.....	6
1.5.3 Fourier Transform Infra-Red (FTIR) spectrophotometer.....	7
1.5.4 Energy Dispersive X-ray Fluorescence Spectrometer (EDXRF).....	8
1.5.5 Electron Probe Micro-Analyzer (EPMA).....	9
1.5.6 Laser Ablation-Inductivity Coupled Plasma-Mass Spectrometer (LA-ICP-MS).....	10
CHAPTER 2 LITERATURE REVIEWS.....	13
2.1 Introduction.....	13
2.2 Natural red plagioclase occurrence in Tibet .....	15
2.3 Plagioclase Occurrence in Inner Mongolia.....	18
2.4 Colored Plagioclase .....	18
2.5 Heat Treatment of Feldspar .....	22
2.6 Diffusion Mechanisms.....	24
2.6.1 Vacancy Mechanism.....	26

	Page
2.6.2 Interstitial Mechanism.....	26
2.6.3 Exchange Mechanism.....	26
2.6.4 Definition About Diffusion.....	28
CHAPTER 3 PHYSICAL PROPERTIES AND INTERNAL FEATURES .....	30
3.1 Introduction.....	30
3.2 Physical and Optical Properties .....	30
3.3 Internal Characteristic .....	38
CHAPTER 4 ANALYTICAL RESULTS.....	41
4.1 Introduction.....	41
4.2 UV-VIS-NIR Spectrophotometric Results .....	41
4.3 Laser Raman Spectroscopic Results.....	44
4.4 Fourier Transform Infra-Red (FTIR) Spectrophotometric Results.....	49
4.5 Energy Dispersive X-ray Fluorescence Spectrometric (EDXRF) Results.....	51
4.6 Electron Probe Micro – Analytical (EPMA) Results.....	54
4.7 Laser Ablation-Inductivity Coupled Plasma-Mass Spectrometric (LA-ICP-MS) Results .....	57
CHAPTER 5 DISCUSSIONS AND CONCLUSIONS.....	70
5.1 Physical Properties.....	70
5.2 Spectroscopic Characteristics .....	74
5.3 Chemical Analyses.....	78
5.4 Conclusions.....	81
REFERENCES .....	82
APPENDICES.....	87
VITA.....	88



## LIST OF TABLES

	Page
Table 1.1 Operation conditions of LA-ICP-MS under this study.....	12
Table 3.1 Physical and optical properties of natural red plagioclase samples (YLA1-YLA3, YD1-YD2, YU1-YU7) and a very light yellow sample, IMA).....	32
Table 3.2 Physical and optical properties of 5 Cu-diffused red plagioclase samples (TA0 - TA2 and DF1-DF2). .....	34
Table 3.3 Pleochroism of 12 natural red plagioclases using dichroscope under daylight (*taken under the gem microscope with incandescent light using the polaroid and diffused plates).....	35
Table 3.4 Pleochroism of 5 Cu-diffused red plagioclases using dichroscope under daylight (*taken under the gem microscope with incandescent light using the polaroid and diffused plates).....	37
Table 3.5 Summary of internal characteristics found in natural and treated red plagioclase samples. ....	40
Table 4.1 EDXRF analyses of feldspar samples presenting as minimum-maximum ranges, averages and standard deviations .....	52
Table 4.2 Representative EPMA analyses of plagioclase samples. ....	56
Table 4.3 LA-ICP-MS spot analyses of representative red plagioclases. ....	58

## LIST OF FIGURES

	Page
Figure 1.1 Flowchart showing the methodology of this research project. ....	4
Figure 1.2 UV-VIS-NIR spectrophotometer, Model Lambda 950 series, Perkin Elmer based at the GIT.....	5
Figure 1.3 Laser Raman spectroscope, Model Renishaw inVia Raman Microscope based at the GIT.....	6
Figure 1.4 Fourier Transform Infra-Red (FTIR) spectrophotometer, Nicolet NEXUS 670 series based at the GIT. ....	7
Figure 1.5 Energy Dispersive X-ray Fluorescence Spectrometer (EDXRF), Model Eagle III microprobe series, EDAX based at the GIT.....	8
Figure 1.6 Electron Probe Micro – Analyzer (EPMA), Model JXA-8100 super probe, JEOL based at the Department of Geology, Faculty of Science, Chulalongkorn University. ....	9
Figure 1.7 Laser Ablation-Inductivity Coupled Plasma-Mass Spectrometer (LA-ICP-MS), an Agilent, Model 7500 series based at the GIT.....	11
Figure 2.1 Structure of plagioclase explaining andesine-labradorite structure. Purple line show the triclinic unit cell in primitive setting while pink line (with labels) correspond to the C-centered setting chosen for unit refinement. Green probability ellipsoids indicate disordered Na, Ca sites bonded to the tetrahedral framework. Orange tetrahedral shown (Si, Al)O <sub>4</sub> tetrahedral with disordered Si and Al distribution. Recalculated for C-centered setting and lattice parameters are a = 8.1703 Å, b = 12.8723 Å, c = 7.1071 Å, alpha 86.551(1)°, beta = 116.175°, gamma = 89.710° (modified after Peretti, 2011). ....	14
Figure 2.2 Yu Lin Gu andesine occurrences as shown by the yellow symbols on this Google map (Coordinate for this locality; 29°03.08'N, 89°20.76'E; 4,102 m from Wang, 2011) (modified after Laurs et al., 2011). ....	16
Figure 2.3 Natural red feldspars were found from shallow pits dug at Yu Lin Gu alluvial fan (Photos by Thanong Leelawatanasuk from investigated field). ....	17

- Figure 2.4 Paths for volume diffusion, grain boundary diffusion, and surface diffusion. Note that volume diffusion can provide many possible paths. This multitude of possible paths allows volume diffusion to be dominant at high temperatures despite the higher mobility expected along the individual short-circuit (surface and grain boundary) paths. If diffusion and reaction throughout a grain is desired, volume diffusion is required. Figure modified from (Manning, 1973)... 25
- Figure 2.5 Schematic representation of the different diffusion mechanisms (a) Vacancy mechanism (b), Interstitial mechanism (c), Direct exchange mechanism and (d) Ring interchange mechanism (modified from Salameh, 2011)..... 27
- Figure 3.1 Distinct pleochroism of the natural red feldspar is clearly observed under London dichroscope (sample no. YD1 (left) and YLA3 (right)). ..... 31
- Figure 3.2 Representative internal features of untreated feldspar samples including (a) colorless zone around fingerprint (YD1), (b) mottled color (red and green) along tubes and twinning (YU3), (c) colorless rim and (d) oriented coarse red tubes with glistening (YU6). ..... 38
- Figure 3.3 Representative internal features of treated feldspar samples show (a) colorless rim, (b) circular of milky red cloud from core to rim (DF2), (c) colorless zone around irregular and (d) straight red tubes (TA2). ..... 39
- Figure 4.1 UV-Vis spectra of untreated red plagioclase (sample no. YLA3) show the polarized absorption bands at about 573 nm (0p) and at 578 nm (90p). ..... 42
- Figure 4.2 UV-Vis spectra of untreated red plagioclase (sample no. YD1) show the distinct polarized absorption bands at about 568 nm (0p) and 591 nm (90p). . 43
- Figure 4.3 UV-Vis spectra of treated red plagioclase (sample no. TA0) show the polarized distinct absorption peaks at about 568 nm (both in 0p and 90p). ..... 43
- Figure 4.4 UV-Vis spectra of untreated very light yellow plagioclase (sample no. IMA) shows the polarized absorption peaks at 382, 420 and 449 nm. .... 44
- Figure 4.5 RAMAN spectrum of natural red plagioclase (sample no. YD2) shows Raman shift peaks at 281, 405, 482, 509, 564 and 792  $\text{cm}^{-1}$ . ..... 45
- Figure 4.6 RAMAN spectrum of treated red plagioclase (sample no. TA1) show Raman shift peaks at 279, 406, 482, 507, 564 and 792  $\text{cm}^{-1}$ . ..... 45
- Figure 4.7 RAMAN spectrum of untreated very light yellow plagioclase (sample no. IMA) shows Raman shift peaks at 281, 406, 483, 509, 565 and 789  $\text{cm}^{-1}$ . ..... 46

Figure 4.8 Raman spectrum databases of albite from the RRUFF Project website ( <a href="http://rruff.info/albite/display=default/X050005">http://rruff.info/albite/display=default/X050005</a> ) (RRUFF).....	46
Figure 4.9 Raman spectrum databases of oligoclase from the RRUFF Project website ( <a href="http://rruff.info/oligoclase/display=default/X050122">http://rruff.info/oligoclase/display=default/X050122</a> ) (RRUFF).....	47
Figure 4.10 Raman spectrum databases of andesine from the RRUFF Project website ( <a href="http://rruff.info/andesine/display=default/X050013">http://rruff.info/andesine/display=default/X050013</a> ) (RRUFF).....	47
Figure 4.11 Raman spectrum databases of labradorite from the RRUFF Project website ( <a href="http://rruff.info/labradorite/display=default/X050108">http://rruff.info/labradorite/display=default/X050108</a> ) (RRUFF) .....	48
Figure 4.12 Raman spectrum databases of bytownite from the RRUFF Project website ( <a href="http://rruff.info/bytownite/display=default/X050033">http://rruff.info/bytownite/display=default/X050033</a> ) (RRUFF).....	48
Figure 4.13 Raman spectrum databases of anorthite from the RRUFF Project website ( <a href="http://rruff.info/anorthite/display=default/X050021">http://rruff.info/anorthite/display=default/X050021</a> ) (RRUFF).....	49
Figure 4.14 FTIR spectrum of natural red plagioclase (sample no. YLA2) shows absorptions related to OH or H <sub>2</sub> O group at the range 3944-3477 cm <sup>-1</sup> and C-H stretching at 2961, 2919 and 2849 cm <sup>-1</sup> .....	50
Figure 4.15 FTIR spectrum of treated red plagioclase (sample no. DF2) shows absorptions related to OH or H <sub>2</sub> O group at the range 3937-3504 cm <sup>-1</sup> and C-H stretching at 2955, 2919 and 2850 cm <sup>-1</sup> .....	50
Figure 4.16 FTIR spectrum of untreated very light yellow plagioclase (sample no. IMA) shows absorptions related to OH or H <sub>2</sub> O group at the range 3937-3562 cm <sup>-1</sup> and C-H stretching at 2919, 2873 and 2849 cm <sup>-1</sup> .....	51
Figure 4.17 Ternary feldspar plots of 18 samples including natural red plagioclase, copper-diffused plagioclase and very light yellow plagioclase. ....	55
Figure 4.18 Comparison between average copper (Cu) contents between natural and treated red plagioclases dividing into colorless rim and inner red areas. ....	59
Figure 4.19 Comparative graph of averaged silver (Ag) contents between natural red and treated red plagioclase dividing into colorless rim and inner red zones.....	60
Figure 4.20 Comparative graph of averaged Iron (Fe) contents between natural red and treated red plagioclase dividing into colorless rim and inner red zones.....	61

Figure 4.21 Comparative graph of averaged manganese (Mn) contents between natural red and treated red plagioclase dividing into colorless rim and inner red zones .....	62
Figure 4.22 Comparative graph of averaged barium (Ba) contents between natural red and treated red plagioclase dividing into colorless rim and inner red zones.....	63
Figure 4.23 Profile plots of Mg, Ti, Mn, Fe, Cu, Sr Ag and Ba in natural red feldspar; 16 spots cross (perpendicular to) the twinning plane from colorless rim (left side) to inner red zone.....	64
Figure 4.24 Profile plots of Mg, Ti, Mn, Fe, Cu, Sr Ag and Ba in natural red feldspar; 16 spots along (parallel to) the twinning plane.....	65
Figure 4.25 Analytical profiles of Mg, Ti, Mn, Fe, Cu, Sr, Ag and Ba in natural red feldspar parallel to the twinning plane (red tube) showing high copper content. ....	65
Figure 4.26 Profile plots of Mg, Ti, Mn, Fe, Cu, Sr, Ag and Ba in treated red feldspar; 36 spots perpendicular to the twinning from colorless rim (left side) to inner red zone.....	66
Figure 4.27 Profile plots of Mg, Ti, Mn, Fe, Cu, Sr, Ag and Ba in treated red feldspar; 42 spots parallel to the twinning from colorless rim (left side) to inner red zone.	67
Figure 4.28 Comparative graph of copper (Cu) contents in treated feldspar (sample no. TA0); 36 spots analyzed perpendicular to twinning planes; Mean and SD were calculated from each area such as colorless (4 spots) light red (8 spots) and red (23 spots).....	68
Figure 4.29 Comparative graph of copper (Cu) content in treated feldspar (sample no. TA0); 42 spots analyzed along the twinning plane; Mean and SD were calculated from each area as colorless (10 spots) light red (10 spots) and red (22 spots). ....	69
Figure 5.1 Distinct dichroism of the natural red plagioclase is clearly observed under London dichroscope (sample no. YD1).....	71
Figure 5.2 Pleochroism of copper-diffused red plagioclase (sample no.TA0) showing moderate grayish red (left) to red (right) under gem microscope using polaroid and diffused plates.....	71

Figure 5.3 Glistening cloud along red zone in natural red plagioclase (sample no. YD1). .....	73
Figure 5.4 Red color layer from rim inwards core in copper-diffused red plagioclase (sample no. TA0).....	73
Figure 5.5 UV-Vis spectra of Cu-diffused red plagioclase (sample no. TA1) show the distinct polarized absorption band at 569.87 nm (0p) and at 571.69 nm (90p). 77	



## CHAPTER 1

### INTRODUCTION

#### 1.1 General Statement

The gem-quality feldspars can be divided into two groups. The first group is alkali feldspars such as orthoclase with adularescence or schiller (moonstone) and microcline with green color (amazonite), and the second group is plagioclase feldspar including oligoclase with adventurescence (sunstone), grey to black feldspar with labradorescence (labradorite). This study is focused on plagioclase feldspars which have red, reddish orange, orangy red and orange colors. Most of the plagioclase feldspar gems with red to orange shade occur naturally in andesine-labradorite range. In 2002, the red 'Congolese' plagioclase feldspar first appeared in the gem market (Fritsch, 2002). Krzemnicki (2004) found labradorites in the Democratic Republic of Congo, which they have deep red color in saturation. The red and green colors of this gem labradorite are attributed by tiny copper colloids. This type of gem from Congo has been sold in the market under the name 'red andesine.' At that time, there was the rumor that 'Congo' andesine might be treated by copper diffusion. Consequently, it caused confusion to many customers and ceased the 'Congo' andesine trading. The new occurrence of red andesine called 'Tibetan sunstone' was found in Tibet at the same time. According to Abdurayim, (2009a), he had collected the samples from Tibet for investigation the natural red andesine and the copper-diffused plagioclase. Hughes (2011), also reported the results of his expedition to Tibet with the international research team in September 2010, to study the reported andesine occurrence in the Shigatse area again. Even though the previous studies emphasized that the cause of color in red andesine was copper, none of them reported about the mechanism in this variety of stone. Therefore, this study is aimed to understand the process or mechanism of copper color causing in the natural red andesine and copper-diffused plagioclase.

#### 1.2 Objective

The main objective of this research is to study the mechanism and cause of red coloring in gem plagioclase.

### 1.3 Scope of Work

The scope of this study was focused on mechanism and cause of red coloring in natural red andesine and copper-diffused red plagioclase.

### 1.4 Methodology

The method of this study can be summarized as a flow chart in Figure 1.1.

1. Literature survey is the first step for this study. Previous works related to plagioclase feldspar, cause of red colors in plagioclase feldspar and copper-diffusion treatment were searched and reviewed. The knowledge gained from the previous works were very helpful for work plan that was designed on the basis of these information.

2. Sample collection was provided by Mr. Thanong Leelawatanasuk from the Gem and Jewelry Institute of Thailand (Public Organization) who visited Tibetan andesine occurrences. All diffused samples were provided by a reputed Chinese gem dealer. These samples were declared to be from light yellow andesine from Inner Mongolia undertaken copper diffusion treatment.

3. Eighteen samples consist of twelve red plagioclase feldspars, one very light yellow plagioclase and five copper-diffused plagioclases were selected for this study. These samples were slab-cut on one side parallel to twinning and then polished for determination of general physical properties and advanced instrumental analyses.

4. Physical and optical properties of all samples were collected using the basic gem equipment at the GIT. These basic properties include refractive indices and birefringence (the different value of minimum and maximum refractive indices) using a refractometer, luminescence under short wave ultraviolet (SWUV, 254 nm), long wave ultraviolet (LWUV, 365 nm) and specific gravity using a hydrostatic balance. Internal features of samples were observed and photographed under a gemological microscope.



5. Raman spectra were collected using a Laser Raman spectroscope. Fourier Transform Infra-Red (FTIR) spectrophotometer and UV-VIS-NIR spectrophotometer were used for collecting the absorption spectra.

6. Semi-quantitative analyses of the major elements and some trace elements were carried out using an Energy Dispersive X-ray Fluorescence Spectrometer (EDXRF).

7. The polished sections were prepared for the quantitative analysis using an Electron Probe Micro-Analyzer (EPMA).

8. Quantitative analysis of trace elements was also carried out using a Laser Ablation-Inductivity Coupled Plasma-Mass Spectrometer (LA-ICP-MS).

9. Data interpretation, discussion and report writing were finally carried out to fulfill the research project.

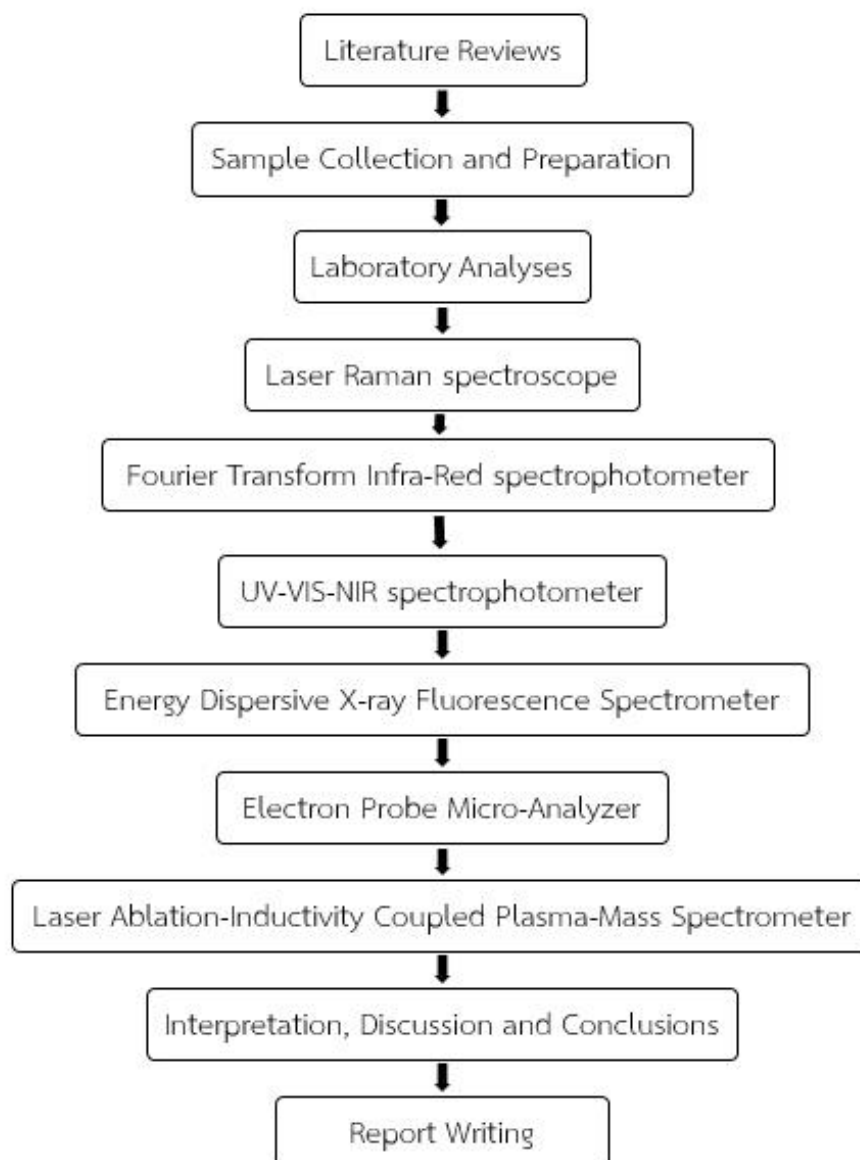


Figure 1.1 Flowchart showing the methodology of this research project.

## 1.5 Advanced Analytical Techniques

### 1.5.1 UV-VIS-NIR spectrophotometer

UV-VIS-NIR spectrophotometer, Model Lambda 950 series, Perkin Elmer (Figure 1.2) based at the GIT was mainly used for the study. This UV-VIS-NIR spectrophotometer contains a light source (tungsten-halogen and deuterium) generating wavelengths over the range of ultraviolet (UV), visible light (VIS) and near infrared (NIR). From basis of the molecular structure and chromophoric elements contained in the sample structure, this spectroscopic technique is applied to investigate the plagioclase samples. This study has been focused on visible light range. Their absorption spectra were examined between 300 and 800 nanometers (nm) with spectral resolution of 2 nm.



Figure 1.2 UV-VIS-NIR spectrophotometer, Model Lambda 950 series, Perkin Elmer based at the GIT.

### 1.5.2 Laser Raman spectroscopy

The Laser Raman spectroscopy, Model Renishaw inVia Raman Microscope (Figure 1.3) based at the GIT was used for this study. Raman spectroscopy is a result of vibrational phenomena of molecular structure activated by the light energy. Laser is the best monochromatic light source. Most Raman spectroscopic studies use laser within the visible range of spectrum. The most famous excitation source is Argon ion gas laser. The wavelength of this laser is in blue-green region between 488.0 and 514.5 nm. Spectrometer, in general, is grating monochromator which dispersion is taken place by selective reflection of the grating surface due to constructive and destructive interference caused by the regularly ruled surface. It is considered to be the most suitable spectrometer for Raman spectroscopy. The stray light is collected by a lens and sent through a monochromator. The elastic Rayleigh scattering light is filtered out while the rest of the collected light is dispersed onto a detector. Detector of Raman spectrometer commonly contains charge couple device (CCD) which yields higher sensitivity (Leelawatanasuk, 2004).



Figure 1.3 Laser Raman spectroscopy, Model Renishaw inVia Raman Microscope based at the GIT.

In this study, the machine was calibrated with silicon plate at its center about 520 nm. The laser source is 514.5 nm. Raman data scan range was set at 250 – 2000  $\text{cm}^{-1}$ , with data acquisition times of 20 seconds and accumulations 2 times with 100% laser power. Raman spectroscopic applications to gemology, most Raman spectrometers are equipped with the microscope that enables the gemologist to focus on the spot to be analyzed. This is quick and non-destructive method for identifying gemstones (Kiefert et al., 2001).

### 1.5.3 Fourier Transform Infra-Red (FTIR) spectrophotometer

Fourier Transform Infra-Red (FTIR) spectrophotometer, Nicolet NEXUS 670 series (Figure 1.4) based at the GIT was used for recording the transmission spectra within the range of near to far infrared. In infrared spectroscopy, IR radiation is passed through a sample. Some of the infrared radiation is absorbed by the sample and some of it passed through (transmitted). The obtained spectrum represents the molecular absorption and transmission, creating a molecular fingerprint of the sample. In this study, measurement of transmission spectra is in a range of 4000-2000  $\text{cm}^{-1}$  which is in the mid infrared range.



Figure 1.4 Fourier Transform Infra-Red (FTIR) spectrophotometer, Nicolet NEXUS 670 series based at the GIT.

#### 1.5.4 Energy Dispersive X-ray Fluorescence Spectrometer (EDXRF)

Energy Dispersive X-ray Fluorescence Spectrometer (EDXRF), Model Eagle III microprobe series, EDAX (Figure 1.5) based at the GIT was used for semi-quantitative analyses of the major elements and some trace elements. The analysis is made by the behavior of atoms when they interact with radiation. When samples are excited with high energy, they become ionized. Energy differences between the electron shells are known and fixed; therefore, the emitted radiation always has characteristic energy and the fluorescent X-rays can be used to detect the abundances of elements which are present in the sample (Shackley, 2011). This method is a non-destructive technique. The X-ray source used in this machine is Rhodium (Rh) X-ray tube. The standard less calibration was applied for all analyses.



Figure 1.5 Energy Dispersive X-ray Fluorescence Spectrometer (EDXRF), Model Eagle III microprobe series, EDAX based at the GIT.

### 1.5.5 Electron Probe Micro-Analyzer (EPMA)

The Electron Probe Micro-Analyzer (EPMA), Model JXA-8100 super probe, JEOL (Figure 1.6) based at the Department of Geology, Faculty of Science, Chulalongkorn University was mainly used for mineral chemical analysis in this study.



Figure 1.6 Electron Probe Micro – Analyzer (EPMA), Model JXA-8100 super probe, JEOL based at the Department of Geology, Faculty of Science, Chulalongkorn University.

The quantitative EPMA analysis is a non-destructive analytical method. Electron beam is focused on the surface of sample at micro-scale and characteristic X-rays are produced from the sample. The characteristic X-rays are detected at specific wavelengths. Their intensities are measured and calibrated with standard to determine concentrations. The EMPA was applied to analyze the major elements (i.e.,  $\text{SiO}_2$ ,  $\text{TiO}_2$ ,  $\text{Al}_2\text{O}_3$ ,  $\text{FeO}$ ,  $\text{CaO}$ ,  $\text{Na}_2\text{O}$  and  $\text{K}_2\text{O}$ ) for recalculation of end-member compositions of all feldspar samples and their concentration of some trace elements such as  $\text{CuO}$  and  $\text{SrO}$ . Standards used for calibration were pure oxides and mineral standards including wollastonite for Si and Ca, corundum for Al, jadeite for Na, potassium titanium phosphate for K and Ti, fayalite for Fe, pure copper for Cu and Strontium Barium Niobate for Sr. Analyses were performed at 15kV (accelerating voltage), with a beam current of about 24 nA and focused beam (probe diameter) smaller than 1  $\mu\text{m}$ .

Measuring times were set at 30 seconds and 10 seconds for peak counts and background counts, respectively. These EPMA analyses were focused on major and minor compositions.

#### **1.5.6 Laser Ablation-Inductivity Coupled Plasma-Mass Spectrometer (LA-ICP-MS)**

Laser Ablation-Inductivity Coupled Plasma-Mass Spectrometry (LA-ICP-MS), an Agilent, Model 7500 series (Figure 1.7) based at the GIT was used for trace element analyses in this study. Low detection limits, multi-element capability and simple ICP-MS spectra, particularly for elements with complex emission spectra such as rare earth elements (REE) (Jarvis, 1988) are able to apply for analyses of elemental distribution in the samples. Laser ablation (LA) can be attached with the system for analyses of the solid samples. Basically, LA-ICP-MS begins with a laser beam focused on the surface sample to generate evaporation of fine particles. The ablated particles are then transported to the secondary excitation source of the Inductivity Coupled Plasma (ICP) that burns the vapor in an argon carrier gas stream. Then the vapor is decomposed, atomized and ionized, before extraction into the mass spectrometer vacuum system for analysis. The excited ions in the plasma torch are subsequently introduced to a mass spectrometer (MS) detector. The MS is a high sensitivity analyzer which can measure the level of part per million (ppm) or part per billion (ppb). The system can be used for both qualitative and quantitative analyses. The NIST glass (NIST 612 and NIST 610), BBMT1 and BNV-1G basalt glass standards were used during LA-ICP-MS trace analyses whereas  $^{26}\text{Al}$  was the internal standard. Data refining was carried out using GLITTER 4.0 software. Operation conditions of LA-ICP-MS are also summarized in Table 1.1. The sensitivity conditions of LA-ICP-MS under this study are collected in Appendix F4.





Figure 1.7 Laser Ablation-Inductivity Coupled Plasma-Mass Spectrometer (LA-ICP-MS), an Agilent, Model 7500 series based at the GIT.

Table 1.1 Operation conditions of LA-ICP-MS under this study.

<u>ICP-MS adjustment : Agilent 7500cs</u>	
Carrier gas flow	0.8 L/min
Plasma gas flow	15.0 L/min Argon
Radio frequency power	1200 W
Radio frequency matching	1.74 V
<u>Laser ablation adjustment : New wave UP-213</u>	
Output energy	12-13 J/cm <sup>2</sup>
Laser energy	50%
Repetition frequency	10 Hz
Crater size	Feldspar sample and standards 55 $\mu$ m
Dwell time	Feldspar : 51 elements Na, Mg, Fe      5 ms Al, Mn          10 ms Other elements 30 ms
External standard	NIST SRM 610
Internal standard	Feldspar Al <sub>2</sub> O <sub>3</sub> = 27wt%
Reference Standard Material	NIST SRM 612, BBM and BNV-1
Repetitions per sample	3
Acquisition time	120 sec
Integration time	0.03 sec

## CHAPTER 2

### LITERATURE REVIEWS

#### 2.1 Introduction

Compositions of the common feldspars can be expressed as a system of  $\text{KAlSi}_3\text{O}_8$  (orthoclase; Or)- $\text{NaAlSi}_3\text{O}_8$  (albite; Ab)- $\text{CaAl}_2\text{Si}_2\text{O}_8$  (anorthite; An). The series between  $\text{KAlSi}_3\text{O}_8$  and  $\text{NaAlSi}_3\text{O}_8$  are known as 'alkali feldspars' whereas those between  $\text{NaAlSi}_3\text{O}_8$  and  $\text{CaAl}_2\text{Si}_2\text{O}_8$  belong to 'plagioclase feldspars'. Members of plagioclase feldspars are given specific names, based on Ca or An content from low to high contents, as albite, oligoclase, andesine, labradorite, bytownite and anorthite, respectively. The feldspar structure consists of an infinite network of  $\text{SiO}_4$  as well as  $\text{AlO}_4$  tetrahedra. The feldspar structure can be considered a stiff derivative of the  $\text{SiO}_2$  structures, by incorporation of Al into the tetrahedral network, and concomitant housing of  $\text{Na}^+$  (or  $\text{K}^+$  or  $\text{Ca}^{2+}$ ) in available voids. When only one  $\text{Si}^{4+}$  (per feldspar formula unit) is substituted by  $\text{Al}^{3+}$ , the structure can be neutralized by incorporation of one  $\text{K}^+$  or one  $\text{Na}^+$ . Similarly when two  $\text{Si}^{4+}$  (per feldspar formula unit) are substituted by  $\text{Al}^{3+}$ , the electric charge of the network can be balanced by a divalent cation such as  $\text{Ca}^{2+}$ . In the plagioclase structure (see Figure 2.1), the amount of tetrahedral Al varies in proportion to the relative amounts of  $\text{Ca}^{2+}$  and  $\text{Na}^+$  so as to maintain electrical neutrality; the more  $\text{Ca}^{2+}$ , the greater amount of  $\text{Al}^{3+}$  (Klein and Hurlbut, 1999).

Other ions which may be present in plagioclase feldspar in very limit amounts include Ti,  $\text{Fe}^{3+}$ ,  $\text{Fe}^{2+}$ , Mn, Mg, Ba and Sr. Most of the iron reported is shown in feldspar analyses to be  $\text{Fe}^{3+}$ . The ion of  $\text{Fe}^{3+}$  usually replaces Al in the structure (Deer et al., 1992).

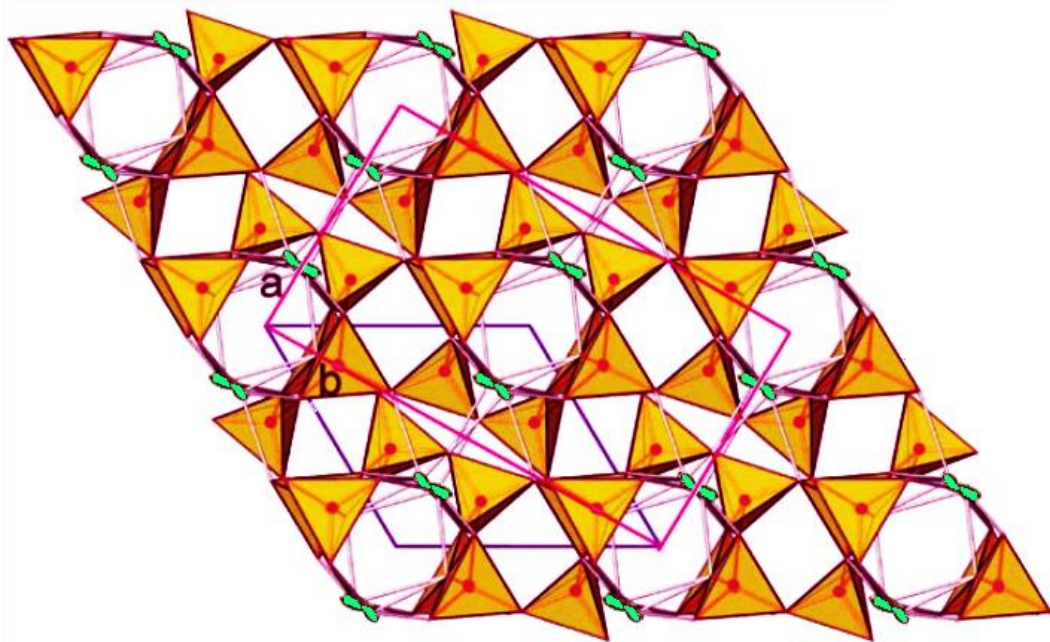


Figure 2.1 Structure of plagioclase explaining andesine-labradorite structure. Purple line show the triclinic unit cell in primitive setting while pink line (with labels) correspond to the C-centered setting chosen for unit refinement. Green probability ellipsoids indicate disordered Na, Ca sites bonded to the tetrahedral framework. Orange tetrahedral shown (Si, Al)O<sub>4</sub> tetrahedral with disordered Si and Al distribution. Recalculated for C-centered setting and lattice parameters are  $a = 8.1703 \text{ \AA}$ ,  $b = 12.8723 \text{ \AA}$ ,  $c = 7.1071 \text{ \AA}$ ,  $\alpha = 86.551(1)^\circ$ ,  $\beta = 116.175^\circ$ ,  $\gamma = 89.710^\circ$  (modified after Peretti, 2011).

## 2.2 Natural red plagioclase occurrence in Tibet

The National Gemstone Testing Center (NGTC) team undertook a field investigation in Bai Lang (Bai Nang) county and Jiangze (Gyangzê ) county in Shigatse (Xigazê) Prefecture, Tibet between 26<sup>th</sup> May and 1<sup>st</sup> June 2010 in order to verify their laboratory works and to investigate the reported red feldspar deposit in Tibet Abdurayim (2009b). The major results and observations were that they did not dig out any 'red feldspar' crystals from solid sedimentary rocks. All the red feldspar samples were dug out or picked up from either loose soils or from the surfaces of alluvial fan. Nine samples were collected from a miners' bag and 15 samples were purchased from a local miner who informed that 14 of these samples were treated. In addition, 11 rock samples, such as diabase, slate, phyllite and basalt were collected in the field. They are major rocks in the alluvial fan. All the red feldspar samples displayed rounded grain without any crystal face. The surfaces appear to have been etched or dissolved. Numbers of small pits were filled by white powder. The white powder on the surfaces could easily be cleaned off. It was difficult to accept that the white powder could have survived from abrasion during geological transportation. They were expected to be minerals associated with alluvial deposit. The red feldspar samples picked up from different places in the alluvial fan have equal sizes ranging from 5 to 10 mm in length. Other minerals typically displayed size distribution (geologically size sorting) from the top to bottom of the valley but there was no evidence of this size sorting for feldspars. The size distribution of the red feldspar was not consistent with normal alluvial sorting of mineral grains. The density and distribution of the red feldspar crystals on the surface and within loose soils vary significantly. In Lhasa and Shigatse, none of the interviewed people knew about the occurrence and existence of the red feldspar in Tibet. Geologically, the east and west of the valley they visited are mountain summits where the bedrocks were exposed (relative height of 200~400 m). The valley from south to north was formed by turbulent flooding. The alluvial fan was a secondary river terrace, comprising mainly black-grey silty slate, phyllite, diabase and basalt. The rock fragments on the surface range from 1–10 cm, depending on the position in the valley. Based on their investigations, they found it hard to believe that there were gem-quality feldspar deposits in the Bai Lang and Jiangze areas of Tibet (Wang et al., 2010).

According to Laurs et al. (2011), the international group visited the Shigatse region of Tibet in late September 2010. Subsequently, they reported the andesine occurrences at Nai Sa-Bainang, Zha Lin village and Yu Lin Gu alluvial fan. Andesines in these areas are associated with alluvial deposits derived from marine sedimentary rocks which are cross-cut by quartz veins. The andesine was recovered from random pits dug in undisturbed locations around the former mining area at Zha Lin provided strong field evidence for a genuine andesine deposit. At Yu Lin Gu area (see Figure 2.2), the group could not confirm the authenticity of the occurrence because andesine was only found at or very near surface of an active alluvial fan and they were not found in the rock outcrops expected to form gem-quality andesine in this area.

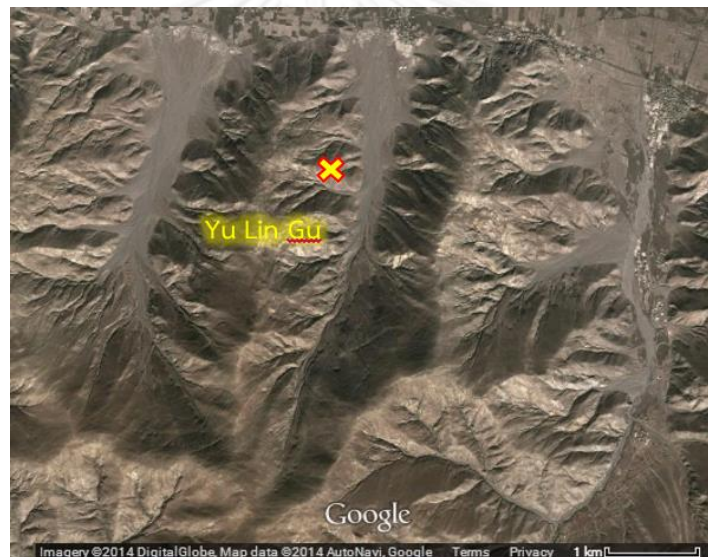


Figure 2.2 Yu Lin Gu andesine occurrences as shown by the yellow symbols on this Google map (Coordinate for this locality; 29°03.08'N, 89°20.76'E; 4,102 m from Wang, 2011) (modified after Laurs et al., 2011).

Himalaya region of Tibet was structurally complex and experienced four major periods of uplift as 55-36, 25-20, 17-12, and 3-0 Ma. All these periods are much younger than flysch deposits (Laurs et al., 2011). Therefore, the geomorphology of these areas are probably different from where the andesine was weathered from its original host rocks and incorporated into sediments derived from the flysch. The mechanical weathering of these rocks created alluvial fan and stream-deposited gravels that appear to contain the pebbles of andesine (see Figure 2.3 (a-d)).



Figure 2.3 Natural red feldspars were found from shallow pits dug at Yu Lin Gu alluvial fan (Photos by Thanong Leelawatanasuk from investigated field).

According to Abduriyim et al. (2011) , the andesine was hosted by alluvial sediments weathered from sedimentary formations consisting mainly of shale and clay-rich sandstone. These were described as Tertiary on the geologic map published by the Chinese Government. On the other hand, Guilmette et al. (2008) reported that the sedimentary formations in this area are much older (Late Triassic). Mechanical weathering of these rocks created stream deposits and alluvial fans that locally contain andesine pebbles. Original host rocks for andesine from Tibet have never been recognized during the field studies. Moreover, expected initial rocks (e.g., basaltic lava) have not been shown on geologic maps of the area.

### 2.3 Plagioclase Occurrence in Inner Mongolia

According to Abduriyim (2009a), pale yellow plagioclases (andesines) from Inner Mongolia were mined from secondary alluvial deposits of sand and gravel in the villages of Shuiquan and Haibouzi, north of Baotou. These stones are expected to be raw material of copper-diffused plagioclase in the market. The mine is situated in the Yinshan tectonic belt, which is in Mesozoic-Cenozoic age. Feldspars have been recovered from an area of approximately 20 km east-west and 5 km north-south. Humic topsoil usually overlies Tertiary (Pliocene) and Cretaceous sand and gravel. Some areas contain layers of tuff or basaltic rock. These andesines are restricted to a light greenish gray, locally iron-stained layer with about 1–3 m thick at several meters below the surface. Mining produces up to 100 tons, annually. The andesine crystals have high transparency and are rounded, except for broken pieces that show well-developed cleavage surfaces. The stones are typically 0.3 to 5.5 cm in diameter, most stones are in the 1–2 cm range. Most of the andesines are pale yellow. Colorless or deep yellow stones are rare, and other colors have not been reported from this area.

### 2.4 Colored Plagioclase

According to Smith (1974), in the eighteenth century, red coloring in feldspar known as the results from inclusions of hematite flakes that are oriented. Light is scattered from this micro-inclusions producing iridescence or schiller or aventurescence. This feldspar has been called sunstone.

Aventurine plagioclase ( $An_{65}$ ) from Modoc County, California was reported by Andersen (1917). It has metallic copper oriented parallel to the b and c axes of the feldspar crystal. However, most samples showing aventurescence contain iron oxide inclusion that merge the concepts of sunstone, aventurine and plate of iron oxide. Therefore, this feldspar unusual has aventurine character caused by metallic copper inclusions.

According to Hofmeister and Rossman (1983) the color of mineral can be produced by minor chemical substituents, inclusions, interference effect from exsolution lamellae, and radiation damage. Yellow color of sanidine and orthoclase, blue to green colors of amazonite may be caused by chemical impurity. Color varieties



are created by inclusions including pink, red, gray, orange and green. Aventurine and schiller effects can also result from inclusions. Gray color is produced by radiation. Exsolution lamellae and oriented intergrowths produce schiller, interference color and chatoyancy. Feldspar is colorless when free of minor substituents, inclusion and exsolution phenomena. In fact, feldspar naturally does not absorb visible light.

Red and green colors of labradorites from Congo are caused by copper; both different colors may be related to different particle sized of tiny copper colloids. Red and green stones from Congo have been sold as red andesine, intermediate composition of the plagioclase solid-solution series (Krzemnicki, 2004).

Color in labradorite from Oregon (USA) is correlated with the concentration of copper. Red labradorite shows the highest copper content (150-200 ppm CuO). The color is further dependent on Cu exsolution temperature, rate of Cu diffusion and aggregation ( $\text{Cu}^0$  colloids) and state of copper ( $\text{Cu}^0$  or  $\text{Cu}^+$ ). Red labradorite, absorption band at 560 to 580 nm combined with a general increasing absorption towards ultraviolet, is attributed to intrinsic absorption by tiny  $\text{Cu}^0$  particles which are too small (<22 nm) to scatter light, and produces a red color. The band-shift from 560 nm towards shorter wavelengths, coupled with a broadening size of the  $\text{Cu}^0$  colloids. As the spectra of the red sample from Congo (RC1 and RC2) are very similar to that from Oregon (RO1) in the 565 nm spectral region, the copper colloids are most probably of a very similar size and measure only a few nanometers (Hofmeister & Rossman, 1985).

Johnston et al. (1991) summarized that sunstones from Oregon contain native copper inclusions that cause aventurescence. On the other hand, aventurescence of sunstones from other localities appear to be caused by hematite inclusions.

According to Nassau (2001), the valence electron configuration of copper is  $3d^{10} 4s^1$ , configuration of copper provides 11 electrons. The 3d band is accordingly filled completely, and the 4s band is half filled to the level marked Cu.

According to Abduriyim (2009b), the natural color Tibetan andesine has been mined using simple hand tools from an alluvial deposit at Bainang County in the Shigatse (Xigazê) area of Tibet. The gem-quality andesine is derived from Tertiary-

Quaternary volcanogenic sediments related to Jurassic-Cretaceous volcanic rocks. Weathering and alluvial transport have resulted in round detrital crystals; most of crystals have orangy-red body color and a few stones have red and green bicolored zones. Top-quality stones in deep red are characterized by fine granular inclusions and some twin lamellae. Poorer qualities of andesine in orange-red and reddish-orange generally contain abundant turbid irregular color patches, tubes, irregular dislocations, and parallel lath-like hollow channels and a few tiny platelets of native copper.

Krzemnicki (2004) described the specimens from Congo as displaying a deeper color saturation, which made these very attractive gemstones. The studied specimens belonged to the labradorite plagioclase feldspar. Microscopically, these stones were rather clean, and contained only some twin lamellae, hollow channels and fine inclusions.

Abduriyim (2009a) studied the copper-diffused red andesine treated in China using materials from Inner Mongolia. Those materials featured pipe-and tube-like structures, discoid fractures, recrystallized white residue filling the lath-like hollow channels, and cloud inclusions that are resemble inclusions in the Tibetan stones. These same features in Tibetan samples might indicate exposure to a thermal reaction underground before eruption of plagioclase-bearing magma.

EPMA chemical analyses indicated a composition range of  $(K_{0.03}Na_{0.46-0.49})_2Ca_{0.46-0.49}Al_{1.43-1.48}Si_{2.51-2.53}O_8$ , the equivalent ratios of albite: anorthite: orthoclase being  $Ab_{46.96-49.79}: An_{46.72-49.94}: Or_{3.03-3.50}$  which indicated andesine composition close to the andesine-labradorite border. The lattice parameters calculated from XRD measurements were  $a_0=8.161-8.193 \text{ \AA}$ ,  $b_0=12.849-12.919 \text{ \AA}$ ,  $c_0=7.105-7.126 \text{ \AA}$ ,  $\alpha=93.26^\circ-93.74^\circ$ ,  $\beta=116.27^\circ-116.38^\circ$ ,  $\gamma=89.93^\circ-90.16^\circ$ . Optical characterization by RI measurement ( $\alpha=1.550-1.551$ ,  $\beta=1.555-1.556$ ,  $\gamma=1.560-1.561$ ) correlated with andesine. LA-ICP-MS analysis indicated the presence of the trace elements, e.g., Li, Mg, K, Sc, Ti, Mn, Fe, Cu, Ga, Sr and Ba. An estimate of degree of structural ordering of Al in tetrahedral sites in Tibetan andesine was made by measuring the parameters  $\Delta=2\theta(1\bar{3}1)-2\theta(131)$  and  $\gamma$ , from the x-ray powder diffraction pattern. Both  $\Delta$  and  $\gamma$  values were plotted as a function of mole percent anorthite (An), and indicated that Tibetan andesine has a low degree of Al/Si ordering with only 22-29 percent of Al lying in the tetrahedral T1(O) site; this indicated that it formed at about 800°C in a volcanic

environment. By plot Ba/Sr versus Ba/Li ratios Tibetan red andesine can be differentiated from andesines of Inner Mongolia. The size of colloidal copper in red Tibetan andesine was smaller than 200 nm, as determined by microstructure observations using TEM.

Fontaine et al. (2010), using nanosecond laser ablation–inductively coupled plasma mass spectrometer (ICPMS), the major and trace compositions of andesines from different origins were determined. Mexican, Oregon, and Asian samples were clearly distinguishable by their major contents (e.g., CaO, SiO<sub>2</sub>, Na<sub>2</sub>O and K<sub>2</sub>O) whereas the compositions of Mongolian, Tibetan and DR Congo materials were within the same range. Since the Li concentration shown to be correlated with the Cu concentration, the formerly proposed differentiation by the Ba/Sr vs. Ba/Li ratio did not distinguish between samples from Tibet and Mongolia. Using femtosecond laser ablation multi-collector ICPMS in high-resolution mode, laboratory diffused samples showed variations up to 3% for <sup>65</sup>Cu/<sup>63</sup>Cu within one mineral due to the diffusion process. Ar isotope ratio measurements proved that heat treatment reduced the amount of radiogenic <sup>40</sup>Ar in the samples, significantly. Only low levels of radiogenic Ar were found in samples collected onsite in both mine locations in Tibet. Together with a high intra-sample variability of the Cu isotope ratio, andesine samples labeled as coming from Tibet were most probably Cu-diffused, using initially colorless Mongolian andesines as starting material. Therefore, in 2010, the only reliable source of colored andesine/labradorite remains in the state of Oregon.

According to Peretti (2011), natural copper andesines from Tibet can be confirmed that they underwent a natural diffusion process associated with hydrothermal fluids. The results of fluid inclusions analysis indicated that solutions contain copper and sulfur with low salinity. Silver concentrations were determined in a few inclusions but it diffused into the surface of copper-bearing andesine only. Copper and silver metals have been known from ore deposits of magmatic-hydrothermal origin. The fractionation was described as the first hydrous silicate magmas produced, followed by crystallization and then volatile rich fluids were separated from the magma. It has been shown in detail that magmatic brine-vapor separation could cause selective metal transport, chemical reactions and other physical processes leading to mineral precipitation. Different geological models might

be responsible for the partitioning between Cu and Ag (e.g., fluid mixing, fluid-rock reaction or vapor separation). However, this study, the fluid compositions found in Tibet andesine provide first indications for similar process.

## 2.5 Heat Treatment of Feldspar

Emmett and Douthit (2009) proved that copper could be easily diffused into the plagioclase feldspar. They conducted their experiments using a variety of andesine/labradorite feldspars. Twenty samples from different sources such as Mexico, Oregon and Mongolia. The diffusion experiment was important to stay below the solidus; they stayed safely below 1250°C. If a copper diffusion experiment was conducted in air the primary copper would be CuO. In the principle CuO could react with plagioclase feldspars to produce a liquid phase below the melting point of CuO at 1235°C and below the solidus of plagioclase. They chose a copper dopant concentration of 1% and a temperature range of 1000 – 1200°C. They embedded the test samples in a refractory oxide powder (ZrO<sub>2</sub>) and placed in alumina crucibles. All polished samples were heat for 160 hours. Three temperatures were used as 1170°C, 1100°C and 1000°C, all ran in air. The results showed that copper can diffuse very rapidly in some samples. In some cases, it appeared that the copper was diffused by bulk or lattice diffusion, and in the others clear pipe or short circuit diffusion was predominant.

Thirangoon (2009) studied 39 light yellow feldspar samples from Oregon, Mongolia and Mexico. The heating experiment was conducted at 1200 °C in air for 50 hours on an alumina felt in a furnace. Temperature of 1200 °C was below the solidus line at 50% anorthite and the 50 hours duration time was less than the time required for Cu diffusion. After heating, the sample appearance showed no apparent improvement. The samples became a little more yellowish and less transparent. Some of the samples from Plush, Oregon, exhibited red schiller cloud before the heating experiment. Mapping analysis using LA-ICP-MS method was performed in all samples to examine the distribution of Cu through the samples. Two unheated samples from Plush, Oregon showed red schiller cloud of Cu platelets. Chemical analysis revealed that Cu was more concentrated in the red cloud area. Before heating, Cu was concentrated only in the red cloud area. Outside the cloud, Cu was not detected. After heating, the red coloration disappeared but the cloud remained. The Cu

concentration in the cloud area decreased while Cu concentration in the area that previously did not contain Cu increased.

Silver incorporation in plagioclases was studied on a set of Inner Mongolian and Tibetan samples. The natural plagioclase material from the Inner Mongolian deposit showed a pale yellow color with various amounts of snowflake-like inclusions, fine particulate clouds, and some growth tubes. These materials were sliced into about 3–3.5 mm thick wafers. Two sets of samples of 10 pieces in each group were diffusion treated. Samples were packed in  $ZrO_2$  powder doped with 1% metallic silver and treated at 1170°C for 31 hours and 180 hours, respectively. To facilitate efficient diffusion, a treatment temperature near 90% of solidus temperature of the material was chosen. Silver distribution profiles in laboratory diffused Inner Mongolian samples and a set of silver-bearing Tibetan samples were analyzed by LA-ICP-MS. Diffusion properties and their implication to incorporation temperature and time scale in these materials were discussed. The results were observed that the distribution of silver concentration profiles in Tibetan and diffused materials from Inner Mongolian were similar. The calculated concentration curves represented the range of time and temperature conditions that could be reasonably produced in the nature or laboratory (Lu et al., 2011).

According to Rossman (2011), the minor potassium content of the feldspars consisted of  $^{40}K$  isotope that slowly decays to  $^{40}Ar$  over geologic time. As long as the feldspar remained in a magmatic system, the temperatures were so high, the radiogenic argon would quickly diffused out of the feldspar. When the crystal cools to near-ambient temperatures, the radiogenic argon would be retained within the crystal and its concentration will build over geologic time. Argon isotope studies of andesine samples returned from the 2010 expedition to Tibet showed that the tested andesines from Yu Lin Gu and Zha Lin contained high concentrations of radiogenic argon, their argon ratio ( $^{40}Ar/^{36}Ar$ ) were high. Additional experiment to test argon retention had been conducted by the laser-heating method. Heating the pale yellow andesine rough for two hours at 200°C, 400°C, 600°C, 800°C and 1000°C. The results showed that 1000°C heating did not extract all the radiogenic argon and indicated that they had not been subjected to a copper diffusion process. A sample previously heated by the laser used in the laser-extraction method was reheat; amount of argon released was much

smaller than the argon release during original heating. But the  $^{40}\text{Ar}/^{36}\text{Ar}$  ratio was much higher. The results show possibly that actual process for diffuse copper into andesine may occur at lower temperature than use in the experiments by Emmett and Douthit (2009).

## 2.6 Diffusion Mechanisms

According to Manning (1973), in practice, diffusion in solids occurs both by volume diffusion through regions of good crystal structure and by a variety of short-circuit diffusion mechanism where atoms move along paths of easy diffusion (See Figure 2.4) These easy diffusion paths usually involve surface or line defects in the crystal such as grain boundaries, dislocation lines or fast diffusion directions on free surfaces. Volume diffusion mechanisms usually depend on the presence of point defects in crystals, such as vacancies or interstitial atoms. According to atomic diffusion theory, the probability of a given possible atom jump actually occurring depends exponentially on the activation energy which must be gathered locally to allow the jump. Since atoms in regions of good crystal structure are more restricted and confined in their motions than atoms on free surfaces or on grain boundaries, diffusion along surfaces or boundaries can usually proceed much more rapidly than can volume diffusion. Therefore, if a diffusant was deposited on a surface and diffusion was allowed to occur, the diffusant normally would penetrate much farther into the crystal along the grain boundaries than through the regions of good crystal structure, where volume diffusion is necessary.

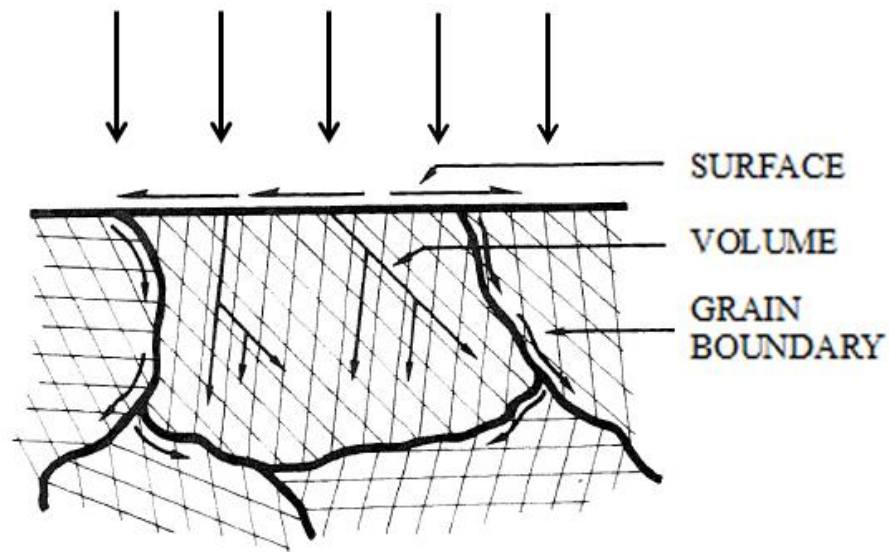


Figure 2.4 Paths for volume diffusion, grain boundary diffusion, and surface diffusion. Note that volume diffusion can provide many possible paths. This multitude of possible paths allows volume diffusion to be dominant at high temperatures despite the higher mobility expected along the individual short-circuit (surface and grain boundary) paths. If diffusion and reaction throughout a grain is desired, volume diffusion is required. Figure modified from (Manning, 1973).

According to Salameh (2011), the diffusion mechanisms were strongly correlated with defects in crystalline solids. Point defects such as vacancies or interstitials and other defect types like dislocations, grain boundaries, phase boundaries and free surfaces often mediated diffusion. Various atomic mechanisms of diffusion in crystals have been identified and are catalogued as follows:

### 2.6.1 Vacancy Mechanism

Vacancies are the most important form of thermally induced atomic defects in metals and ionic crystals. Diffusion by vacancy mechanism is very dominant in face centered cubic (FCC), body-centered cubic (BCC) and hexagonal closed packed (HCP) metals and solid solution alloys because the activation energy for this mechanism comprises the energy required to create a vacancy and that required to move it is relatively small in these structures (Murch, 1991).

This mechanism, one atom from the atoms surrounding the vacant site diffuses to it and creates a vacancy in their original position during diffusion (see Figure 2.5 (a)). This will produce random shifts of atoms from one lattice position to another as a result of atom jumping. Since the vacancies are thermally induced, the rate of diffusion increases rapidly with increasing temperature in this process.

### 2.6.2 Interstitial Mechanism

In the interstitial mechanism (see Figure 2.5 (b)), the atom diffuses by jumping from one interstitial site to one of its neighboring sites where the interstitial starts from an equilibrium position, reaches the saddle-point configuration and settles again on an adjacent interstitial site. When the jump is completed, no permanent displacement of the matrix atoms remains. In this mechanism, no defect is necessary to mediate interstitial jumps and therefore no defect formation energy contributes to the activation energy of diffusion. This mechanism is relevant for diffusion of small atoms such as H, C, N, and O in metals and other materials because small atoms fit in interstitial sites and they do not greatly displace the solvent atoms from their normal lattice sites. This diffusion is a thermally activated process, so the diffusion by interstitial mechanism increased by increasing temperature.

### 2.6.3 Exchange Mechanism

In the direct exchange mechanism (see Figure 2.5 (c)), two atoms move simultaneously and exchange their positions. In the most of the crystal structures this mechanism requires large distortions to squeeze the atoms through; this entails a high activation barrier and makes this process energetically unfavorable.



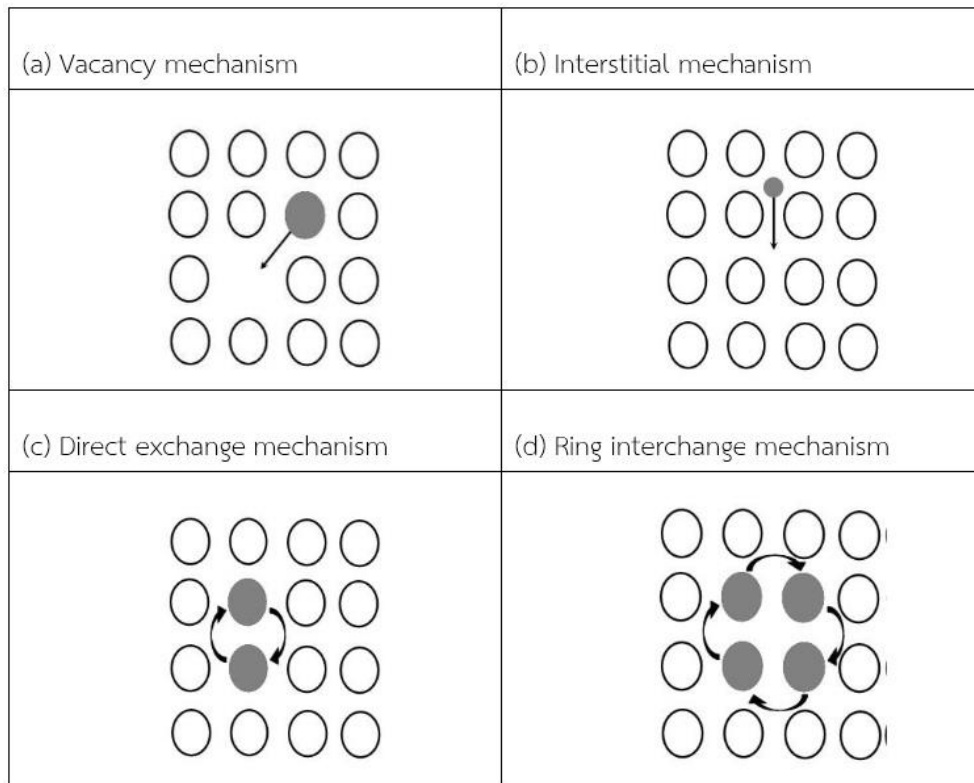


Figure 2.5 Schematic representation of the different diffusion mechanisms (a) Vacancy mechanism (b), Interstitial mechanism (c), Direct exchange mechanism and (d) Ring interchange mechanism (modified after Salameh, 2011)

According to Zener (1950), the ring mechanism see Figure 2.5 (d), three or more atoms rotate as a group by one atom distance. The required lattice distortions are not as great as in a direct exchange; therefore, the ring mechanism has lower activation energy but it requires more collective atomic motion which makes this more complicated mechanism unlikely for most crystalline substances.

#### 2.6.4 Definition About Diffusion

**Fick's First law** (IUPAC, 1999) : This law states the relationship between the flux vector  $J_i$  and the concentration gradient  $\nabla c_i$  of the diffusing species  $i$ :  $J_i = -D\nabla c_i$  where  $D$  is the diffusion coefficient or diffusivity. In three dimensions, this is a second-rank tensor. The dimension of  $D$  is  $\text{m}^2/\text{s}$ . For the concentration, the units can be chosen, the units for the flux depend on this choice, e.g., with  $c_i$  in  $\text{mol}/\text{m}^3$ ,  $J_i$  is expressed in  $\text{mol}/\text{m}^2/\text{s}$ . The flux, and therefore also the diffusion coefficient, has to be chosen relative to a *frame of reference*. For planar diffusion along the  $x$  direction the equation reduces to the scalar expression  $J_i = -D (\partial c_i / \partial x)$ .

**Fick's Second law** (IUPAC, 1999): This law states the relationship between the concentration gradient  $\nabla c_i$  of the species  $i$  and the rate of change of its concentration  $\partial c_i / \partial t$  caused by its diffusion at a given point in the system:  $\partial c_i / \partial t = \nabla(D\nabla c_i)$  where  $D$  is the diffusion coefficient or diffusivity. For planar diffusion along the  $x$  direction this equation reduces to :  $\partial c_i / \partial t = \partial / \partial x [D(c_i)(\partial c_i / \partial x)]$

When  $D$  is independent of concentration it takes the form  $\partial c_i / \partial t = D(\partial^2 c_i / \partial x^2)$

**Hetero diffusion** (IUPAC, 1999): The diffusion of foreign atoms in a material is called hetero diffusion (also called *impurity diffusion* or *solute diffusion*).

**Lattice diffusion** (IUPAC, 1999): A diffusion process which takes place through the bulk lattice of the crystal and excludes such mechanisms as short circuit diffusion along dislocations, grain boundary diffusion, and surface diffusion. Also called *bulk diffusion* or *volume diffusion*.

**Pipe diffusion** (IUPAC, 1999): Diffusion which takes place along a dislocation line.

**Short circuit diffusion** (IUPAC, 1999) : Any diffusion process occurring via grain boundaries, surfaces or dislocations. Short circuit diffusion mechanisms often cause diffusion in polycrystalline materials to proceed more quickly than in single crystals.

According to Poirier and Poirier (1985), vacancies were point defects and it was easily conceivable that they might migrate along the highly imperfect cores of linear or two-dimensional crystalline defects, more rapidly than in the bulk of the crystal. Indeed, there was good evidence that vacancies diffuse easily along dislocations (pipe diffusion) and grain boundaries (grain-boundary diffusion).

**Surface diffusion** (IUPAC, 1999): Diffusion takes place on a surface.

**Tracer diffusion** (IUPAC, 1999): Tracer diffusion refers to the migration of a tagged atom through a material of which it is a component.

**Tracer diffusion coefficient** (IUPAC, 1999): The diffusion coefficient  $D_i^*$  is defined by Fick's First law for an isotopic ally labeled atom. The term is usually restricted to the particular simple situation in which a tracer isotope in very dilute concentration is diffused into an otherwise homogeneous material with no driving forces other than the concentration gradient of the tracer itself.

In a homogeneous material, the mean square displacement  $\langle x_i^2 \rangle$  of the tracer  $i$  in the x-direction, as derived from the tracer concentration profile, is related to the tracer diffusion coefficient  $D_i^*$  by the Einstein formula for Brownian motion  $\langle x_i^2 \rangle = 2D_i^* t$  where  $t$  is the diffusion time. Often the tracer diffusion coefficient is not distinguished from the self-diffusion coefficient. This is only justified if diffusion is taken place by uncorrelated atom jumps. For interstitial diffusion of particles A in an elemental crystal A, this is the case, but for diffusion via a vacancy mechanism this does not hold. The tracer diffusion coefficient and self-diffusion coefficient are generally related by the correlation factor.

**Vacancy mechanism** (IUPAC, 1999): A mechanism where diffusion is made possible by the exchange of positions between the diffusing species and a vacancy.

According to Ruzeng et al. (2005), Fick's law is important in understanding the process of sapphire diffusion treatment. The diffusion coefficient of a coloring ion can reflect the diffusion ability of ions and diffusion velocity in general. The thickness of the diffusion layer at different temperatures and times using the diffusion coefficient were obtained also.

## CHAPTER 3

### PHYSICAL PROPERTIES AND INTERNAL FEATURES

#### 3.1 Introduction

The plagioclase feldspar samples used in this study were provided by Mr. Thanong Leelawatanasuk, Head of Gem Testing Laboratory, the Gem and Jewelry Institute of Thailand (Public Organization). He visited Tibetan andesine occurrences along with the international research team for sample collection and field observation in 2010. The natural red plagioclase samples were collected from Yu Lin Gu area and the copper-diffused red plagioclase samples were bought from a Chinese dealer who confirmed that these samples have been undertaken copper diffusion. He also declared that these samples are from the Inner Mongolia.

Eighteen samples were divided into two groups including thirteen natural plagioclases (twelve red stones and one very light yellow sample) and five copper-diffused plagioclases. All samples were then polished one side parallel to c crystal axis for determination of the general gemological and physical properties and subsequently analyzed by advanced instruments.

#### 3.2 Physical and Optical Properties

Plagioclase samples were collected using the basic gemological equipments. Colors of these plagioclase samples are mostly light red to red and one sample is light yellow. The refractive indices (RI) are 1.560 to 1.562 for  $n_{\gamma}$  and 1.550 to 1.555 for  $n_{\alpha}$ , birefringences range between 0.007 to 0.010. Specific gravity (SG) values measured using a hydrostatic balance are about 2.63 to 2.68 (see Tables 3.1 and 3.2). These properties fall within the general ranges of feldspar.

In addition, ultraviolet lamps; both short wave (SWUV) and long wave (LWUV), were used for observation of fluorescence of these plagioclase samples. Fluorescence of untreated and treated red samples are similarly inert to very weak red under SWUV and inert to weak pinkish orange under LWUV whereas fluorescence of the untreated very light yellow sample is weak pinkish orange under SWUV and inert

under LWUV. Pleochroism of all red plagioclase samples using dichroscope under daylight are reported in Tables 3.3 and 3.4.

The natural red plagioclases show pleochroism only from colorless to green whereas the red hue does not show pleochroism (see Figure 3.1 and Table 3.3), although their color appearances are red. However, natural red plagioclases possess uneven color as red, green and colorless. The obvious pleochroism color could not be observed in the treated red feldspars (mostly red to dark red). Both groups of red samples have colorless rim, but these colorless rim areas do not show pleochroism. In this study, pleochroism appears only in the inner area of the stones (see Table 3.3).

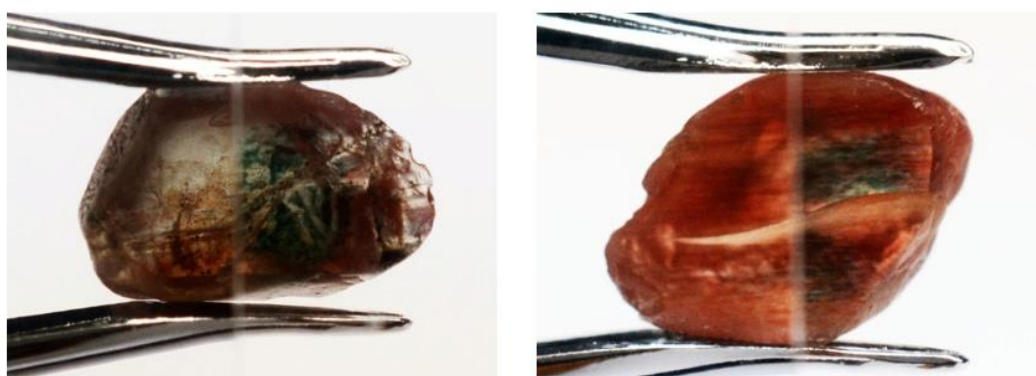


Figure 3.1 Distinct pleochroism of the natural red feldspar is clearly observed under London dichroscope (sample no. YD1 (left) and YLA3 (right)).

Table 3.1 Physical and optical properties of natural red plagioclase samples (YLA1-YLA3, YD1-YD2, YU1-YU7) and a very light yellow sample, IMA).






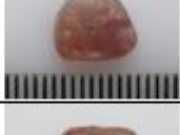


Sample name	Weight (ct)	SG	Ri	BF	Size (mm)	Photo
YLA1	1.44	2.68	1.562-1.555	0.007	9.87x7.03x3.69	
YLA2	3.21	2.68	1.560-1.552	0.008	9.83x6.86x6.61	
YLA3	2.04	2.67	1.561-1.553	0.008	9.96x6.99x5.30	
YD1	2.18	2.67	1.560-1.551	0.009	11.06x7.18x3.94	
YD2	2.75	2.66	1.560-1.552	0.008	10.36x6.93x6.45	
YU1	3.44	2.68	1.562-1.554	0.008	9.04x6.01x7.62	
YU2	2.26	2.67	1.561-1.553	0.008	8.64x6.78x4.40	
YU3	7.00	2.67	1.560-1.552	0.008	12.74x9.20x7.32	

Table 3.1 continued


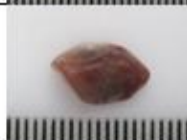



Sample name	Weight (ct)	SG	RI	BF	Size (mm)	Photo
YU4	3.70	2.66	1.561-1.552	0.009	14.65x10.30x4.46	
YU5	2.09	2.68	1.561-1.553	0.008	10.93x7.03x4.48	
YU6	2.17	2.67	1.561-1.553	0.008	10.36x7.83x4.87	
YU7	5.06	2.67	1.561-1.554	0.007	17.98x7.66x6.47	
IMA	19.1	2.67	1.560-1.553	0.007	24.01x11.60x8.72	

Table 3.2 Physical and optical properties of 5 Cu-diffused red plagioclase samples (TA0 - TA2 and DF1-DF2).



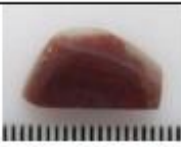


Sample name	Weight (ct)	SG	RI	BF	Size (mm)	Photo (scale in mm)
TA0	18.09	2.67	1.560-1.553	0.007	19.93x15.91x8.44	
TA1	7.23	2.67	1.561-1.553	0.008	11.89x10.86x7.76	
TA2	5.79	2.68	1.560-1.552	0.008	16.15x8.88x5.34	
DF1	1.58	2.63	1.560-1.550	0.010	8.53x7.05x6.43	
DF2	5.48	2.67	1.562-1.555	0.007	9.53x7.79x7.28	



Table 3.3 Pleochroism of 12 natural red plagioclases using dichroscope under daylight  
 (\*taken under the gem microscope with incandescent light using the polaroid and diffused plates).








Sample no.	Pleochroism (color)	Photo*
YD1	Strong/colorless to green (Focus on colorless area)	
YD2	Moderate/light green to green (Focus on colorless area)	
YLA1	Weak/colorless to light green (Focus on colorless area)	
YLA2	Weak/colorless to light green (Focus on colorless area)	
YLA3	Strong/colorless to green (Focus on colorless area)	
YU1	Weak/colorless to light green (Focus on colorless area)	
YU2	Weak/colorless to light green (Focus on colorless area)	

Table 3.3 continued

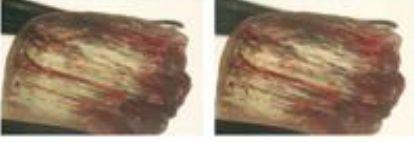
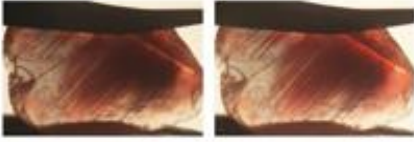
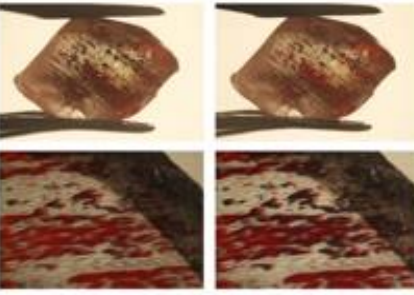

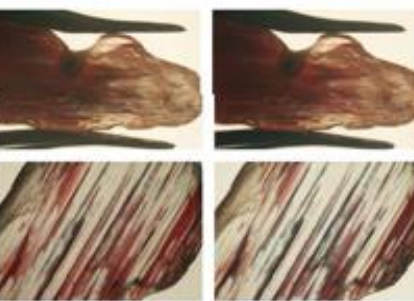


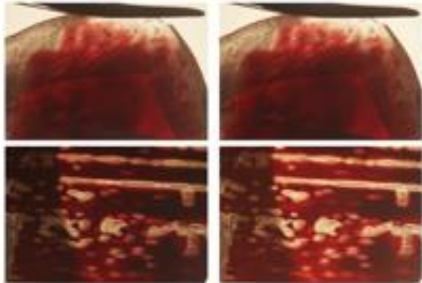

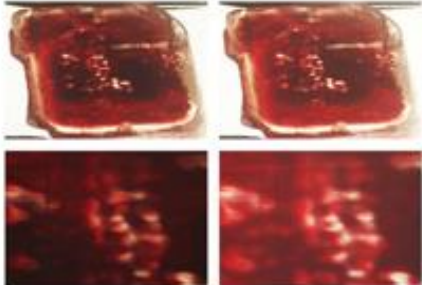
Sample no.	Pleochroism (color)	Photo*
YU3	Moderate/colorless to light green (Focus on colorless area)	
YU4	Weak/colorless to light green (Focus on colorless area)	
YU5	Moderate/colorless to green (Focus on colorless area)	
YU6	Weak/light green to green (Focus on colorless area)	
YU7	Moderate/colorless to green (Focus on colorless area)	

Table 3.4 Pleochroism of 5 Cu-diffused red plagioclases using dichroscope under daylight (\*taken under the gem microscope with incandescent light using the polaroid and diffused plates).

Sample no.	Pleochroism (color)*	Photo
TA0	Moderate/grayish red to red	
TA1	Very weak/grayish red to red	
TA2	None	
DF1	None	
DF2	Weak/colorless to green (Focus on colorless area)	

### 3.3 Internal Characteristic

Internal features were investigated and their photos were taken under a gem microscope. Some crucial internal features (as shown in Figures 4 and 5) include oriented tubes, fingerprints, irregular tubes, colorless rim, colorless zone around fingerprint or fracture, mottled colors (red and green), milky cloud along red zone, glistering cloud along red zone and red color layer from rim towards core. Although, internal features in natural and treated stones are quite similar, the red color layers from rim towards core were not found in the natural feldspar samples whereas mottled color (red and green) and glistering cloud along red zone were not found in the treated feldspar samples. Summary of internal characteristics found in untreated and treated red feldspar samples are presented in Table 3.5.

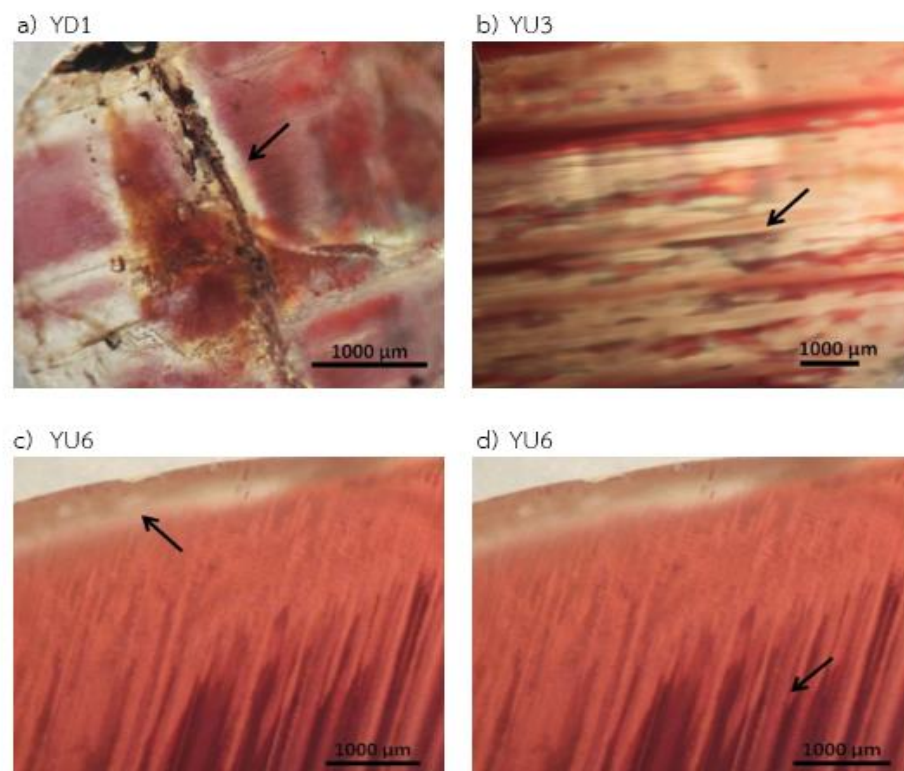


Figure 3.2 Representative internal features of untreated feldspar samples including (a) colorless zone around fingerprint (YD1), (b) mottled color (red and green) along tubes and twinning (YU3), (c) colorless rim and (d) oriented coarse red tubes with glistering (YU6).

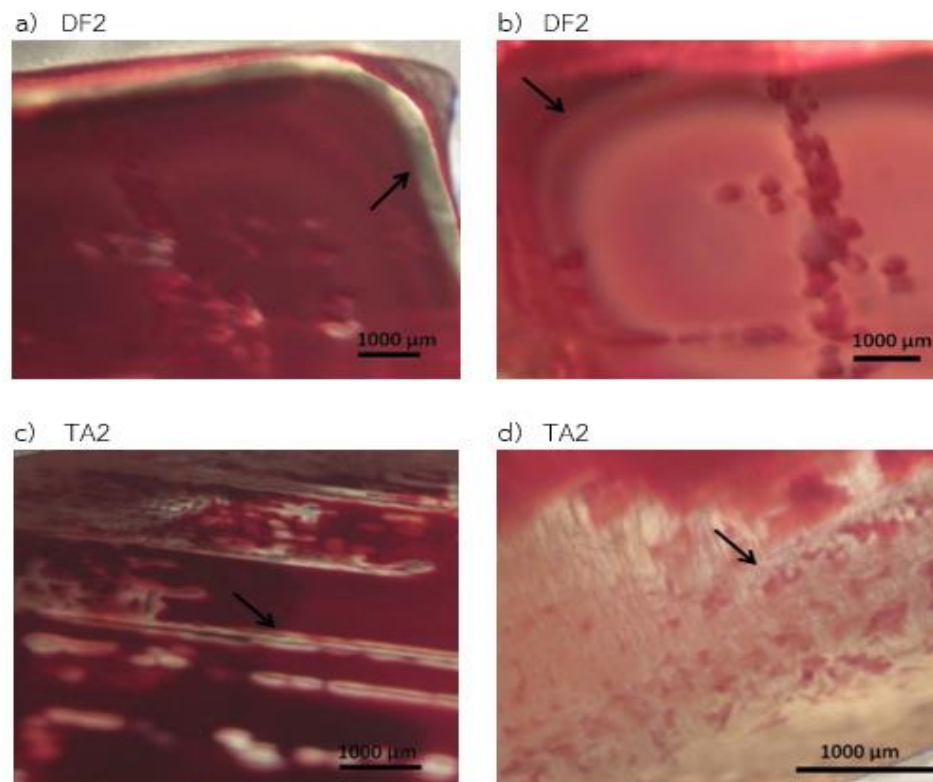


Figure 3.3 Representative internal features of treated feldspar samples show (a) colorless rim, (b) circular of milky red cloud from core to rim (DF2), (c) colorless zone around irregular and (d) straight red tubes (TA2).

All internal characteristics found in natural and treated red plagioclase samples are summarized in Table 3.5. Several internal features were recognized in both groups of plagioclase samples; they are oriented tubes, irregular tubes, colorless rim, colorless zones around tubes and fingerprints or fractures, mottled or uneven colors of red and green, milky cloud along red zone. Some untreated samples showed glistering cloud, which was not found in treated samples. On the other hand, red layers from rim towards inner core were found only in the treated samples.

Table 3.5 Summary of internal characteristics found in natural and treated red plagioclase samples.

Internal characteristic of plagioclase feldspar	Untreated	Treated
1. Oriented tubes	✓	✓
2. Irregular tubes	✓	✓
3. Colorless zone from surface (rim)	✓	✓
4. Colorless zone around red tubes	✓	✓
5. Colorless zone around fingerprint or fracture	✓	✓
6. Mottled color (red and green)	✓	✓
7. Milky cloud along red zone	✓	✓
8. Glistering cloud along red zone	✓	-
9. Red color layer from rim towards inner core	-	✓



## CHAPTER 4

### ANALYTICAL RESULTS

#### 4.1 Introduction

This research focuses on mechanism and cause of red coloring in gem plagioclase feldspar. Therefore, the advanced analytical techniques are expected to be the most important tools to differentiate natural red plagioclase from copper-diffused plagioclase. UV-VIS-NIR spectrophotometer, Electron Probe Micro-Analyzer (EPMA) and Laser Ablation-Inductivity Coupled Plasma-Mass Spectrometer (LA-ICP-MS) were mainly used for this study. Moreover, Laser Raman spectroscopy, Fourier Transform Infra-Red (FTIR) spectrophotometer and Energy Dispersive X-ray Fluorescence Spectrometer (EDXRF) were additionally engaged to investigate the nature and specific features of samples.

#### 4.2 UV-VIS-NIR Spectrophotometric Results

An UV-VIS-NIR spectrophotometer, Model Lambda 950 series, Perkin Elmer was engaged for investigation within the wavelength of 300 to 800 nm (UV-Visible region). Since, all plagioclase samples are in the triclinic system, it is difficult to find their optic axis. To set sample for using with this instrument, the polarized spectra of each sample oriented in the position which show maximum pleochroism under dichroscope observation. These results cannot be defined to exact spectra are gamma, alpha or beta. Therefore, in this study, two directions of polarized spectra when the filter was perpendicular at 0 and 90 degree called '0p' and '90p', respectively.

UV-Vis spectrum of natural red plagioclase samples show range of distinct absorption band at about 568 to 599 nm (0p) and at 573 to 595 nm (90p) (see Appendix A). Two samples (YLA3 and YD1 see Figures 4.1 and 4.2) that have strong pleochroism (colorless to green) show more obvious different absorption than those of the samples with weak to moderate pleochroism. The UV-Vis spectra of treated red plagioclases (copper-diffused feldspar) show distinct range of absorption band at 568 to 597 nm (0p) and at 568 to 579 nm (90p) (see Appendix A). The absorption patterns of samples in both 0p and 90p are quite similar as the treated red feldspar sample (TA0 see Figure

4.3). The copper-diffused feldspars show similar distinct absorption band at about 570 to 590 nm; these were also recognized in natural red feldspar samples.

The natural plagioclase (IMA) with very light yellow shows the absorption peaks at 382, 420 and 449 nm (see Figure 4.4). Bands near 380, 420, and 450 nm may be due to  $\text{Fe}^{3+}$  in tetrahedral sites as suggested by Hofmeister and Rossman (1985). This sample has no pleochroism, no different in hue color. Therefore, it was investigated only one direction for polarized spectrum.

The results of polarized spectra in range near 560 nm should be the absorption of red color caused by  $\text{Cu}^0$  (Hofmeister and Rossman, 1985), and the spectra that shift to right as 590 nm should be the absorption of green color. According to Hofmeister and Rossman (1985), a board polarized band at 670 nm produced the absorption minimum in green.

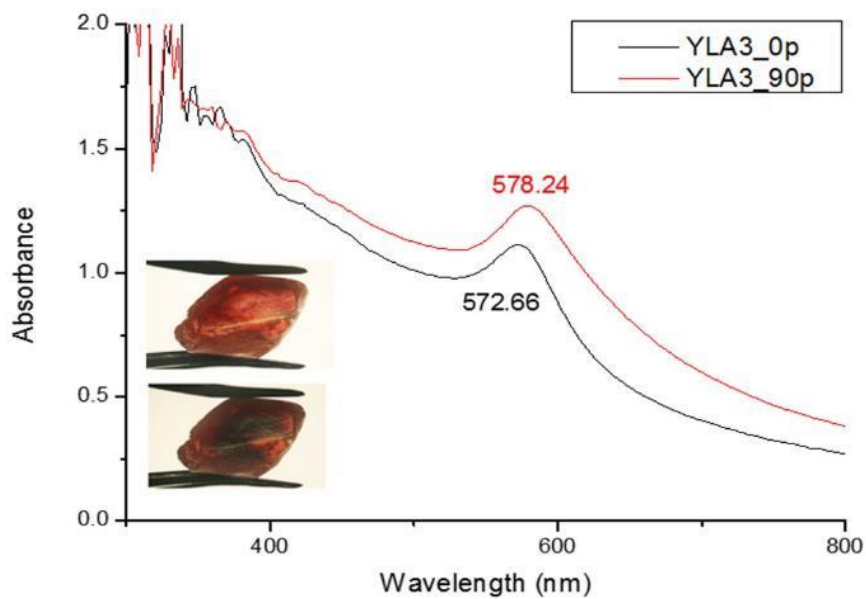


Figure 4.1 UV-Vis spectra of untreated red plagioclase (sample no. YLA3) show the polarized absorption bands at about 573 nm (0p) and at 578 nm (90p).



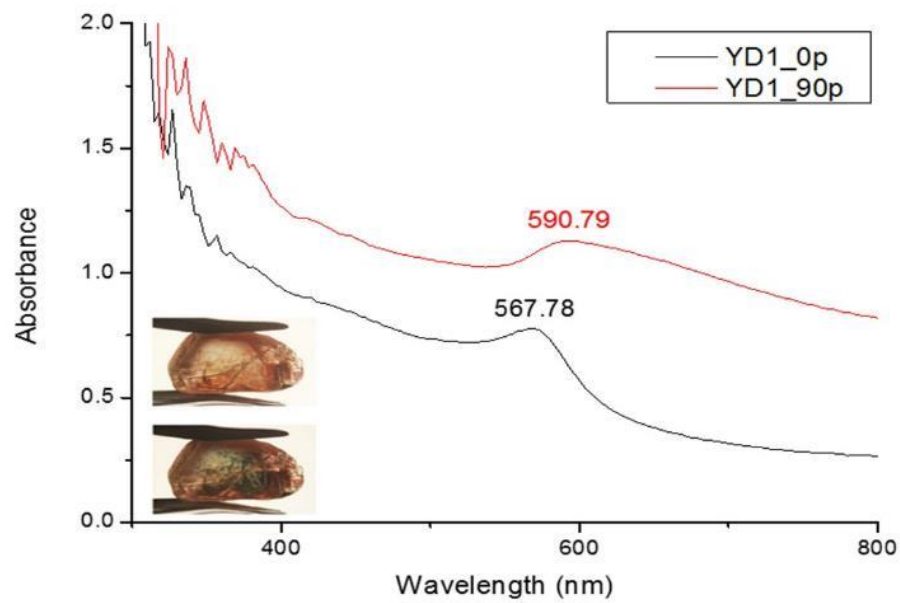


Figure 4.2 UV-Vis spectra of untreated red plagioclase (sample no. YD1) show the distinct polarized absorption bands at about 568 nm (0p) and 591 nm (90p).

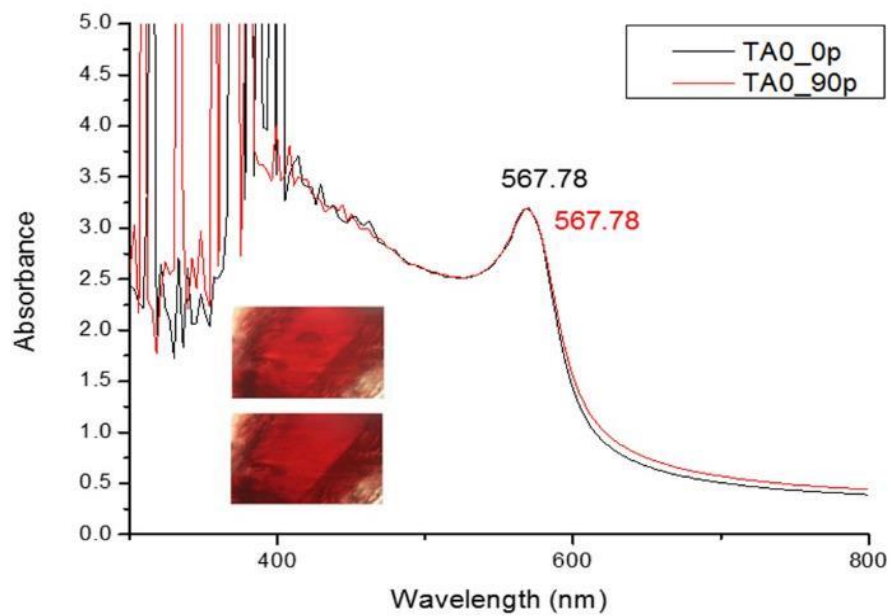


Figure 4.3 UV-Vis spectra of treated red plagioclase (sample no. TA0) show the polarized distinct absorption peaks at about 568 nm (both in 0p and 90p).

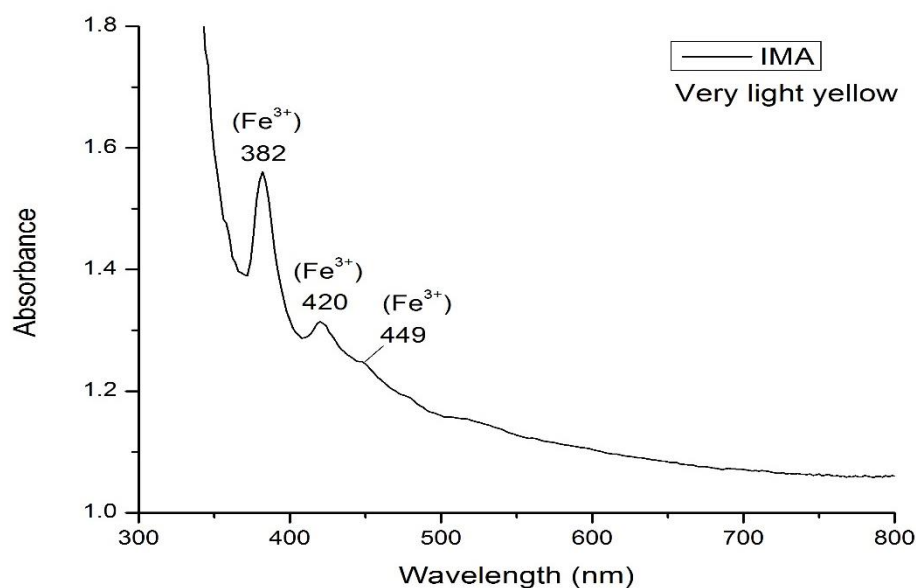


Figure 4.4 UV-Vis spectra of untreated very light yellow plagioclase (sample no. IMA) shows the polarized absorption peaks at 382, 420 and 449 nm.

### 4.3 Laser Raman Spectroscopic Results

Raman spectroscopy was set at the scanning range of 250–2000  $\text{cm}^{-1}$ . All the results are collected in Appendix B. The representative samples including natural red plagioclase (sample no. YD2), copper-diffused red plagioclase (sample no. TA1) and natural very light yellow plagioclase (sample no. IMA) contain many peaks at about 281, 406, 482, 509, 564 and 792  $\text{cm}^{-1}$  (see Figures 4.5 - 4.7). However, all spectra, in general, show similar Raman shift pattern of feldspar reference database as reported by Freeman et al. (2003). Raman spectrum databases of plagioclase feldspar from the RRUFF Project website contain abelite, oligoclase, andesine, labradorite, bytownite and anorthite, respectively. (see Figures 4.8 - 4.13)

All plagioclase samples show range of Raman shift peaks series at 281, 406, 482, 509, 564 and 792  $\text{cm}^{-1}$  are comparable to the pattern of andesine-labradorite of the RRUFF database.

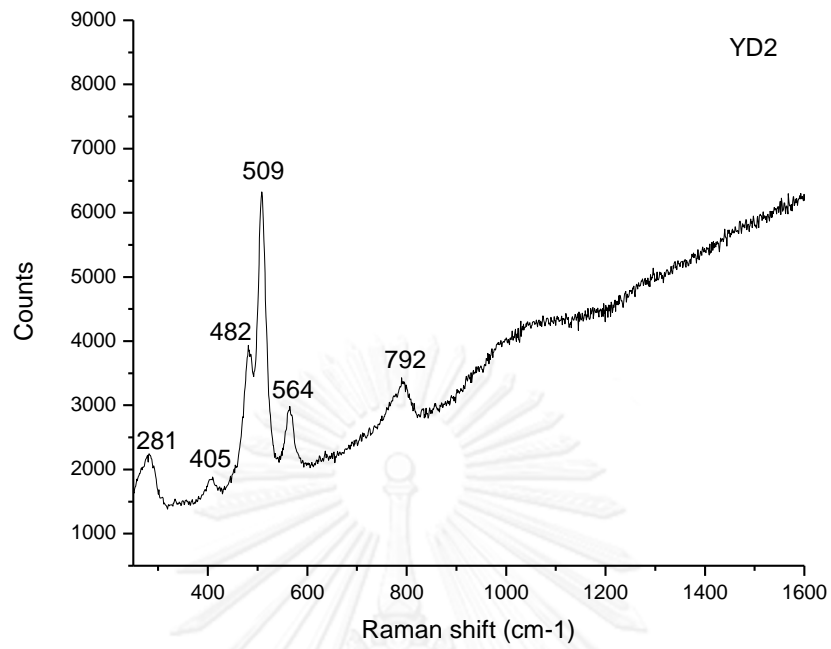


Figure 4.5 RAMAN spectrum of natural red plagioclase (sample no. YD2) shows Raman shift peaks at 281, 405, 482, 509, 564 and 792  $\text{cm}^{-1}$ .

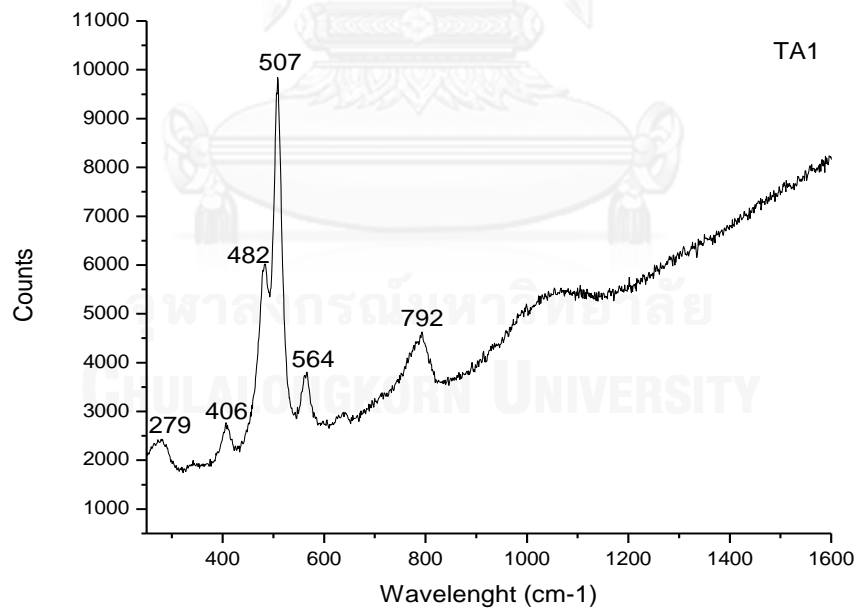


Figure 4.6 RAMAN spectrum of treated red plagioclase (sample no. TA1) show Raman shift peaks at 279, 406, 482, 507, 564 and 792  $\text{cm}^{-1}$ .

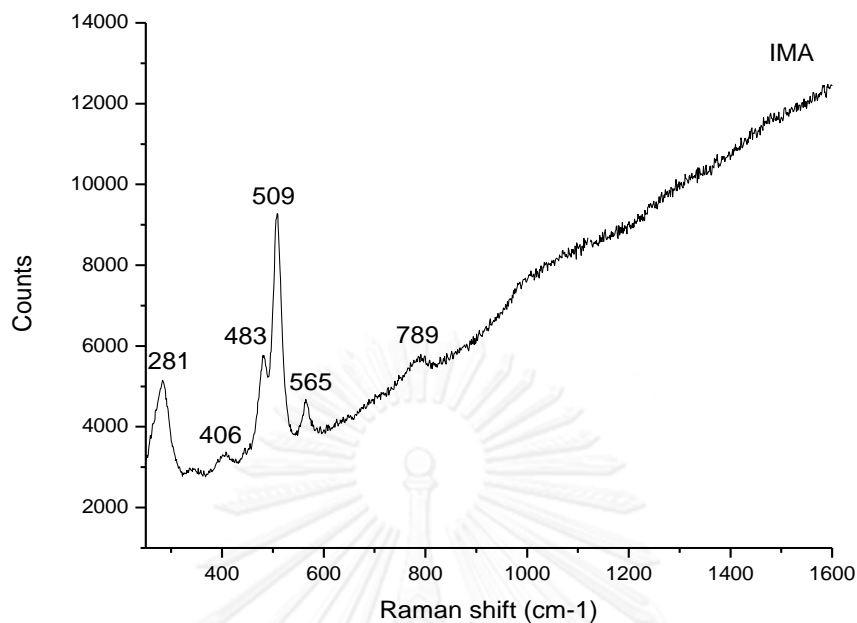


Figure 4.7 RAMAN spectrum of untreated very light yellow plagioclase (sample no. IMA) shows Raman shift peaks at 281, 406, 483, 509, 565 and 789  $\text{cm}^{-1}$ .

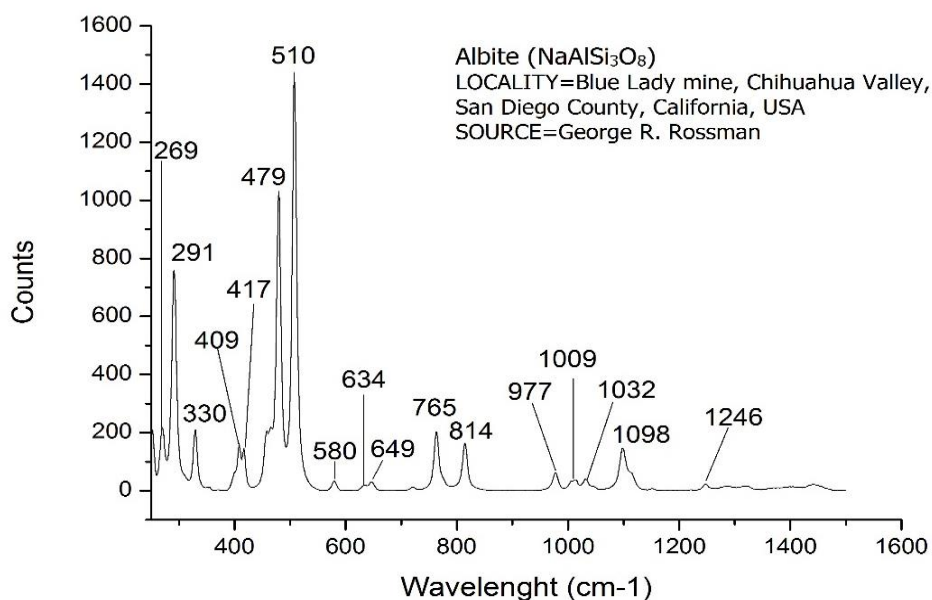


Figure 4.8 Raman spectrum databases of albite from the RRUFF Project website (<http://rruff.info/albite/display=default/X050005>) (RRUFF)

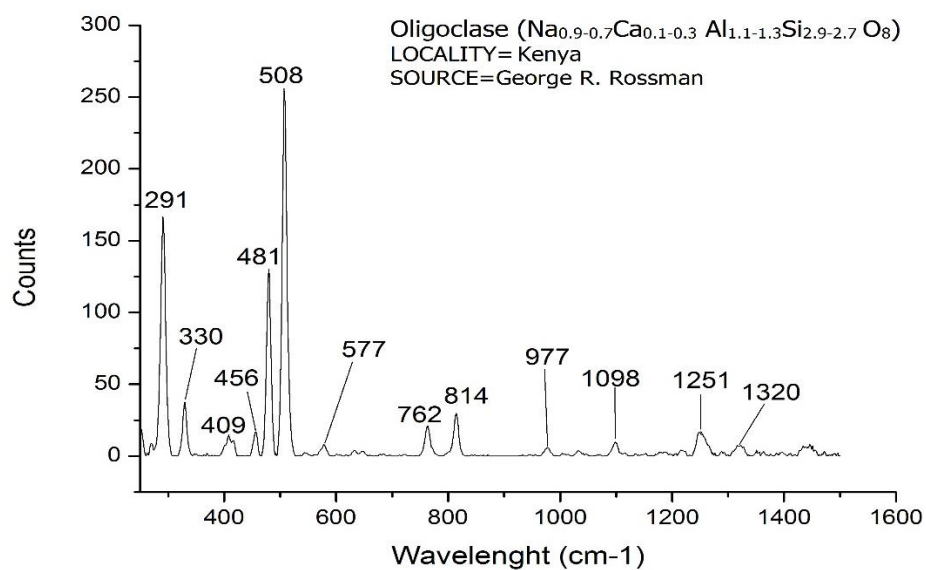


Figure 4.9 Raman spectrum databases of oligoclase from the RRUFF Project website (<http://rruff.info/oligoclase/display=default/X050122>) (RRUFF)

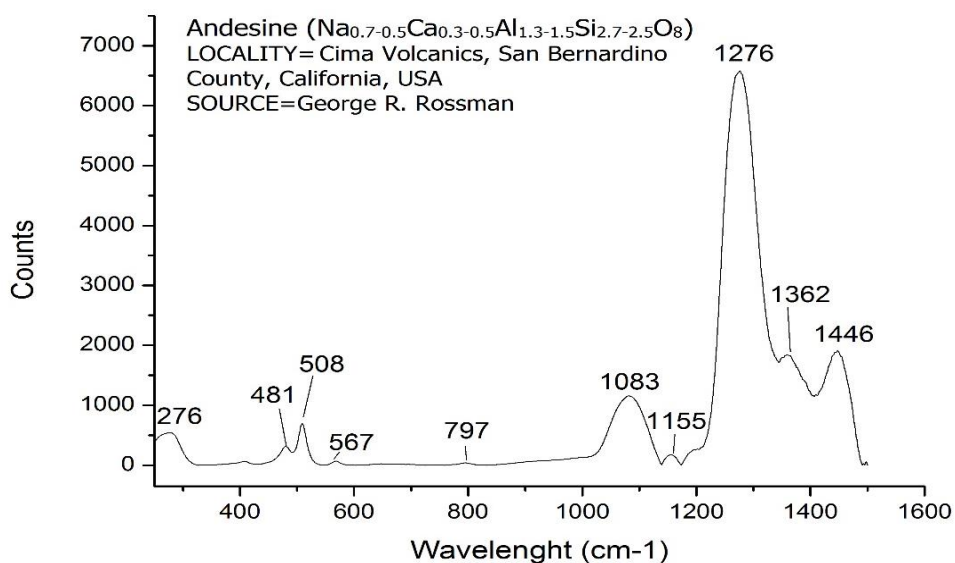


Figure 4.10 Raman spectrum databases of andesine from the RRUFF Project website (<http://rruff.info/andesine/display=default/X050013>) (RRUFF)

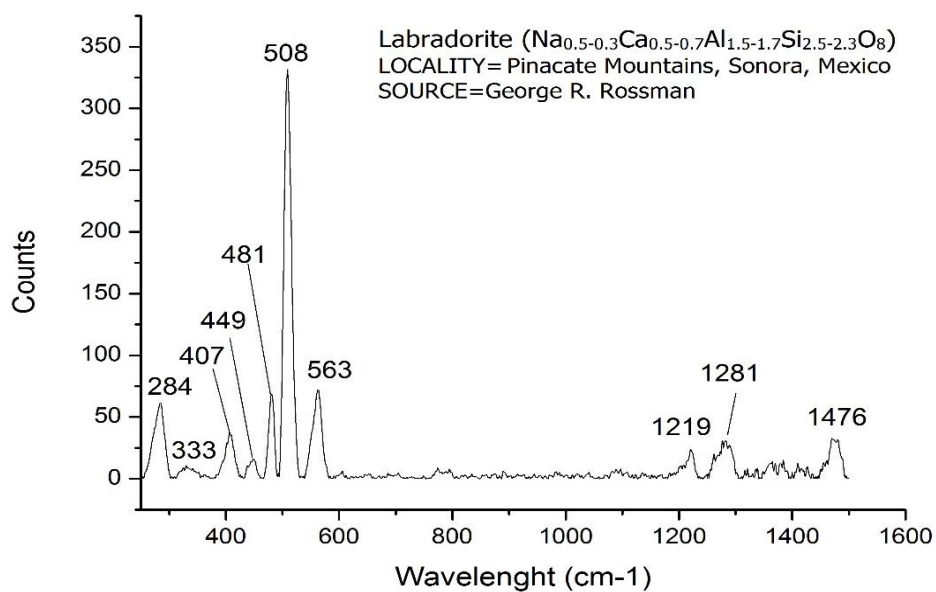


Figure 4.11 Raman spectrum databases of labradorite from the RRUFF Project website (<http://rruff.info/labradorite/display=default/X050108>) (RRUFF)

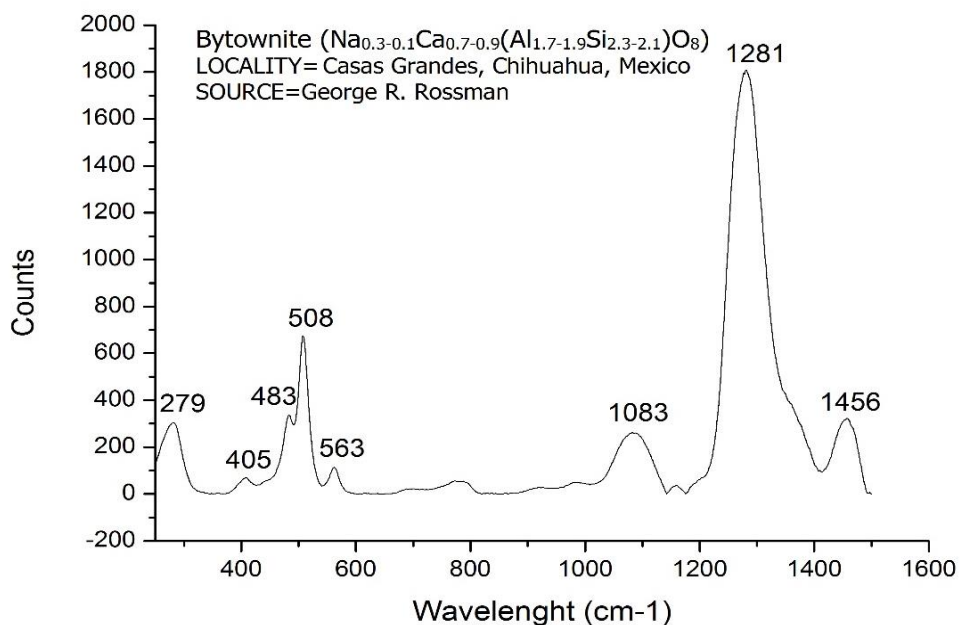


Figure 4.12 Raman spectrum databases of bytownite from the RRUFF Project website (<http://rruff.info/bytownite/display=default/X050033>) (RRUFF)

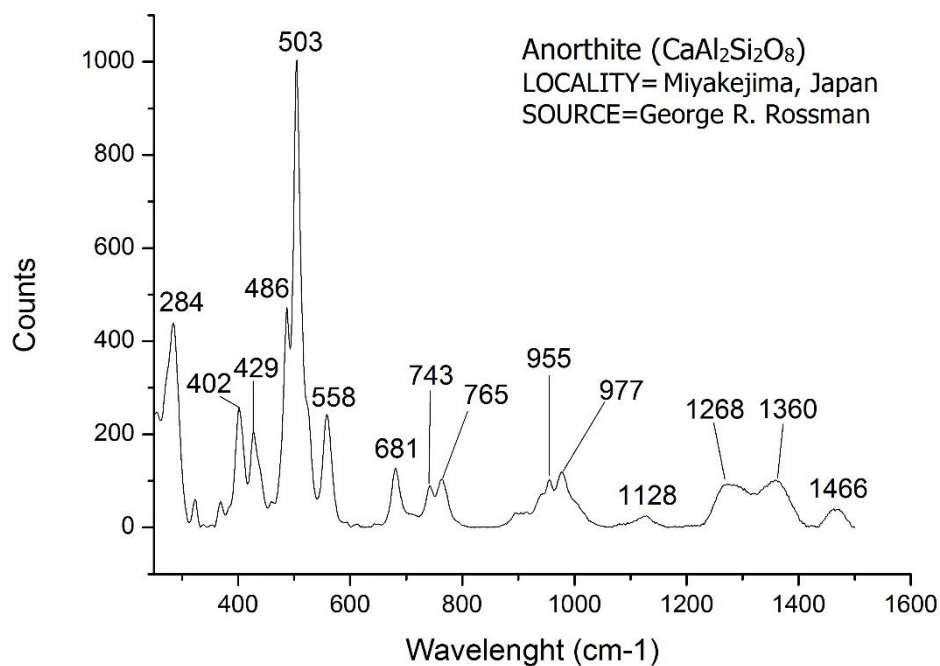


Figure 4.13 Raman spectrum databases of anorthite from the RRUFF Project website (<http://rruff.info/anorthite/display=default/X050021>) (RRUFF)

#### 4.4 Fourier Transform Infra-Red (FTIR) Spectrophotometric Results

For Infrared Spectroscopy, all spectra gained from plagioclase samples were scanned within in range of 4000 to 2000  $\text{cm}^{-1}$  and collected in Appendix C. According to Stuart (2004) about the infrared spectroscopy region, representative FTIR spectra of natural red plagioclase (sample no. YLA2), copper-diffused plagioclase (sample no. DF2) and natural very light yellow plagioclase (sample no. IMA) are shown in Figures 4.14 - 4.16, respectively. They show consistency of two main absorption bands caused by OH- or  $\text{H}_2\text{O}$  at about 3900 to 3400  $\text{cm}^{-1}$  and C-H stretching at 2960 to 2849  $\text{cm}^{-1}$ .

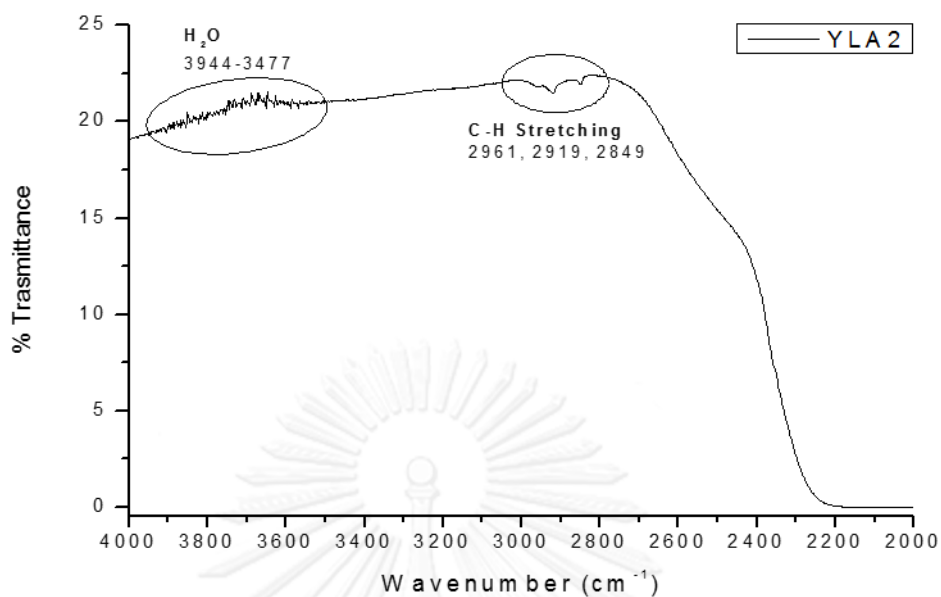


Figure 4.14 FTIR spectrum of natural red plagioclase (sample no. YLA2) shows absorptions related to OH or H<sub>2</sub>O group at the range 3944-3477 cm<sup>-1</sup> and C-H stretching at 2961, 2919 and 2849 cm<sup>-1</sup>.

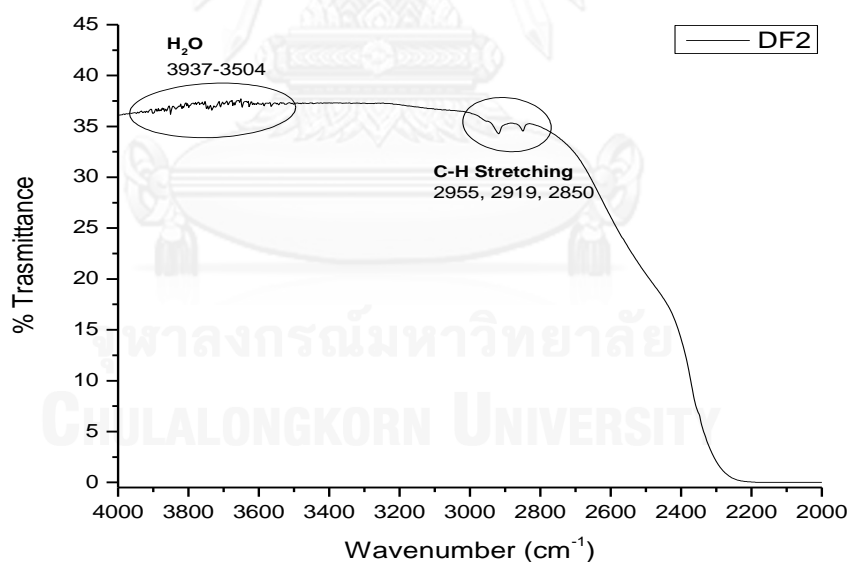


Figure 4.15 FTIR spectrum of treated red plagioclase (sample no. DF2) shows absorptions related to OH or H<sub>2</sub>O group at the range 3937-3504 cm<sup>-1</sup> and C-H stretching at 2955, 2919 and 2850 cm<sup>-1</sup>.



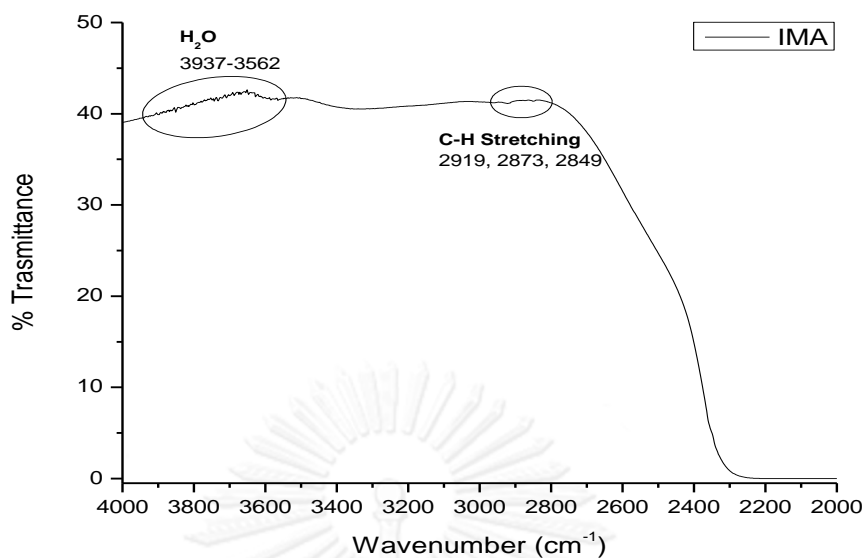


Figure 4.16 FTIR spectrum of untreated very light yellow plagioclase (sample no. IMA) shows absorptions related to OH or H<sub>2</sub>O group at the range 3937-3562 cm<sup>-1</sup> and C-H stretching at 2919, 2873 and 2849 cm<sup>-1</sup>.

#### 4.5 Energy Dispersive X-ray Fluorescence Spectrometric (EDXRF) Results

Major and trace elements of 18 feldspar samples were analyzed and reported as wt% oxides, i.e., SiO<sub>2</sub>, TiO<sub>2</sub>, Al<sub>2</sub>O<sub>3</sub>, Fe<sub>2</sub>O<sub>3</sub>, K<sub>2</sub>O, Na<sub>2</sub>O, CaO, CuO and SrO. All of the analytical results are listed in Appendix D. Each sample was collected for 2 to 26 analytical points, based on variety of color observed on the sample surfaces. These data are summarized as ranges of minimum and maximum, average and standard deviation as shown in Table 4.1. These semi-qualitative EDXRF analyses with standardless calibration are automatically normalized to 100%.

Table 4.1 EDXRF analyses of feldspar samples presenting as minimum-maximum ranges, averages and standard deviations

Group of samples	Spots	Oxides	Min. – Max. (wt%)	Mean (wt%)	S.D. (wt%)
Natural red plagioclase (12 samples)	26	SiO <sub>2</sub>	61.83 - 63.26	62.62	0.41
		TiO <sub>2</sub>	0.04 - 0.08	0.06	0.01
		Al <sub>2</sub> O <sub>3</sub>	26.14 - 26.81	26.52	0.19
		Fe <sub>2</sub> O <sub>3</sub>	0.35 - 0.39	0.37	0.01
		K <sub>2</sub> O	0.27 - 0.35	0.31	0.02
		Na <sub>2</sub> O	4.14 - 2.15	2.93	0.55
		CaO	6.48 - 7.03	6.74	0.14
		CuO	0.06 - 0.18	0.10	0.03
		SrO	0.31 - 0.36	0.34	0.01
Natural very light yellow plagioclase (1 sample)	2	SiO <sub>2</sub>	62.64 - 62.74	62.69	0.07
		TiO <sub>2</sub>	0.05 - 0.06	0.06	0.01
		Al <sub>2</sub> O <sub>3</sub>	26.59 - 26.61	26.60	0.02
		Fe <sub>2</sub> O <sub>3</sub>	0.37 - 0.39	0.38	0.01
		K <sub>2</sub> O	0.29 - 0.29	0.29	0.00
		Na <sub>2</sub> O	2.60 - 2.74	2.67	0.10
		CaO	6.96 - 6.99	6.97	0.02
		CuO	0.01 - 0.01	0.01	0.00
		SrO	0.33-0.34	0.33	0.01

Table 4.1 continued

Group of samples	Spots	Oxides	Min. – Max. (wt%)	Mean (wt%)	S.D. (wt%)
Copper-diffused red plagioclase (5 samples)	18	SiO <sub>2</sub>	59.19 - 63.41	62.15	1.02
		TiO <sub>2</sub>	0.04 - 0.11	0.06	0.02
		Al <sub>2</sub> O <sub>3</sub>	26.25 - 28.20	26.89	0.54
		Fe <sub>2</sub> O <sub>3</sub>	0.32 - 0.40	0.35	0.03
		K <sub>2</sub> O	0.27 - 0.34	0.31	0.02
		Na <sub>2</sub> O	2.16 - 5.05	3.06	0.88
		CaO	6.33 - 7.28	6.76	0.28
		CuO	0.07 - 0.10	0.08	0.01
		SrO	0.31 - 0.39	0.34	0.02

Twelve natural red samples (26 analytical spots): SiO<sub>2</sub> varies from about 61.83 to 63.26 wt% with an average of  $62.62 \pm 0.41$  wt% , TiO<sub>2</sub> varies from about 0.04 to 0.08 wt% with an average of  $0.06 \pm 0.01$  wt% , Al<sub>2</sub>O<sub>3</sub> varies from about 26.14 to 26.81 wt% with an average of  $26.52 \pm 0.19$  wt% , Fe<sub>2</sub>O<sub>3</sub> varies from about 0.35 to 0.39 wt% with an average of  $0.37 \pm 0.01$  wt% , K<sub>2</sub>O varies from about 0.27 to 0.35 wt% with an average of  $0.31 \pm 0.02$  wt% , Na<sub>2</sub>O varies from about 4.14 to 2.15 wt% with an average of  $2.93 \pm 0.55$  wt% , CaO varies from about 6.48 to 7.03 wt% with an average of  $6.74 \pm 0.14$  wt% , CuO varies from about 0.06 to 0.18 wt% with an average of  $0.10 \pm 0.03$  wt% and SrO varies from about 0.31 to 0.36 wt% with an average of  $0.34 \pm 0.01$  wt%.

Natural very light yellow sample (2 analytical spots): SiO<sub>2</sub> varies from about 62.64 to 62.74 wt% with an average of  $62.69 \pm 0.07$  wt% , TiO<sub>2</sub> hardly varies from about 0.05 to 0.06 wt% with an average of  $0.06 \pm 0.01$  wt% , Al<sub>2</sub>O<sub>3</sub> hardly varies from about 26.59 to 26.61 wt% with an average of  $26.60 \pm 0.02$  wt% , Fe<sub>2</sub>O<sub>3</sub> hardly varies from about 0.37 to 0.39 wt% with an average of  $0.38 \pm 0.01$  wt% , K<sub>2</sub>O has 0.29 wt% (not varies) , Na<sub>2</sub>O varies from about 2.60 to 2.74 wt% with an average of  $2.67 \pm 0.10$  wt% , CaO varies from about 6.96 to 6.99 wt% with an average of  $6.97 \pm 0.02$  wt% , CuO has 0.01 wt% (not varies) and SrO hardly varies from about 0.33 to 0.34 wt% with an average of  $0.33 \pm 0.01$  wt% oxides.

Five copper-diffused or treated red samples (18 analytical spots): SiO<sub>2</sub> varies from about 59.19 to 63.41 wt% with an average of 62.15 ± 1.02 wt%, TiO<sub>2</sub> varies from about 0.04 to 0.11 wt% with an average 0.06 of ± 0.02 wt% , Al<sub>2</sub>O<sub>3</sub> varies from about 26.25 to 28.20 wt% with an average of 26.89 ± 0.54 wt% , Fe<sub>2</sub>O<sub>3</sub> varies from about 0.32 to 0.40 wt% with an average of 0.35 ± 0.03 wt% , K<sub>2</sub>O varies from about 0.27 to 0.34 wt% with an average of 0.31 ± 1.02 wt% , Na<sub>2</sub>O varies from about 2.16 to 5.05 wt% with an average of 3.06 ± 0.88 wt%, CaO varies from about 6.33 to 7.28 wt% with an average of 6.76 ± 0.28 wt%, CuO varies from about 0.07 to 0.10 wt% with an average of 0.08 ± 0.01 wt% and SrO varies from about 0.31 to 0.39 wt% with an average of 0.34 ± 0.02 wt%.

As the results, all three samples have compositions of plagioclase feldspar. Although they show the same ranges of main composition, trace elements particularly copper, cause of red color in feldspar (Hofmeister and Rossman, 1985), can be detected with high uncertainty. These semi-qualitative EDXRF analyses with standardless calibration are unlikely appropriate for detailed study in the cause of red coloring in feldspar. Electron Probe Micro-Analysis (EPMA) and Laser Ablation Inductivity-Coupled Plasma-Mass Spectrometry (LA-ICP-MS) would yield more accuracy of trace analyses. They were used for quantitative analyses of these feldspar samples.

#### **4.6 Electron Probe Micro – Analytical (EPMA) Results**

Minerals chemical analyses using EPMA of eighteen samples including 12 natural red samples (sample nos. YLA1-YLA3, YD1-YD2 and YU1-YU7), very light yellow plagioclase feldspar (sample no. IMA) and 5 treated red samples (sample nos. TA0, TA1-TA2 and DF1-DF2) were carried out. Representative EPMA analyses are summarized in Table 4.2 and more analyses are listed in Appendix E.

Natural red samples (12 samples): yield averages of 57% SiO<sub>2</sub>, 27% Al<sub>2</sub>O<sub>3</sub>, 10% CaO and 5% NaO<sub>2</sub> with trace amounts of about 0.07% TiO<sub>2</sub>, 0.4%wt FeO, 0.5% K<sub>2</sub>O, 0.07% CuO and ≤0.01% SrO.

Natural very light yellow sample: contains approximately 58% SiO<sub>2</sub>, 27% Al<sub>2</sub>O<sub>3</sub>, 10% CaO and 5% NaO<sub>2</sub> with trace amounts of about 0.03% TiO<sub>2</sub>, 0.4% FeO, 0.5% K<sub>2</sub>O and 0.02% CuO.

Copper-diffused or treated red samples (5 samples): yield averages of 56% SiO<sub>2</sub>, 27% Al<sub>2</sub>O<sub>3</sub>, 10% CaO and 5% NaO<sub>2</sub> with trace amounts of 0.05% TiO<sub>2</sub>, 0.3% FeO, 0.5% K<sub>2</sub>O and 0.06% CuO.

In summary, chemical compositions of all samples have similar ranges approximately 56-58% SiO<sub>2</sub>, 27% Al<sub>2</sub>O<sub>3</sub>, 10% CaO and 5% NaO<sub>2</sub> with trace amounts of TiO<sub>2</sub>, FeO, K<sub>2</sub>O, CuO and SrO.

Based on 8 Oxygen (O), recalculated chemical formula of these feldspars vary in atomic proportions of K<sub>3-5</sub>, Na<sub>44-50</sub> and Ca<sub>48-51</sub>. Ternary atomic plots of Ca-Na-K ratios (Figure 4.17) show intermediate calcium content (48-51%, An<sub>48-51</sub>). All samples are in the same compositional range of andesine-labradorite.

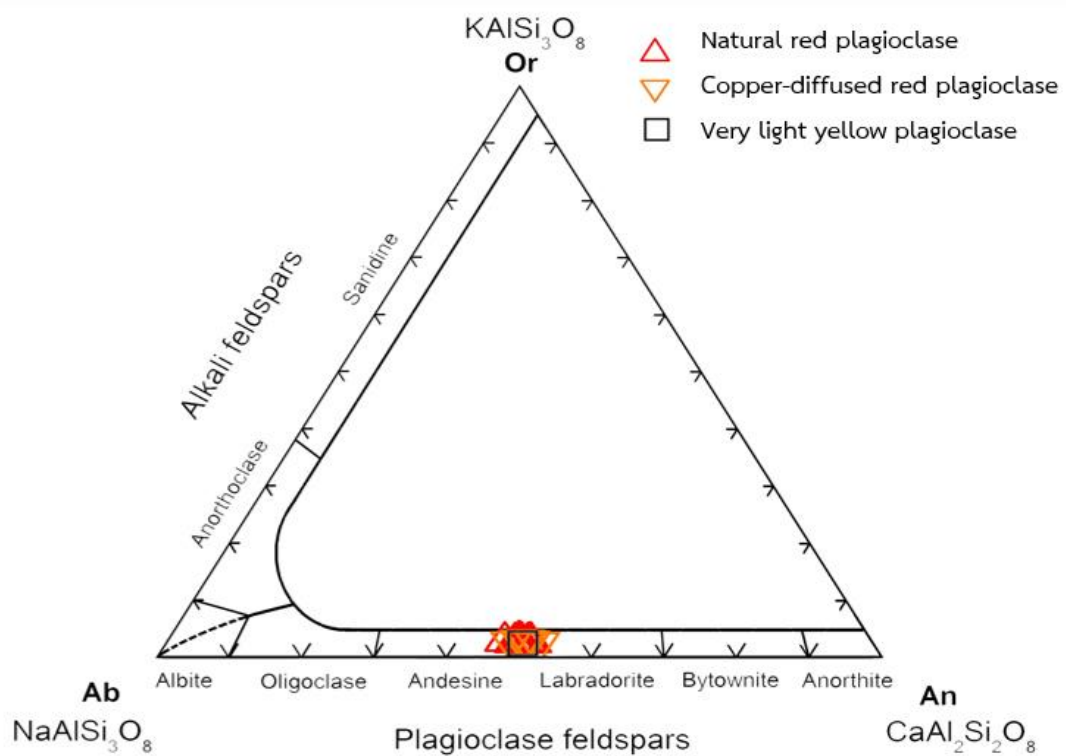


Figure 4.17 Ternary feldspar plots of 18 samples including natural red plagioclase, copper-diffused plagioclase and very light yellow plagioclase.

Table 4.2 Representative EPMA analyses of plagioclase samples.

Sample	Natural Red Plagioclase					Treated Red Plagioclase				
	YU3	YU4	YU5	YU6	YU7	TA0	TA1	TA2	DF1	DF2
SiO <sub>2</sub>	58.39	55.65	55.82	58.24	58.35	58.00	55.97	55.14	55.58	55.96
TiO <sub>2</sub>	0.07	0.04	0.09	0.07	0.07	0.13	0.04	0.06	0.00	0.06
Al <sub>2</sub> O <sub>3</sub>	26.33	27.44	27.40	26.34	26.47	26.61	27.25	27.28	27.51	27.65
FeO*	0.33	0.43	0.41	0.30	0.41	0.37	0.34	0.33	0.32	0.31
CaO	9.02	10.03	9.98	9.24	9.12	9.14	9.85	9.73	9.30	10.10
Na <sub>2</sub> O	5.40	4.81	5.23	5.16	5.14	5.28	5.15	5.35	5.37	5.02
K <sub>2</sub> O	0.49	0.74	0.45	0.46	0.46	0.46	0.46	0.51	0.00	0.43
CuO	0.05	0.09	0.09	0.11	0.07	0.05	0.10	0.05	0.00	0.08
SrO	0.00	0.00	0.00	0.00	0.01	0.00	0.03	0.00	0.00	0.00
Total	100.10	99.28	99.51	99.93	100.17	100.06	99.21	98.45	98.09	99.60
Formula 8(O)					Formula 8(O)					
Si	2.612	2.530	2.530	2.538	2.610	2.598	2.540	2.525	2.529	2.529
Ti	0.002	0.001	0.003	0.001	0.002	0.004	0.001	0.002	0.002	0.002
Al	1.389	1.471	1.465	1.465	1.396	1.405	1.458	1.473	1.482	1.473
Fe <sup>3+</sup>	0.000	0.000	0.000	0.000	0.000	0.000	0.000	0.000	0.000	0.000
Fe <sup>2+</sup>	0.203	0.113	0.079	0.110	0.246	0.201	0.106	0.041	0.111	0.119
Na	0.468	0.424	0.460	0.449	0.446	0.459	0.453	0.475	0.452	0.439
Ca	0.432	0.489	0.485	0.480	0.437	0.439	0.479	0.477	0.464	0.489
K	0.028	0.043	0.026	0.029	0.026	0.026	0.026	0.030	0.028	0.025
Cu	0.002	0.003	0.003	0.001	0.002	0.002	0.003	0.002	0.003	0.003
Sr	0.000	0.000	0.000	0.000	0.000	0.000	0.001	0.000	0.000	0.000
Total	4.939	4.967	4.977	4.968	4.926	4.938	4.969	4.989	4.968	4.965
%Ab	50.42	44.34	47.38	46.85	49.04	49.66	47.30	48.36	47.85	46.10
%An	46.58	51.14	49.96	50.17	48.07	47.50	49.95	48.63	49.19	51.31
%Or	2.99	4.52	2.66	2.99	2.89	2.84	2.75	3.01	2.96	2.59

#### 4.7 Laser Ablation-Inductivity Coupled Plasma-Mass Spectrometric (LA-ICP-MS) Results

LA-ICP-MS analyses are mostly collected in Appendix F1 and the representative samples were summarized in Table 4.3, including natural red plagioclases (sample nos. YU1, YU4, YU6 and YLA2) and treated red plagioclases (sample nos. TA0, TA1, TA2 and DF2). The results from LA-ICP-MS spot analyses were separately used in two ways. Plots concentration profile of natural and treated red plagioclase samples were investigated, initially. Subsequently, all the results were calculated statistically for trace element concentrations.

Some previous works (i.e., Hofmeister and Rossman (1985); Krzemnicki (2004); Abdurimyim(2009b)) reported that copper is the most crucial cause of red color in feldspar. Therefore, LA-ICP-MS analyses were focused on copper contents which should be the main cause of red coloring in both natural and treated red feldspar. In addition, the other elements were obtained from LA-ICP-MS analyses such as silver (Ag) and iron (Fe) were also emphasized in this study in detail for differentiation.

The average contents of magnesium (Mg), titanium (Ti), manganese (Mn), iron (Fe), strontium (Sr) and barium (Ba) of representative samples of both groups are in similar ranges. Therefore, some trace elements, e.g., copper (Cu), silver (Ag), iron (Fe), manganese (Mn) and barium (Ba) were used for profile plots along perpendicular direction and parallel direction to the twinning planes (sample nos. YU1, YU6 and TA0). Then comparison of average contents of all red samples were made. This study is aimed to recognize diffusion profiles of natural and treated stones.

Moreover, both red plagioclase groups usually show colorless rim. Therefore, inner red color zones and outer colorless areas are compared statistically in term of trace element concentrations. This may lead to differentiation of natural and treated stones which were undertaken different processes.

Table 4.3 LA-ICP-MS spot analyses of representative red plagioclases.

Sample no.	Natural Red Plagioclase (ppm)				Treated Red Plagioclase (ppm)			
	YU1	YU4	YU6	YLA2	TA0	TA1	TA2	DF2
<b>Major elements</b>								
Na	36964.87	35645.41	38206.75	41044.29	37411.58	40155.11	40143.53	39207.61
Al	142897.64	142897.63	142897.59	142897.61	142897.64	142897.61	142897.61	142897.59
Si	263137.72	252060.23	260700.53	262283.25	254937.38	256023.08	255679.05	257190.63
Ca	70943.16	70815.75	66465.83	68919.47	66475.19	68128.95	66411.07	71590.53
<b>Minor elements</b>								
Li	8.0	26.7	67.6	8.4	10.6	18.8	41.4	21.9
Be	bdl	bdl	bdl	bdl	0.2	bdl	bdl	bdl
B	6.0	3.3	3.5	4.3	4.5	3.3	4.0	5.4
Mg	420.3	309.3	413.7	412.8	413.8	412.7	430.7	428.6
Ti	364.7	359.5	360.7	364.9	347.5	370.8	361.9	336.8
V	1.8	1.6	1.5	1.9	1.4	1.8	1.8	1.6
C	bdl	1.2	bdl	bdl	bdl	bdl	bdl	bdl
Mn	36.8	31.2	34.0	37.7	28.6	38.0	35.9	33.7
Fe	2688.5	2948.2	2913.1	2804.2	2346.9	2737.6	2655.2	1812.2
Co	0.9	0.5	0.6	0.6	0.5	0.5	0.6	0.8
Ni	2.5	5.6	3.1	0.4	bdl	bdl	bdl	0.3
Cu	310.8	604.8	963.9	539.3	378.6	613.0	550.3	486.5
Zn	2.3	2.3	2.9	2.7	2.1	2.2	2.5	2.7
Ga	16.2	16.4	17.8	18.2	15.3	18.2	17.8	16.3
Ge	0.9	0.7	0.8	0.8	0.6	0.9	0.9	0.5
Rb	0.8	0.9	0.8	1.0	0.7	1.0	1.0	0.8
Sr	1069.0	1132.0	1030.0	1119.4	901.0	1140.8	1116.7	1003.4
Y	0.2	0.2	0.1	0.2	0.2	0.2	0.2	0.2
Zr	0.0	bdl	bdl	bdl	0.0	bdl	bdl	bdl
Nb	bdl	bdl	bdl	bdl	bdl	bdl	bdl	bdl
Mo	bdl	bdl	bdl	bdl	bdl	bdl	bdl	bdl
Ag	790.3	0.5	466.7	207.4	bdl	bdl	bdl	bdl
Sn	0.3	2.4	1.4	0.8	0.2	0.7	1.1	0.6
Sb	bdl	bdl	bdl	bdl	bdl	bdl	bdl	bdl
Cs	bdl	bdl	bdl	bdl	bdl	bdl	bdl	bdl
Ba	125.3	132.9	133.2	145.3	124.5	146.3	145.7	100.4
La	1.2	1.7	1.1	1.7	1.2	1.8	1.7	1.4
Ce	2.3	2.8	2.3	2.9	2.1	2.9	2.7	2.5
Pr	0.3	0.3	0.3	0.3	0.2	0.3	0.3	0.3
Nd	0.8	0.8	0.8	0.9	0.9	0.8	0.9	0.9
Sm	0.4	0.1	0.3	0.1	0.2	0.2	0.1	0.2
Eu	0.5	0.4	0.4	0.5	0.4	0.6	0.5	0.4
Gd	bdl	0.2	bdl	bdl	0.2	0.1	bdl	0.1
Tb	bdl	bdl	bdl	bdl	bdl	bdl	0.0	bdl
Dy	bdl	0.1	bdl	bdl	bdl	bdl	bdl	bdl
Ho	bdl	bdl	bdl	bdl	bdl	bdl	bdl	bdl
Er	bdl	bdl	bdl	bdl	bdl	bdl	bdl	bdl
Tm	bdl	bdl	bdl	bdl	bdl	bdl	bdl	bdl
Yb	bdl	bdl	bdl	bdl	bdl	bdl	bdl	bdl
Lu	bdl	bdl	bdl	bdl	bdl	bdl	bdl	bdl
Hf	bdl	bdl	bdl	bdl	bdl	bdl	bdl	bdl
Ta	bdl	bdl	0.0	bdl	bdl	bdl	bdl	bdl
W	bdl	bdl	bdl	bdl	bdl	bdl	bdl	bdl
Pb	0.5	0.4	0.5	0.5	0.4	0.4	0.4	0.4
Bi	bdl	bdl	bdl	bdl	0.0	bdl	bdl	bdl
Th	bdl	bdl	bdl	bdl	bdl	bdl	bdl	bdl
U	bdl	bdl	bdl	bdl	bdl	0.0	bdl	bdl

bdl: below detection limit



Copper (Cu): varies from about 311 to 1417 ppm with an average of  $797.57 \pm 185.37$  ppm in natural red feldspar and about 379 to 833 ppm with an average of  $491.38 \pm 36.41$  ppm in treated red feldspar. The average Cu content in natural red samples is almost two times higher than that of treated red samples.

For natural red samples, the Cu contents in colorless areas varies from about 311 to 1020 ppm with an average of  $760.70 \pm 154.76$  ppm whereas those in red areas varies from about 436 to 1417 ppm with an average of  $815.72 \pm 202.10$  ppm. The average Cu content of inner red areas and colorless rim appear to be the same range (see Figure 4.18).

For treated red samples, the Cu contents in colorless areas varies from 444 to 833 ppm with an average of  $509.43 \pm 61.16$  ppm whereas those in red area varies from 379 to 613 ppm with an average of  $488.02 \pm 28.62$  ppm. The average copper content from colorless areas (rim) is higher than content from red area (inner).

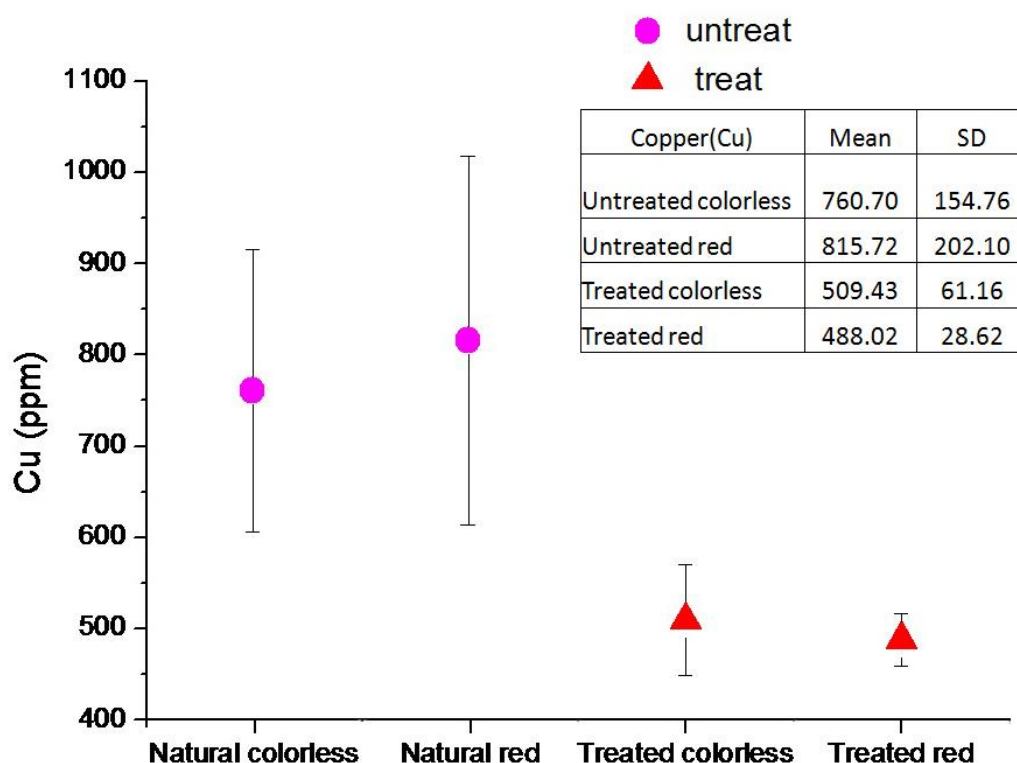


Figure 4.18 Comparison between average copper (Cu) contents between natural and treated red plagioclases dividing into colorless rim and inner red areas.

Silver (Ag): is  $\leq 790$  ppm with an average of  $91.01 \pm 196.96$  ppm in natural red red feldspar and about  $\leq 1$  ppm with an average of  $0.01 \pm 0.07$  ppm in treated red feldspar. Although, average Ag content of natural red samples appear to be higher than those of the treated samples, they have very high uncertainties (see Figure 4.19).

For natural red samples, the Ag contents in colorless areas are  $\leq 790$  ppm with an average of  $91.01 \pm 196.96$  ppm whereas those in red areas are  $\leq 710$  ppm with an average of  $74.20 \pm 157.08$  ppm. These appear to be the same range with high uncertainty.

For treated red samples, the Ag contents in colorless areas  $\leq 1$  ppm with an average of  $0.04 \pm 0.15$  ppm whereas those in red areas are  $\leq 0.30$  ppm. Then they are actually negligible.

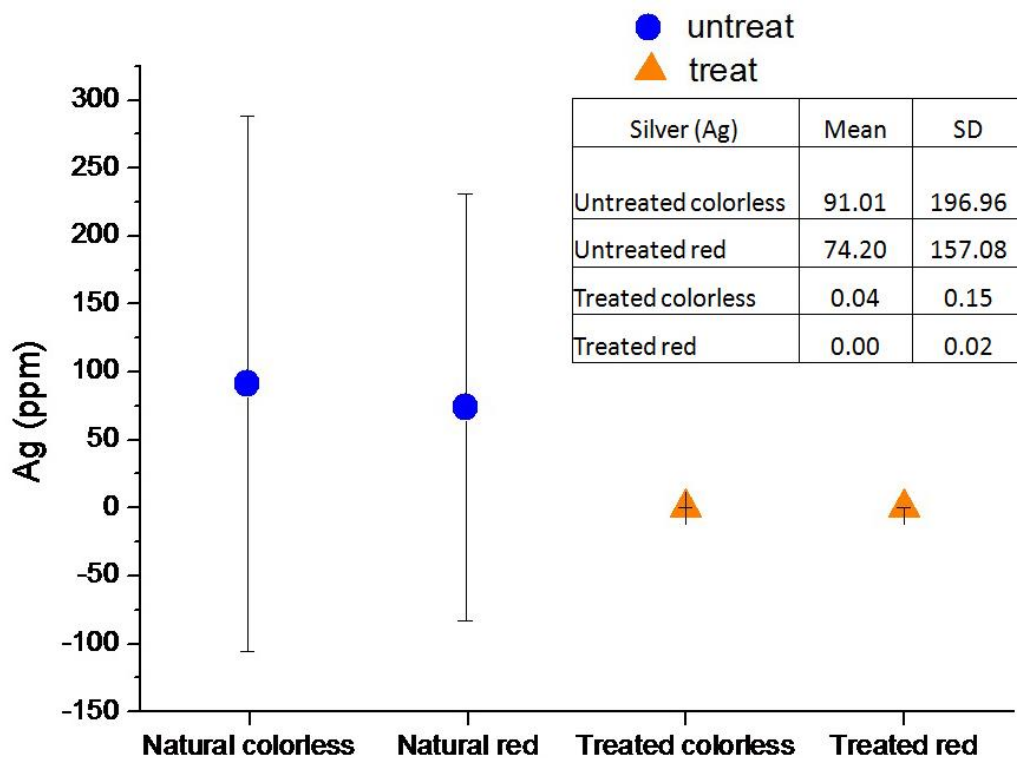


Figure 4.19 Comparative graph of averaged silver (Ag) contents between natural red and treated red plagioclase dividing into colorless rim and inner red zones.

Iron (Fe): varies from about 1858 to 3164 ppm with an average of  $2570.55 \pm 331.54$  ppm in natural plagioclases and about 1536 to 2810 ppm with an average of  $2075.68 \pm 302.73$  ppm) in treated plagioclases. The average of Fe content in natural samples is slightly higher than treated samples. Fe content is much higher than others trace elements such as manganese, copper, silver and barium (Figure 4.20).

For natural red samples, the iron contents in colorless areas varies from 1858 to 3164 ppm with an average of  $2401.50 \pm 391.62$  ppm) whereas those in red areas varies from 1888 to 3062 ppm with an average of  $2656.26 \pm 275.05$  ppm). Their average iron content from inner red areas is higher than content from colorless rim.

For treated red samples, the iron contents in colorless areas vary from 1535.86 to 2809.88 ppm with an average of  $2203.56 \pm 308.66$  ppm and in red areas varies from 1578.99 to 2737.57 ppm with an average of  $2051.94 \pm 296.25$  ppm. They appear to be the same range.

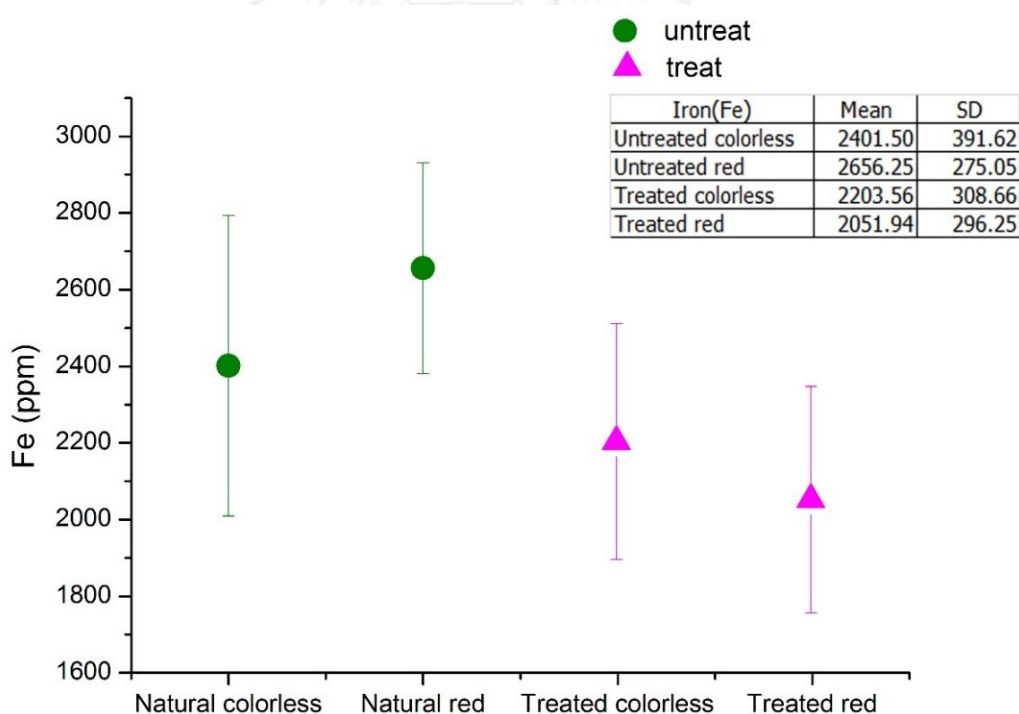


Figure 4.20 Comparative graph of averaged Iron (Fe) contents between natural red and treated red plagioclase dividing into colorless rim and inner red zones.

Manganese (Mn): varies from 30 to 40 ppm with an average of  $34.38 \pm 2.00$  ppm in natural red plagioclases and about 29 to 38 ppm with an average of  $32.78 \pm 1.16$  ppm in treated plagioclases. Both groups contain similar range of Mn (Figure 4.21).

For natural red samples, the Mn contents in both colorless areas (30 to 40 ppm with an average of  $34.19 \pm 2.08$  ppm) red areas (30 to 40 ppm with an average of  $34.66 \pm 1.88$  ppm) are obviously equal.

For treated red samples, the manganese contents in both colorless areas (29 to 36 ppm with an average of  $32.42 \pm 1.55$  ppm) red areas (29 to 38 ppm with an average of  $32.85 \pm 1.07$  ppm) are quite equal contents.

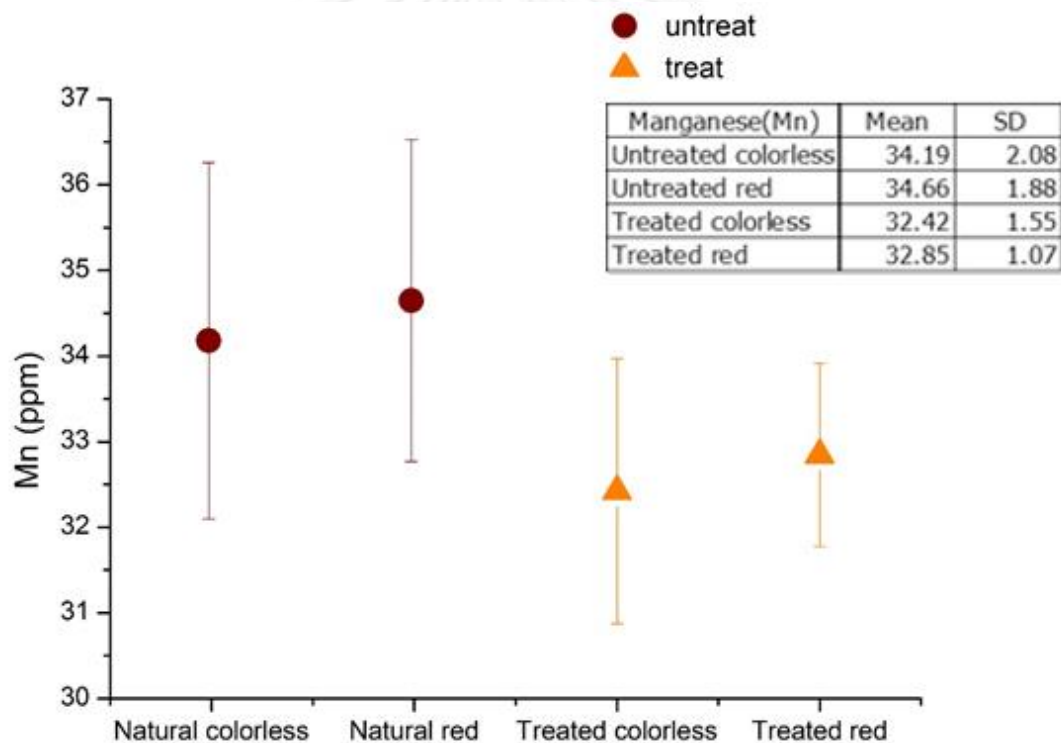


Figure 4.21 Comparative graph of averaged manganese (Mn) contents between natural red and treated red plagioclase dividing into colorless rim and inner red zones

Barium (Ba): varies from 122 to 171 ppm with an average of  $135.01 \pm 5.39$  ppm in natural red plagioclases and about 88 to 154 ppm with an average of  $111.40 \pm 21.09$  ppm in treated plagioclases. The average of Ba content of natural red samples is slightly higher than that of treated samples (Figure 4.22).

For natural red samples, the Ba content in colorless areas vary from about 122 to 152 ppm with an average of  $137.16 \pm 4.93$  ppm and red areas vary from 113 to 171 ppm with an average of  $134.15 \pm 5.47$  ppm which they are the same ranges.

For treated red samples, the Ba contents in colorless areas vary from 88 to 154 ppm with an average of  $116.59 \pm 23.05$  ppm and red areas vary from 88 to 149 ppm with an average of  $110.44 \pm 20.61$  ppm which appear to be the same range.

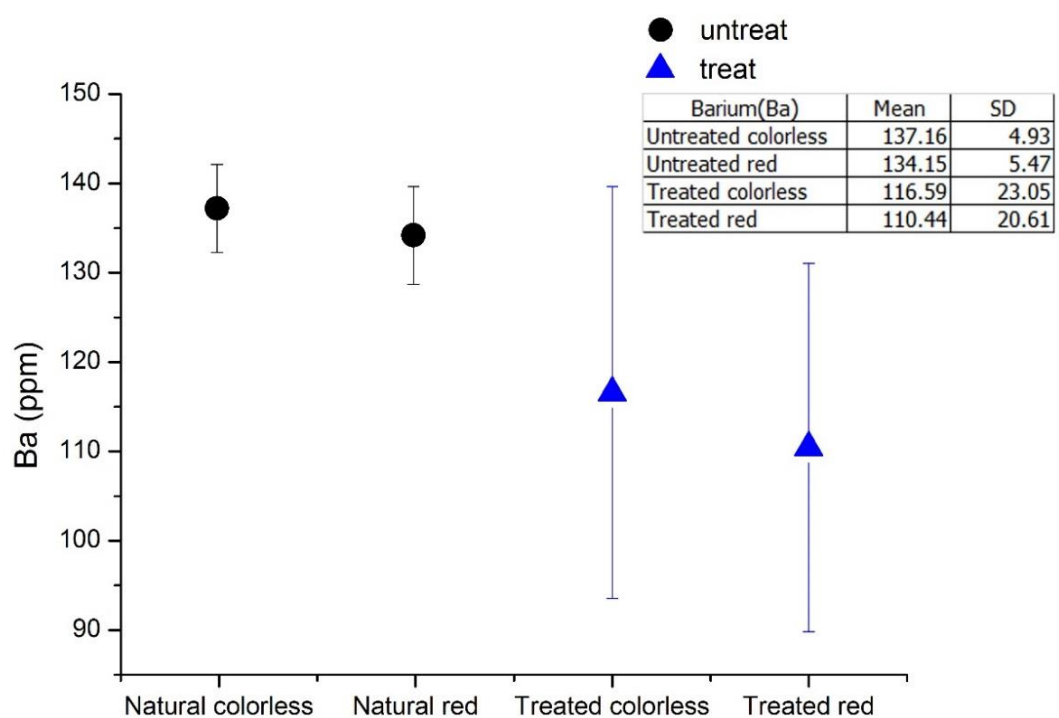


Figure 4.22 Comparative graph of averaged barium (Ba) contents between natural red and treated red plagioclase dividing into colorless rim and inner red zones.

The trace element profiles including magnesium (Mg), titanium (Ti), manganese (Mn), iron (Fe), copper (Cu), strontium (Sr), silver (Ag) and barium (Ba) of natural sample no. YU1 were plotted in two directions perpendicular (Figure 4.23) and parallel (Figure 4.24) to twinning plane, only profile plot of copper show the concentration as diffusion from inner red outwards colorless rim. On the other hand, profile plots of silver show diffusion from colorless rim inwards core.

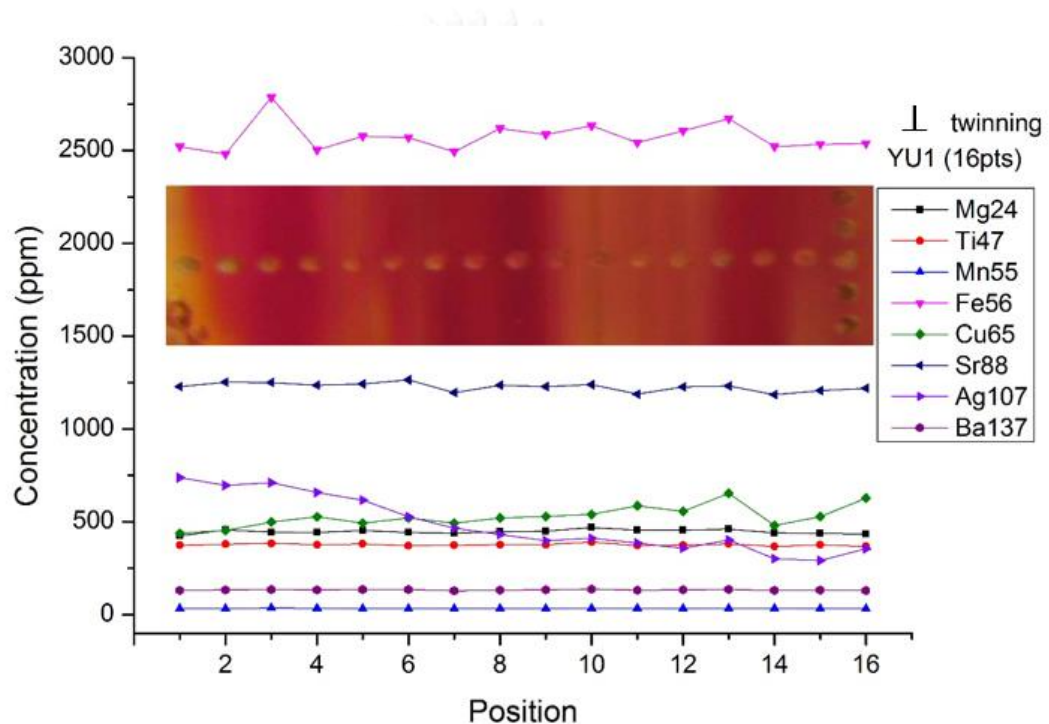


Figure 4.23 Profile plots of Mg, Ti, Mn, Fe, Cu, Sr Ag and Ba in natural red feldspar; 16 spots cross (perpendicular to) the twinning plane from colorless rim (left side) to inner red zone.

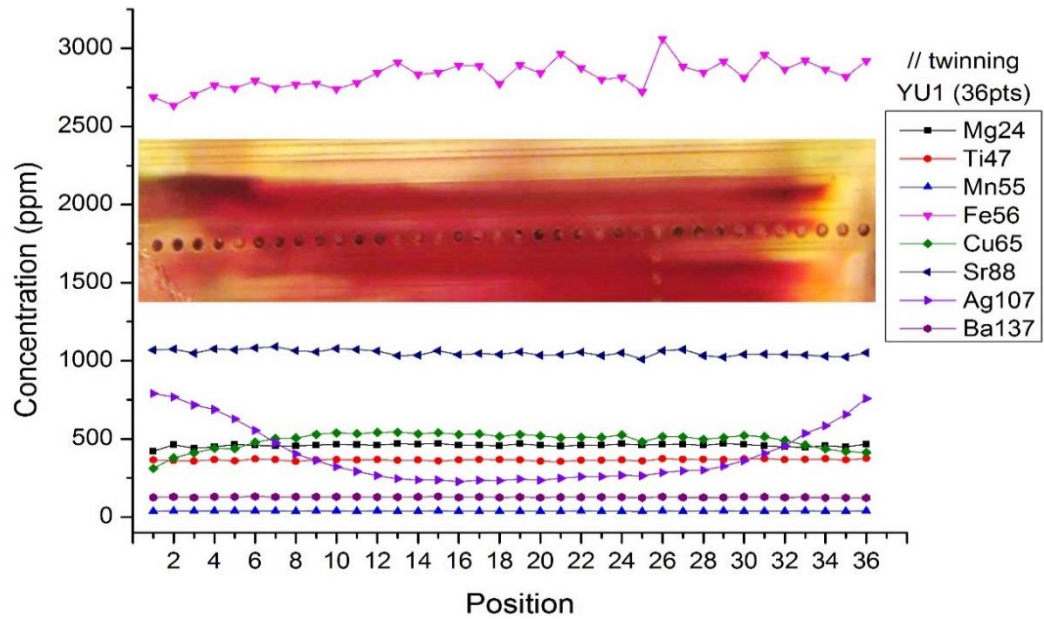


Figure 4.24 Profile plots of Mg, Ti, Mn, Fe, Cu, Sr Ag and Ba in natural red feldspar; 16 spots along (parallel to) the twinning plane.

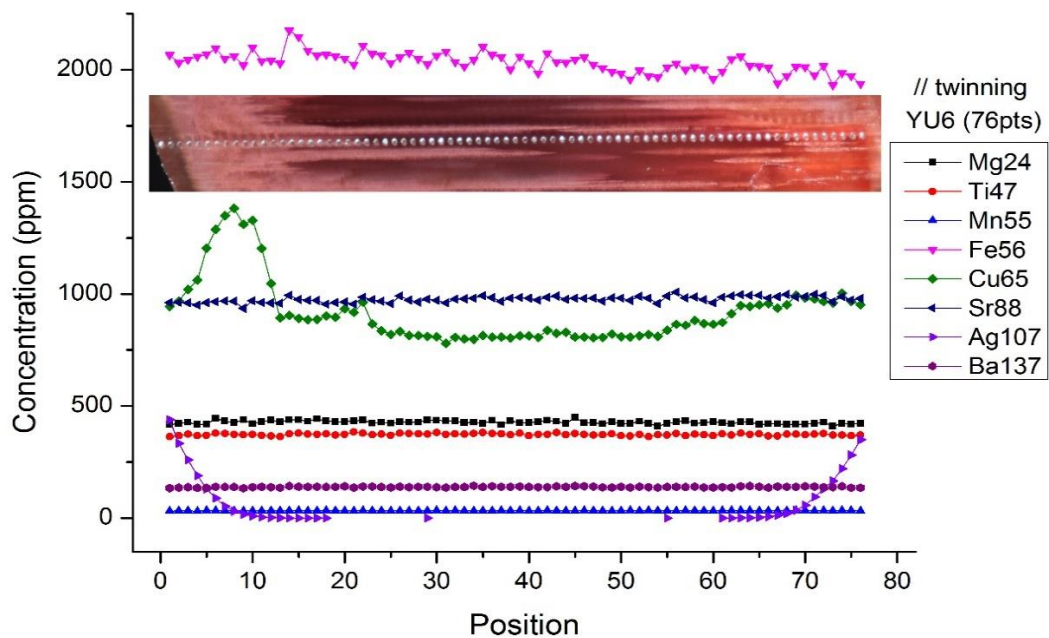


Figure 4.25 Analytical profiles of Mg, Ti, Mn, Fe, Cu, Sr, Ag and Ba in natural red feldspar parallel to the twinning plane (red tube) showing high copper content.

Analyses of natural red samples (sample nos. YU1 and YU6) show profile along a red twinning plan of copper increasing towards core (Figure 4.25). However, analytical profile perpendicular to the twinning (sample no. YU1) shows high copper content in intense red areas.

Whereas the trace element of treated red sample (TA0) was profile plotted in two directions perpendicular (Figure 4.26) and parallel (Figure 4.27) to the twinning plane show no variation of copper and silver contents.

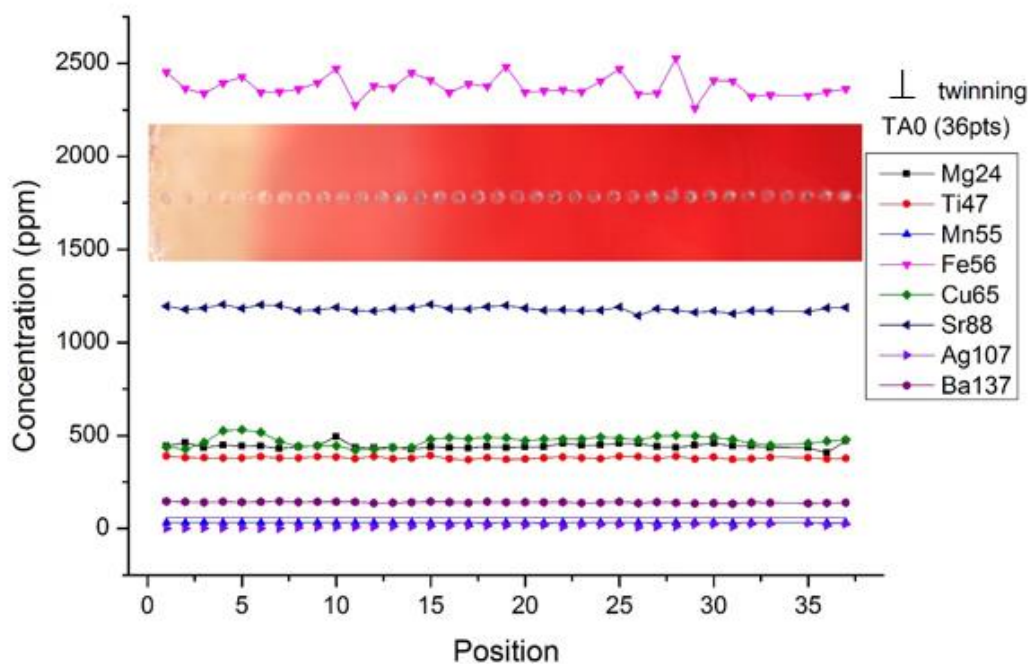


Figure 4.26 Profile plots of Mg, Ti, Mn, Fe, Cu, Sr, Ag and Ba in treated red feldspar; 36 spots perpendicular to the twinning from colorless rim (left side) to inner red zone.



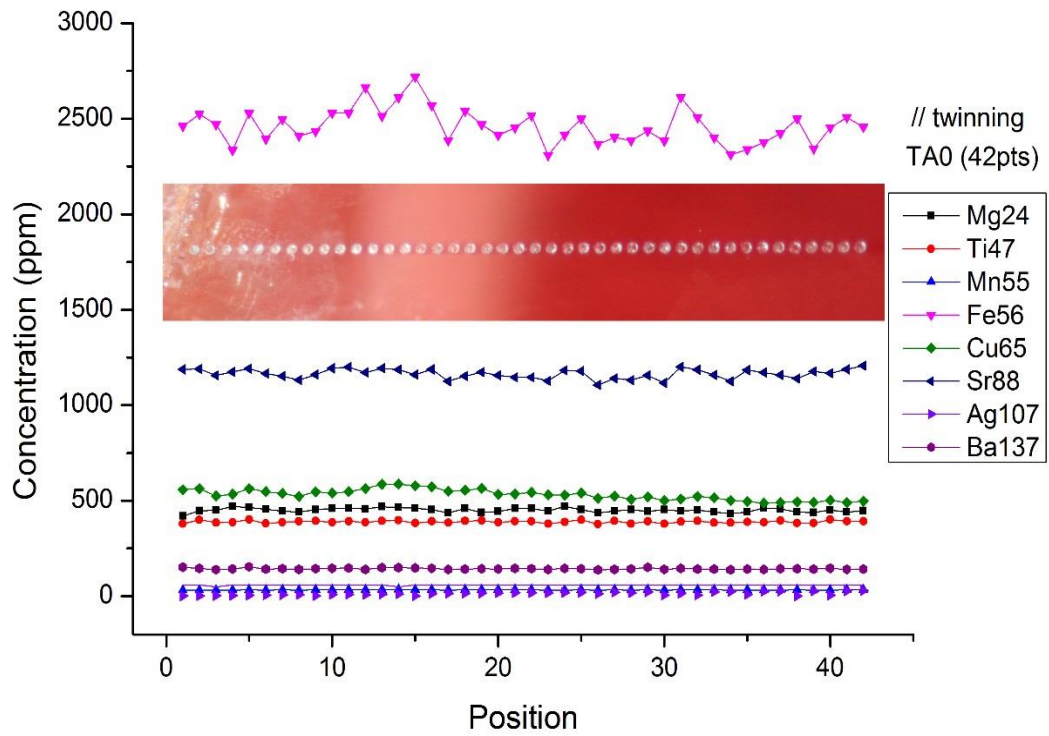


Figure 4.27 Profile plots of Mg, Ti, Mn, Fe, Cu, Sr, Ag and Ba in treated red feldspar; 42 spots parallel to the twinning from colorless rim (left side) to inner red zone.

Comparative copper contents in treated red feldspar, sample no. TA0, containing three color zones (i.e., colorless, light red and red area) from rim to inner core are present in Figures 4.28 - 4.29. The treated red plagioclases have red color layers between light red and red. Most light red areas are related to cloud; therefore, light red color from outer (sample no. TA0) may be caused by cloud inclusion.

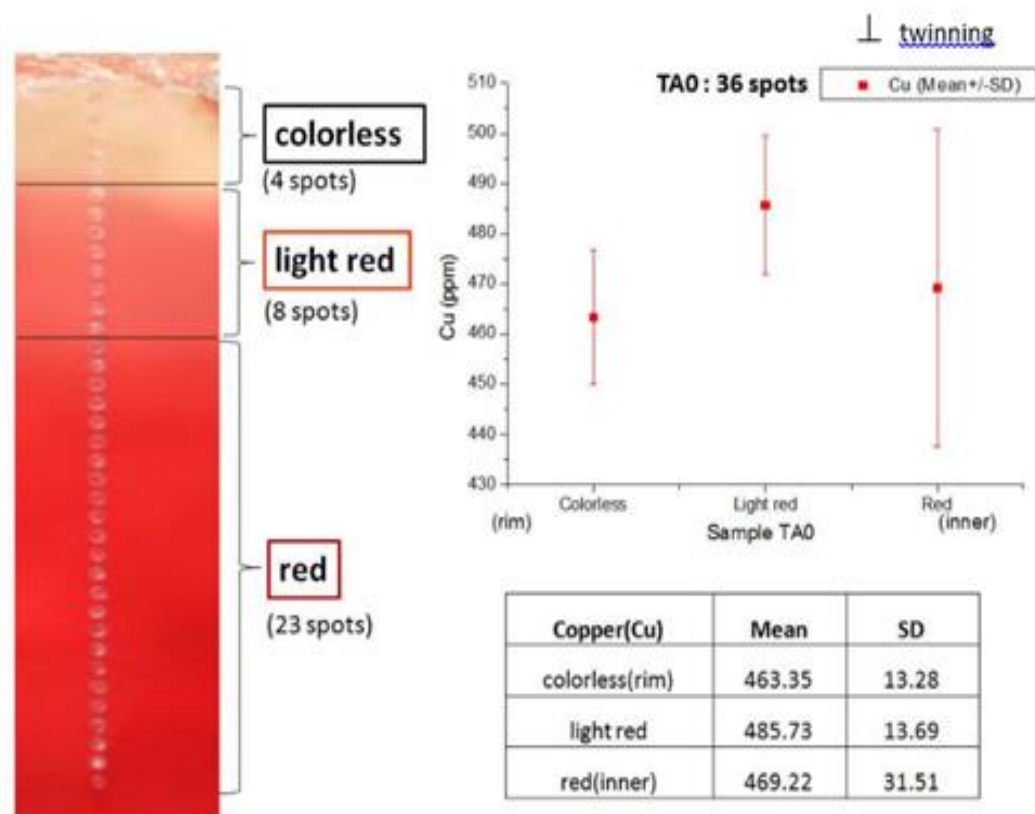


Figure 4.28 Comparative graph of copper (Cu) contents in treated feldspar (sample no. TA0); 36 spots analyzed perpendicular to twinning planes; Mean and SD were calculated from each area such as colorless (4 spots) light red (8 spots) and red (23 spots).

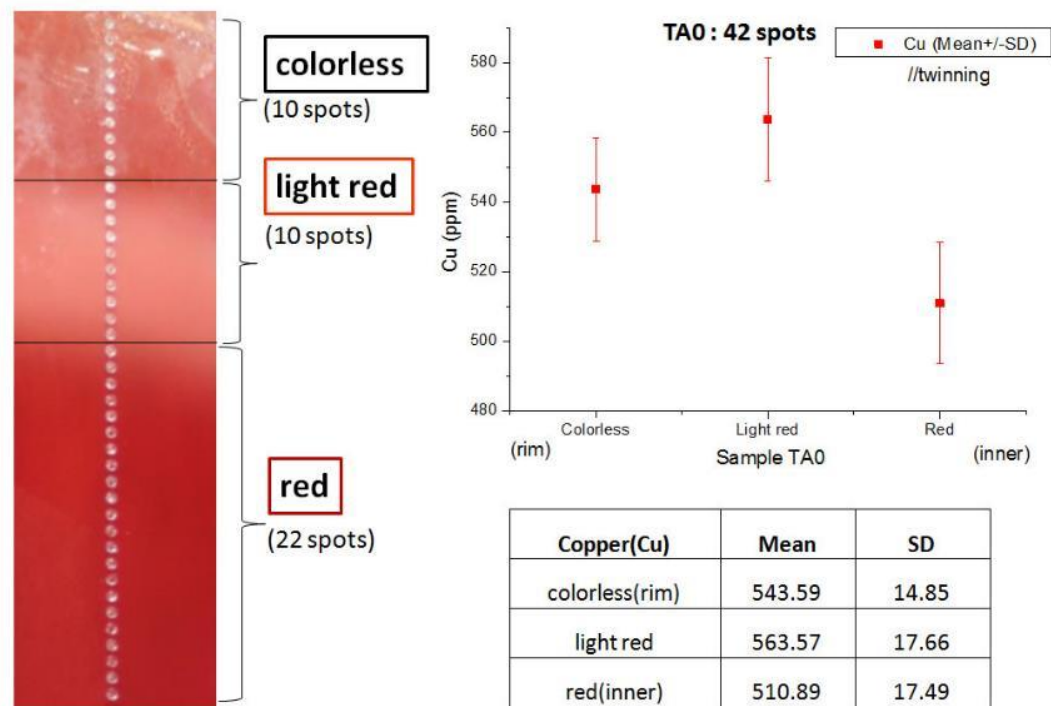


Figure 4.29 Comparative graph of copper (Cu) content in treated feldspar (sample no. TA0); 42 spots analyzed along the twinning plane; Mean and SD were calculated from each area as colorless (10 spots) light red (10 spots) and red (22 spots).

As the results, this treated red sample shows that copper contents along twinning plane (average  $528.86 \pm 28.52$  ppm) are higher than those analyzed perpendicular to twinning direction (average  $472.24 \pm 27.60$  ppm). Copper contents of light red area appear to be higher than those in the inner red area. In term of statistic, they are in the same range. Standard deviation of the sample results (red area) is too high and covers range of the other parts of colorless and light red. It cannot be used to conclude this information.

More profiles of natural and treated red plagioclases are collected in Appendix F3. Moreover, Cu and Ag profiles can also be observed in natural red plagioclases which appear to be related to diffusion process. This will be discussed later.

## CHAPTER 5

### DISCUSSIONS AND CONCLUSIONS

#### 5.1 Physical Properties

The samples in this study can be divided into two groups. The first group contains 12 natural red plagioclases from Yu Lin Gu, Tibet. The second group contains 5 copper-diffused red plagioclases which their raw materials are expected from Mongolia. Therefore, a very light yellow plagioclase from Mongolia was collected for reference under this study.

The first group, rough plagioclases from Tibet are light red to red without bicolored red- green sample. On the other hand, Tibetan samples previously reported by Abduriyim (2009a) are deep red, reddish orange, orange-red and some stones are bicolored red-green.

The second group, copper-diffused red plagioclases from Mongolia are red to intense red. These colors are relatively darker than those of the natural red plagioclases from Tibet. A Chinese dealer declared to Mr. Thanong Leelawatanasuk who provides the studied samples that all samples were treated by copper-diffusion in China and raw materials are from Inner Mongolia. Also, Abduriyim (2009a) reported similarly that copper-diffused red andesine from Inner Mongolia had been used for treatment in China.

Most studied plagioclase samples both from Tibet and Inner Mongolia appear to have similar physical properties that were also previously reported for andesine from Congo (Fritsch, 2002), Tibetan and Inner Mongolia plagioclase (Abduriyim & Kobayashi, 2008) . Their refractive indices range from 1.550 to 1.562 which are lower than the RI range (1.560-1.572) of labradorite from Oregon, USA (reported by Fritsch, 2002).

According to Krzemnicki (2004), pleochroism of labradorite from Congo and Oregon are very weak in red sample to distinct in green sample while andesines from Congo (Fritsch, 2002) are very weak as found similarly in Tibetan andesine Abduriyim (2009a). Very weak pleochroism is also recognized in the natural red samples of the

first group under this study but after the samples were polished, these stones show more obvious uneven color. Colorless zones distributed throughout with mottle red and green colors. Under dichroscope, most natural red samples showed weak to strong pleochroism between green and colorless whereas red areas did not change (see Figure 5.1). The second sample group (Cu-diffused plagioclase) show unclearly pleochroism from colorless to green color; this may due to intense red even deeper than the natural red plagioclase. However, color in some particular areas may change weakly- moderately from red to grayish red or colorless to green under gem microscope using polaroid and diffused plates (see Figure 5.2).

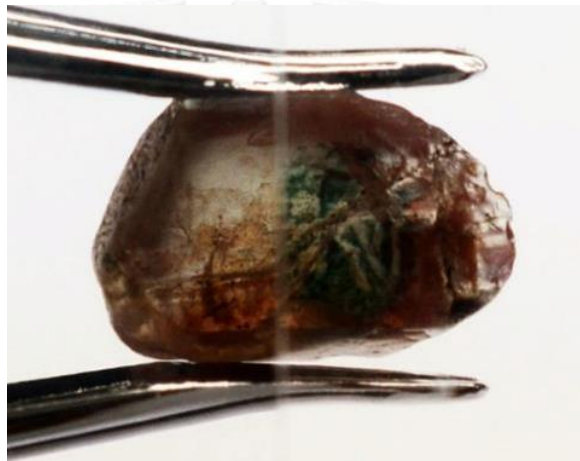


Figure 5.1 Distinct dichroism of the natural red plagioclase is clearly observed under London dichroscope (sample no. YD1).

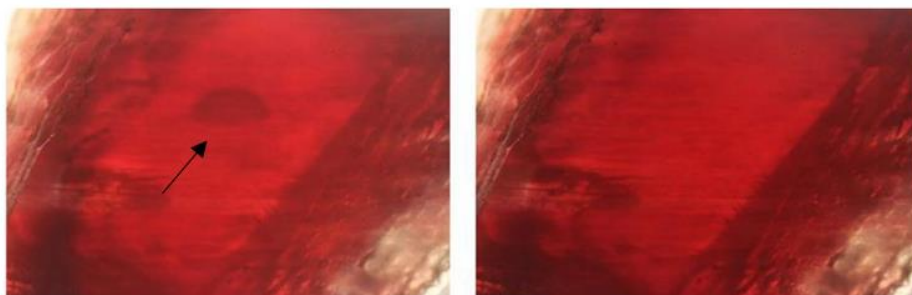


Figure 5.2 Pleochroism of copper-diffused red plagioclase (sample no.TA0) showing moderate grayish red (left) to red (right) under gem microscope using polaroid and diffused plates.

According to Abduriyim (2009a), Tibetan natural samples usually show twin lamellae parallel to the [010] presenting as parallel lath-like hollow channels or pipe-like tubes. They showed irregular color patches caused by milky turbidity of fine particle inclusions; moreover, fissures and leaf-like discoid fractures also present. Only one sample displayed aventurescence. These reported inclusions are resemble to those found in the samples under this study.

However, the internal characteristics of samples in both sample groups under this study are quite similar to each other. Their inclusions included oriented tubes, fingerprint, irregular tubes, colorless zone around fingerprint or fracture, mottle color (red and green), milky cloud along red zone and colorless rim called as white rim (McClure, 2009; Peretti, 2011). Some distinctive features between both groups are some glistering cloud along red zone in natural red plagioclase (Figure 5.3) and red color layer from rim towards core in copper-diffused red plagioclase (see also Figure 5.5). The interesting features in red feldspar are aventurescence effect (schiller or glistering) and red clouds that relate to the red color of stone.

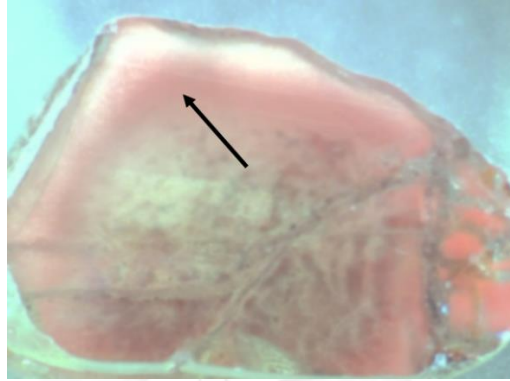


Figure 5.3 Glistening cloud along red zone in natural red plagioclase (sample no. YD1).

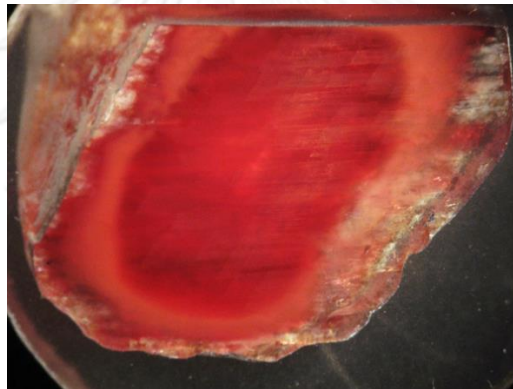


Figure 5.4 Red color layer from rim inwards core in copper-diffused red plagioclase (sample no. TA0).

Since the eighteenth century, red coloring in feldspar has known as results of hematite flake inclusions that are oriented when light is scattered they may produce schiller (iridescence or aventurescence). These feldspars may be called ‘sunstone’ (Smith, 1974). According to Henn (2004), aventurescent oligoclase feldspars from Oregon, USA that has colorless with red tabular inclusions are responsible to the pale red color. They contain euhedral hematite inclusions which cause aventurescence by the reflection of light from these tiny red platelets. This effect can occur from metallic copper inclusions. Andersen (1917) had initially reported aventurine plagioclase (An<sub>65</sub>) from Modoc County, California which they have metallic copper oriented parallel to the b and c of crystal axes. After Hofmeister and Rossman (1985) studied the gem quality labradorite, they found red color from the intrinsic absorption of colloidal Cu<sup>0</sup>

particles that are too small to scatter light (<22 nm). Tibetan andesine was confirmed metallic copper smaller than 200 nm by TEM. These colloidal inclusions are concluded to be small particles of metallic copper ( $\text{Cu}^0$ ).

Andersen (1915) suggested that play of light caused by reflections from thin visible oriented lamella in feldspar is aventurization. This effect distinguishes from red cloudy because it does not involve strong reflections from thin oriented lamellae. Therefore, the glistering and red clouds were found in some studied samples may be the main cause of red color. But the glistering should be occurred by nano-copper particles oriented along twinning plane that different from copper platelet inclusion in sunstones from Ponderosa mine. These copper platelet inclusions could be observed under microscope (50x) (Johnston et al., 1991). In this study, clouds or small particles in natural red plagioclase were observed under microscope (70x); however, a few of small copper inclusions display schiller effect. For copper-diffused red plagioclases, their intense red color layer is distinguished from the natural red plagioclase.

## 5.2 Spectroscopic Characteristics

All samples were collected Raman spectra. Characteristic peaks of Raman spectrum of high-temperature plagioclase (intermediate Na, Ca mixture) are  $509\pm 1$ ,  $482\pm 2$ ,  $284\pm 3$  and  $179\pm 4$   $\text{cm}^{-1}$  (Freeman et al., 2003). All samples in both plagioclase groups showed similar Raman-shift peaks at about 281, 406, 482, 509, 564 and 792  $\text{cm}^{-1}$ . These are matched very well with the typical Raman spectra of plagioclase. These Raman spectra are similar to plagioclase databases from the RRUFF Project website (source of all samples from Rossman, R. G.), especially patterns of andesine, labradorite and bytownite.



Fourier Transform Infra-Red (FTIR), according to Hofmeister and Rossman (1983), the infrared absorption is frequently observed in the 3600-3300  $\text{cm}^{-1}$  region as a result of minor amount of structural water in the feldspar. The infrared spectra of all plagioclase samples under this study show consistency of two main absorption bands including OH- or H<sub>2</sub>O at about 3900 to 3400  $\text{cm}^{-1}$  and C-H stretching at about 2960 to 2849  $\text{cm}^{-1}$  (as suggested by Stuart (2004). Representative infrared spectra of natural orange-red, reddish orange, deep red and bicolored red-green Tibetan andesines reported by Abduriyim (2009a) are unlikely to be related to OH- or H<sub>2</sub>O- absorptions. However, these spectra could not distinguish any difference between natural red plagioclase from Tibet and copper-diffused red plagioclase from Inner Mongolia.

All substances can appear as colloid under the appropriate conditions which may not relate to chemical composition and colloid condition (Greenland, 1917). According to Hofmeister and Rossman (1983), the color of mineral can be produced by minor chemical substituents, inclusions, interference effect from exsolution lamellae and radiation damage. Many colors may be created by inclusions as pink, red, gray, orange and green. Aventurine and schiller effects also result from inclusions. Exsolution lamellae and oriented intergrowth features may produce interference color, schiller and chatoyancy in gemstones.

To identify the cause of color in gemstone, many gem testing laboratories use UV-VIS-NIR spectrophotometry. According to Rada et al. (2011), transition metal ions possess characteristics of optical absorption spectra that are mostly extended in the UV-visible spectrum depending on the valence state and coordination number of the transition metal which is consequence of d level state. Therefore, the characteristics absorption spectra of the transition metal ions were used to study the red coloring in plagioclase.

This study focuses the cause of red coloring and schiller in the plagioclase samples. These might be occurred from the copper inclusions as reported in some previous works, i.e., sunstone from Lake County, Oregon. Red color is cause by a weekly polarized absorption band centered at 560 nm or 570 nm, the red are from the intrinsic absorption of colloidal Cu<sup>0</sup> particles that are too small to scatter light (<22 nm) whereas green color is caused primarily by a board polarized band around 670 nm. It

produces an absorption minimum in the green which may be caused by  $\text{Cu}^{1+}/\text{Cu}^0$  IVCT or  $\text{Cu}^0$  pairs by Hofmeister and Rossman (1983) and Hofmeister and Rossman (1985). Red labradorites from Congo and Oregon show two distinct absorption bands at 565 and 380 nm due to copper (Krzemnicki, 2004) and deep red Tibetan andesine displays predominant absorption near 565 nm with weak absorption at 320 nm. Reddish orange has main absorption shifting to 567 nm with weak absorption at 320 nm and very weak absorptions at 423 and 450 nm due to  $\text{Fe}^{3+}$  (Abduriyim, 2009a).

All red plagioclase samples were studied in two directions of polarized spectra when the filter was parallel and perpendicular at 0 degree (0p) and 90 degree (90p), respectively. The natural red plagioclase samples show range of distinct absorption bands at 568 to 599 nm (0p) and at 573 to 595 nm (90p). The polarized spectra show different absorption that relates to distinctive pleochroism color in some sample (e.g., sample nos. YLA3 and YD1 see Figure 3.1). The absorption spectra distinctively shift towards red region as present in the one natural red sample (sample no. YD1). It has strong pleochroism (colorless to green when focus on colorless area), its polarized absorption spectra shows distinctive band at about 568 nm (0p) and at 591 nm (90p) (see Figure 4.2). Comparative absorption spectra of copper-diffused red plagioclase that have very weak pleochroism showing similar polarized absorption spectra at about 570 nm (0p) and 572 nm (90p) (see Figure 5.5).

Spectroscopic results of all red samples in both groups help to confirm that all samples are plagioclase that red coloring is caused by copper. Although, both groups have some different distinctive pleochroism and UV-Vis spectra which show some different absorption shifts in perpendicular polarized spectra. But these results are overlapping between some natural red plagioclases and copper-diffused red plagioclases. The green color can be seen obviously in natural red samples whereas the copper-diffused red samples have intense red throughout the whole stones.

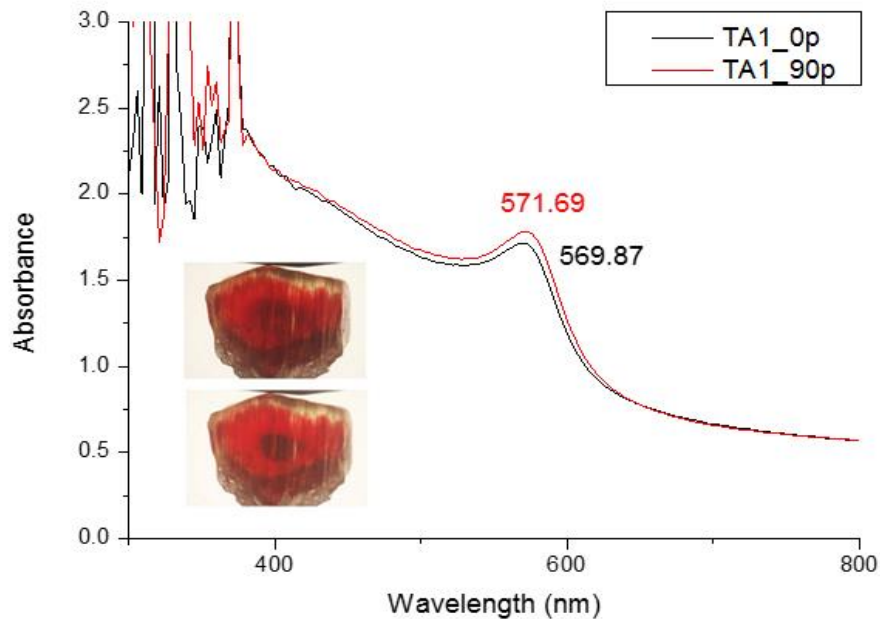


Figure 5.5 UV-Vis spectra of Cu-diffused red plagioclase (sample no. TA1) show the distinct polarized absorption band at about 570 nm (0p) and 572 nm (90p).

According to Hofmeister and Rossman (1983), feldspar is naturally colorless when it is in the pure form without any minor substituent, inclusion and exsolution phenomena. It does not absorb light in the visible portion of spectrum. The natural very light yellow plagioclase from Mongolia (sample no. IMA) shows the absorption peaks at 382, 420 and 449 nm due to  $\text{Fe}^{3+}$ , this result is similar to absorption of colorless feldspar from Inner Mongolia reported by Abduriyim (2009a) and Abduriyim (2009b). The sample IMA has not shown absorption band at 560-565 nm but some natural red plagioclases have unclear absorption peak about at 380 nm (see Appendix A).

### 5.3 Chemical Analyses

In this study, the EDXRF analyses collected the element oxides of all plagioclase samples, both major and minor elements can be analyzed as semi-qualitative composition. Therefore, these results cannot be used to study trace elements in specific area. It is better procedure to use the EMPA analyses for recalculate end-member content of all the plagioclase samples. As the results, both groups of samples from Tibet and Inner Mongolia revealed the overlapping in range of andesine-labradorite which is similar to results of Abduriyim (2009a).

Regarding to the previous works, cause of color in feldspar have been suggested to be involved significantly by tiny inclusions. Hofmeister and Rossman (1983), feldspar may yield several colors depending on various colors of inclusions. Based on this study, physical properties and spectroscopic characteristics of all investigated samples indicate that red color in plagioclase should be caused by schiller effect of copper colloid inclusions. This idea is supported by the same results as reported by Abduriyim et al. (2011); Andersen (1917); Hofmeister and Rossman (1985); Krzemnicki (2004); Peretti (2011).

Copper appears to be a crucial trace element as analyzed by LA-ICP-MS. Their spot analyses were profile plotted for both natural red plagioclase and Cu-diffused red plagioclase samples. This study use even spot size (55  $\mu\text{m}$ ) distance between spots of 100  $\mu\text{m}$  along straight lines. Two directions, perpendicular and parallel to twinning plane, were set for all profile analyses. These designed experiment is different from those reported by Peretti (2011).

Trace element profiles (Appendix F3), in natural red sample, show diffusion from inner red outwards colorless rim (sample s YU1 and YU4); moreover, sample YU6 also shows high copper concentrate along red tube. Whereas profile plots of silver show diffusion from colorless rim inwards core (samples YU1 and YU6). These results are similar to results reported by Peretti (2011). This evidence may indicate copper diffusion along twinning plane. According to Abduriyim (2009a), red and green color variation appear to have been involved by copper exsolution temperature. They are related to rate of Cu diffusion and aggregation of  $\text{Cu}^0$  colloids as well as oxidation state of copper ( $\text{Cu}^0$  or  $\text{Cu}^+$ ) (Hofmeister and Rossman, 1985; Krzemnicki, 2004).

Regarding to feldspar structure, copper cannot be substituted into the tetrahedral network. Therefore, the copper should be form as  $\text{Cu}^0$  colloids particles which formed as inclusion. It is probably the main cause of red coloring. However, their color may be changed to colorless which is probably caused by  $\text{Cu}^0$  oxidized from  $\text{Cu}^+$ . Valence electron configuration of copper is  $3d^{10} 4s^1$  with 11 electrons, the  $3d$  band is filled completely whereas the  $4s$  band is half filled to the level marked Cu (Nassau, 2001). This copper state ( $\text{Cu}^+$ ) is stable. It does not absorb light in the visible portion of spectrum when feldspar is colorless and without inclusion (Arem, 2011; A. M. Hofmeister & Rossman, 1983). However, the weak zone in crystal structure of plagioclase feldspar are usually follow twinning plane in which the copper inclusions can be located and oriented along (001) and (010) directions as reported by Hofmeister and Rossman (1985). Ponderosa mine sunstones also have copper platelets oriented on (001), (010) and probably (100) directions. Although, natural and treated red plagioclases under this study unclearly show platelet inclusions but most red tubes and red cloud orientate along twinning plane which they are suspected to be copper micro-inclusion.

Copper contents of red plagioclase compared to data of Peretti (2011), the copper-diffused red feldspars contain various contents. Treated red feldspars reported by Peretti (2011) yield similar results of treated samples under this study. However, he reported copper contents in some treated feldspars are extremely high about 3490 ppm (sample no. 10722-Cu that was copper-diffused by Emmett). On the other hand, natural red plagioclases from Yu Lin Gu, Tibet contain 311 to 1426 ppm Cu. Therefore, the copper content of different processes could be higher than content in the natural red plagioclase. In the chapter 4, the results were reported as natural red samples from Yu Lin Gu, Tibet have higher Cu content than the copper-diffused plagioclases from Inner Mongolia.

Three color zones, colorless, light red and red were also statistically distinguished for Cu content. Copper contents in treated red plagioclase sample show higher concentration from outer colorless rim to inner re core. This is crucial evidence to support surface diffusion by artificial treatment. According to Emmett and Douthit (2009), copper diffusion experiment used  $ZrO_2$  containing 1% copper metal and run in air with temperature range  $1000^{\circ}C - 1200^{\circ}C$ , the copper can diffuse in the plagioclase. Process of treatment, formula of flux and powder, is still secret or unclear about how to change colorless raw material to intense red color.

The natural red plagioclases from Yu Lin Gu, Tibet, were confirmed that their origin is the natural red plagioclase source (Abduriyim et al., 2011). But, it is difficult to prove when copper occurred in the natural red samples during the geological process. Copper contents (core>rim) might indicate that copper had already inside the plagioclase feldspar; subsequently, mechanism related to temperature and pressure may lead to generation of copper colloidal particles causing red color. After copper maybe changed in oxidation state, other colors can be produced. Consequently, red samples show uneven color with green and colorless; moreover, some samples may show glistering.

## 5.4 Conclusions

The main objective of this research is to study the mechanism and cause of red coloring in gem plagioclase feldspar.

Base on analytical results obtained from 18 samples, it can be concluded that the red color of feldspar is caused by copper and the mechanism of copper diffusion taken place along a dislocation line as 'pipe diffusion' and 'surface diffusion'. The concluding remarks are listed below:

1. The cause of red coloring in both natural red and copper-diffused red plagioclases should be (nano-particles) copper colloid particles. Many results are supported this cause of red color. e.g., red or glistering cloud along tube or twinning plane. UV-Vis spectra show the distinct absorption band at 566 - 599 nm probably due to  $\text{Cu}^0$  colloid which has absorption pattern similar to all red plagioclase samples reported in previous works.

2. Treated red plagioclase shows intense red and color layer with cloud whereas the natural red plagioclase contains the glistering cloud inclusion. Both natural and treated red plagioclase show colorless rim but the average copper content in treated red samples are getting high at the outer rim and less copper content toward inner zone.

3. The mechanism of copper diffusion taken place along a dislocation line as pipe diffusion can be seen in both sample groups. The analytical results show comparative copper profile along tube or twinning plane and cross directions. In natural red sample, contents of copper along twinning planes have possibility of red color with higher copper concentration. Relatively, the perpendicular direction has higher copper content only positions of red zone. The copper-diffused sample, using statistic copper content, can be proven that copper diffused from the surface related to their internal feature as red color layer. Thus, the copper-diffused plagioclase sample has the mechanism of both pipe diffusion and surface diffusion.

## REFERENCES

- Abduriyim, A. (2009a). A Mine Trip to Tibet and Inner Mongolia: Gemological Study of Andesine Feldspar. from GIA. <http://www.gia.edu/research-resources/news-from-research/andesine-mines-Tibet-Inner-Mongolia.pdf>
- Abduriyim, A. (2009b). The characteristics of red andesine from the Himalaya Highland Tibet. *The Journal of Gemmology*, 31(5-8), 283-298.
- Abduriyim, A., & Kobayashi, T. (2008). Gem News International: Gemological properties of andesine collected in Tibet and Inner Mongolia. *Gems & Gemology*, 44(4), 371-373.
- Abduriyim, A., McClure, S. F., Rossman, G. R., Leelawatanasuk, T., Hughes, R. W., Laurs, B. M., . . . Emmett, J. L. (2011). RESEARCH ON GEM FELDSPAR FROM THE SHIGATSE REGION OF TIBET. *Gems & Gemology*, 47(2), 167-180.
- Andersen, O. (1915). On aventurine feldspar. *American Journal of Sociology*, 40, 351-398.
- Andersen, O. (1917). Aventurine feldspar from California. *American Mineralogist*, 2, 91.
- Arem, J. E. (2011). Gem feldspars and feldspars treatments Retrieved August 12, 2012 <http://www.jewelersethicsassociation.com/docs/GEM%20FELDSPARS.pdf>
- Deer, W. A., Howie, R. A., & Zussman, J. (1992). *An Introduction to the Rock Forming Minerals* (2 ed.). London: Longman.
- Emmett, J., & Douthit, T. (2009). Copper diffusion in plagioclase. from GIA <http://www.gia.edu/research-resources/news-from-research/Cu-diffusion-Emmett.pdf>
- Fontaine, G. H., Hametner, K., Peretti, A., & Günther, D. (2010). Authenticity and provenance studies of copper-bearing andesines using Cu isotope ratios and element analysis by fs-LA-MC-ICPMS and ns-LA-ICPMS. *Analytical and Bioanalytical Chemistry*, 398, 2915-2928.
- Freeman, J. J., Wang, A., Kuebler, K. E., & Haskin, L. A. (2003, June 10, 2014). *RAMAN SPECTROSCOPIC CHARACTERIZATION OF THE FELDSPARS – IMPLICATIONS FOR*



*IN SITU SURFACE MINERAL CHARACTERIZATION IN PLANETARY EXPLORATION. .*

Paper presented at the Lunar and Planetary Science

- Fritsch, E. (2002). Gem News International : Red andesine feldspar from Congo. . *Gems & Gemology*, 38(1), 94-95.
- Guilmette, C., Hébert, R., Dupuis, C., Wang, C., & Li, Z. (2008). Metamorphic history and geodynamic significance of high grade metabasites from the ophiolitic mélange beneath the Yarlung Zangbo ophiolites, Xigaze area Tibet *Journal of Asian Earth Sciences*, 32, 423–437.
- Hofmeister, A. M., & Rossman, G. R. (1983). Color in Feldspars. *Reviews in Mineralogy*, 2, 271 - 280.
- Hofmeister, A. N., & Rossman, G. R. (1985). Exsolution of metallic copper from Lake County labradorite. *Geology*, 13, 644-647.
- Hughes, R. W. (2011). Andesine: Timeline of a controversy. Retrieved August 1, 2011, from GIA, <http://www.gia.edu/research-resources/news-from-research/timeline-hughes.pdf>
- IUPAC. (1999). Definitions of terms for diffusion in the solid *Pure and Applied Chemistry*, 71, 1307-1325.
- Jarvis, K. E. (1988). Inductively coupled plasma mass spectrometry: a new technique for the rapid or ultra-trace level determination of the rare-earth elements in geological materials *Chemical Geology*, 68, 31-39.
- Johnston, C. L., Gunter, M. E., & Knowles, C. R. (1991). Sunstone labradorite from the Ponderosa Mine, Oregon. *Gems & Gemology*, 27(4), 220-233.
- Kiefert, L., Hänni, H. A., & Ostertag, T. (2001). Raman Spectroscopic Applications to Gemmology *Handbook of Raman Spectroscopy*: CRC Press.
- Klein, C., & Hurlbut, C. S. (1999). *Manual of Mineralogy* (21 ed.). USA: John Wiley & Sons.
- Krzemnicki, M. S. (2004). Red and green labradorite feldspar from Congo. *The Journal of Gemmology*, 29(1), 15-23.

- Lauris, B. M., Abduriyim, A., & Isatelle, F. (2011). Geology and field studies of reported andesine occurrences in the Shigatse region of Tibet. from GIA. <http://www.gia.edu/research-resources/news-from-research/geology-lauris.pdf>.
- Leelawatanasuk, T. (2004). *Relationship between magnesium and iron content in some olivine and Raman Spectroscopy*. Chulalongkorn University.
- Lu, R., Dubinsky, E. V., Douthit, T. R., & Emmett, J. L. (2011). Silver Incorporation in Inner Mongolian and Tibetan Andesine. from GIA. <http://www.gia.edu/research-resources/news-from-research/silver-lu.pdf>.
- Manning, J. R. (1973). *Diffusion kinetics and mechanisms in sample crystals*. . Paper presented at the Geochemical transport and kinetics, a conference at Airlie House, Virginia.
- McClure, S. F. (2009). Observations on Identification of Treated Feldspar. from GIA <http://www.gia.edu/research-resources/news-from-research/identification-treated-feldspar.pdf>.
- Murch, G. E. (1991). Diffusion in Crystalline Solids. In R. W. By Cahn, P. Haasen and E.J. Kramer (eds). (Ed.), *Materials Science and Technology* (Vol. 5): VCH Weinheim
- Nassau, K. (2001). *The physical and chemistry of color* (2 ed.). New York: John Wiley & Sons
- Peretti, A. (2011). Distinguishing Natural Tibetan Copper-Bearing Andesine from its Diffusion-Treated Counterparts Using Advanced Analytical Methods. *Contributions to Gemology*, 10, 105.
- Poirier, J., & Poirier, P. (1985). *Creep of Crystals: High-Temperature Deformation Processes in Metals, Ceramics and Minerals*. New York: Cambridge University Press.
- Rada, S., Dehelean, A., & Culea, E. (2011). Dual role of the six-coordinated lead and copper ions in structure of the copper-lead-tellurate glasses. *Journal of Alloys and Compounds*, 509, 321-325.

- Rossman, G. R. (2011). Argon Isotope Studies of Andesine Collected During the 2010 Expedition to Tibet. from GIA. <http://www.gia.edu/research-resources/news-from-research/argon-rossman.pdf>.
- RRUFF. Retrieved July 10, 2014. <http://rruff.info/albite/display=default/X050005>  
<http://rruff.info/oligoclase/display=default/X050122>  
<http://rruff.info/andesine/display=default/X050013>  
<http://rruff.info/labradorite/display=default/X050108>  
<http://rruff.info/bytownite/display=default/X050033>
- Ruzeng, Y., Yuan, Y., & Hongyi, X. (2005). Sapphire diffusion treatment and behavior of iron and titanium. *The Journal of Gemmology*, 29(7-8), 455-460.
- Salameh, B. (2011). Thermal-Stimulated Diffusion in Crystalline Solids A New Theoretical Approach. *European Journal of Scientific Research*, 50(1), 59-66.
- Shackley, M. S. (2011). An Introduction to X-Ray Fluorescence (XRF) Analysis in Archaeology *X-Ray Fluorescence Spectrometry (XRF) in Geoarchaeology* (pp. 7-44). London: Springer.
- Smith, J. V. (1974). Chemical and Textural Properties. *Feldspar Minerals* (Vol. 2, pp. 690): Springer-Verlag Heidelberg.
- Stuart, B. (2004). *Infrared spectroscopy: fundamentals and applications*. England: John Wiley & Sons
- Thirangoon, K. (2009). Observation on effects of heating and copper diffusion in feldspar (An on-going research). Retrieved September 10, 2009, from GIA <http://www.gia.edu/research-resources/news-from-research/heating-Cu-diffusion-feldspar2.pdf>.
- Wang, W., Lan, Y., Lu, T., Jiang, W., Chen, C., Li, Q., . . . J., X. (2011). Documental report of geological field investigation on “red feldspar” in Tibet, China. *Journal of Gems & Gemmology*, 13(1), 1-5.
- Wang, W., Lan, Y., Lu, T., Jiang, W., Chen, C., Li, Q., . . . Xie, J. (2010). Letters to the Editors : Geological field investigation on the reported occurrence of ‘red feldspar’ in Tibet. *Gem & Jewellery*, 19(4), 44-45.

Zener, C. (1950). Ring diffusion in metals. *Acta Crystallographica*, 3, 346-354.



## APPENDICES

**Appendix A** : UV-VIS-NIR spectra of 17 feldspar samples which consist of 12 untreated samples and 5 treated samples

**Appendix B** : RAMAN spectra of 18 feldspar samples which consist of 13 untreated samples and 5 treated samples

**Appendix C** : RAMAN spectra of 18 feldspar samples which consist of 13 untreated samples and 5 treated samples

**Appendix D** : EDXRF analyses of 18 feldspar samples which consist of 13 untreated samples and 5 treated samples; 2 – 6 spots analyses per sample were collected.

**Appendix E** : EPMA result of 18 feldspar samples which consist of 13 untreated samples and 5 treated samples

**Appendix F1** : LA-ICP-MS chemical analyses of 17 plagioclase samples (12 untreated red plagioclase and 5 treated red plagioclase samples)

**Appendix F2** : LA-ICP-MS chemical spot analyses of 17 plagioclase samples (5 elements; Mn, Fe, Cu, Ag and Ba) in red and colorless areas of each samples

**Appendix F3** : Concentration profiles (Cu and Ag) in ppm of untreated red feldspar (sample nos. YU1, YU4, YU5 and YU6) and treated red feldspar (sample no. DF2) determined using LA-ICP-MS

**Appendix F4** : Sensitivity of LA-ICP-MS analyses in this study

**Appendix G** : Internal characteristic of 10 plagioclase feldspars

(All in CD)

## VITA

Miss Namrawee Susawee was born on November 23, 1981 in Chiang Mai, Thailand. She graduated with bachelor degree in Gemology from the Department of Geology, Faculty of Science, Chiang Mai University in 2004. At present, she works at Gem Testing Laboratory, The Gem and Jewelry Institute of Thailand and also studied in Master program in Geology at Chulalongkorn University.

